



Theses and Dissertations

2006-06-02

Compliant Mechanism Suspensions

Timothy Melvin Allred
Brigham Young University - Provo

Follow this and additional works at: <https://scholarsarchive.byu.edu/etd>

 Part of the [Mechanical Engineering Commons](#)

BYU ScholarsArchive Citation

Allred, Timothy Melvin, "Compliant Mechanism Suspensions" (2006). *Theses and Dissertations*. 434.
<https://scholarsarchive.byu.edu/etd/434>

This Thesis is brought to you for free and open access by BYU ScholarsArchive. It has been accepted for inclusion in Theses and Dissertations by an authorized administrator of BYU ScholarsArchive. For more information, please contact scholarsarchive@byu.edu, ellen_amatangelo@byu.edu.

COMPLIANT MECHANISM SUSPENSIONS

by

Timothy M. Allred

A thesis submitted to the faculty of

Brigham Young University

in partial fulfillment of the requirements for the degree of

Master of Science

Department of Mechanical Engineering

Brigham Young University

August 2003

BRIGHAM YOUNG UNIVERSITY

GRADUATE COMMITTEE APPROVAL

of a thesis submitted by

Timothy M. Allred

This thesis has been read by each member of the following graduate committee and by majority vote has been found to be satisfactory.

Date

Larry L. Howell, Chair

Date

Spencer P. Magleby

Date

Robert H. Todd

BRIGHAM YOUNG UNIVERSITY

As chair of the candidate's graduate committee, I have read the thesis of Timothy M. Allred in its final form and have found that (1) its format, citations, and bibliographical style are consistent and acceptable and fulfill university and department style requirements; (2) its illustrative materials including figures, tables, and charts are in place; and (3) the final manuscript is satisfactory to the graduate committee and is ready for submission to the university library.

Date

Larry L. Howell
Chair, Graduate Committee

Accepted for the Department

Brent L. Adams
Graduate Coordinator

Accepted for the College

Douglas M. Chabries
Dean, College of Engineering and Technology

ABSTRACT

COMPLIANT MECHANISM SUSPENSIONS

Timothy M. Allred
Department of Mechanical Engineering

Master of Science

This thesis has explored the use of compliant mechanisms in vehicle suspension systems, specifically where a compliant mechanism acts as part of the wheel locating mechanism and as the energy storage element. A compliant mechanism has the potential of reducing part count, joints, and manufacturing and assembly costs of a suspension system. Fatigue failure has been found to be a limiting design constraint which competes with space and weight constraints. Controlling wheel motion in response to control forces has also been shown to be an important functional requirement for a compliant suspension system. Vehicle applications that are best suited for the use of compliant suspension systems are those that are low weight, have low energy storage requirements, and do not require precise vehicle handling characteristics. New compliant suspension concepts have been explored that support the wheel in 3-dimensions to minimize undesired wheel motions. These new concepts demonstrate increased stiffness and decreased stress due to

control forces. Of these concepts, the compliant A-Arm proves to be the most promising candidate for future development. It has added advantages of lower space requirements, lower number of extra joints and rigid links, and simpler design for manufacture and assembly. The stiffness, stress, and kinematic characteristics of the compliant A-Arm configuration have been explored. This configuration has a non-linear force-deflection curve that is facilitated by the stress-stiffening effects of large deflections. A closed-form linear stiffness solution and a pseudo-rigid-body model has also been developed to aid in the initial design of the compliant A-Arm in a suspension system.

TABLE OF CONTENTS

CHAPTER 1 Introduction	1
1.1 Thesis Objective	4
1.2 Research Justification	5
1.2.1 Benefits of Compliant Mechanisms in Suspensions Systems	5
1.2.2 Contributions	5
1.3 Thesis Outline	6
 CHAPTER 2 Background & Literature Review	 9
2.1 Suspension Systems	9
2.1.1 Applications	9
2.1.2 Functions of a Suspension System	10
2.1.3 Design Considerations	11
2.1.4 Classifications and Examples	19
2.1.5 Current Suspension Research	22
2.2 Compliant Mechanisms	23
2.2.1 Pseudo-Rigid-Body-Model	24
2.2.2 Compliant Mechanism Synthesis	25
2.2.3 Type Synthesis	25
2.2.4 Vibration Analysis	26
2.3 Use of Compliant Mechanisms in Suspensions	26
2.3.1 Leaf Spring	26
2.3.2 Examples	29
2.3.3 Other Examples	31
 CHAPTER 3 Understanding the Design of a Compliant Suspension System	 33
3.1 Compliant Mechanisms and Suspension Functional Requirements	33
3.2 Important Functional Requirements and Design Constraints of a Compliant Suspension System	36
3.2.1 Fatigue	36
3.2.2 Creep	40
3.2.3 Control Forces and Wheel Deflections	41
3.2.4 The Effect of Compliant Solutions on other Suspension Properties ..	48
3.2.5 Other Considerations	49

3.3 Design Conclusions	50
3.4 Possible Vehicle Applications	51
CHAPTER 4 Concept Exploration	55
4.1 Solution Objectives	56
4.2 Rigid-Body Replacement Synthesis	56
4.2.1 Double A-Arm 4-Bar Mechanism	57
4.2.2 McPherson Strut	59
4.2.3 Trailing Arm	60
4.2.4 Multi-link Mechanism	61
4.3 Other Mechanism Concepts	62
4.3.1 Straight Line Mechanisms	63
4.3.2 Compliant Linear Motion Mechanisms	64
4.3.3 A-Arm Configuration	65
CHAPTER 5 Concept Evaluation and Comparisons	69
5.1 Wheel Deflections and Control Forces	69
5.1.1 Concepts	70
5.1.2 Deflection Results	73
5.1.3 Discussion of Deflection Results	75
5.1.4 Stress Results from Analysis of Control Forces	76
5.1.5 Discussion of Stress Results	76
5.1.6 Conclusions on Mechanism Response to Control Forces	78
5.2 Space and Weight Constraints on Stress Reduction	78
5.3 Other Comparisons	80
5.4 Concept Evaluation Conclusions	80
CHAPTER 6 Compliant A-Arm	83
6.1 Justification for Further Analysis	83
6.2 Analysis with Beam Elements	84
6.2.1 Stiffness Results	85
6.2.2 Deflection Path	86
6.3 Linear Closed-Form Solution of Stiffness Results	88
6.4 Test Results	95
6.5 Non-linear FEA Results	97
6.5.1 Reaction Loads, Deflections, and Stress	99
6.6 Non-Linear Stiffness and Stress Predictions	102
6.6.1 Pseudo-Rigid-Body Model	105
6.7 Compliant A-Arm Suspension Design	117
6.8 Conclusion	123

CHAPTER 7 Conclusions and Future Work	125
7.1 Conclusions	125
7.2 Future Work	128
7.2.1 Suspension A-Arm Mechanism Configurations	128
7.2.2 Techniques for Decreasing Stress and Weight	130
7.2.3 Proper Ground Clearance	131
7.2.4 Compliant Suspension Used in Parallel with Extra Energy Storage Device	132
APPENDIX Linear Closed Form Solution of Compliant A-Arm	139
A.1 Spherical Joint Approximation	142
A.2 Fixed Joint Connection	143

LIST OF TABLES

TABLE 3.1	Identification of Suspension Functional Specifications, Compliant Mechanism Characteristics and Important Design Constraints.....	35
TABLE 3.2	Vehicle Application Information	52
TABLE 5.1	Mechanism Concept Configuration Characteristics	72
TABLE 5.2	Wheel Attitude Changes (radians).....	74
TABLE 5.3	Bending and Direct Stress due to Control Forces.....	77
TABLE 6.1	Physical Test Prototype Specifications	96
TABLE 6.2	Reaction Loads	98

LIST OF FIGURES

Figure 1.1	Traditional leaf spring suspension configuration [1].....	2
Figure 1.2	Kinematic 4-bar linkage suspension system [2]	3
Figure 2.1	Kinematic 4-bar linkage suspension system [2]	11
Figure 2.2	Quarter-car model two-mass system.....	12
Figure 2.3	Camber and scrub	16
Figure 2.4	Toe angle.....	16
Figure 2.5	Control forces	17
Figure 2.6	Common automobile independent suspensions [2]	21
Figure 2.7	Common solid-axle automotive suspensions [2].....	22
Figure 2.8	Example of how the pseudo-rigid-body model converts (a) a flexible segment into (b) a rigid-link mechanism	24
Figure 2.9	Leaf spring configurations [1]	28
Figure 2.10	Kinematic lever radius of a leaf spring (Matschinsky, 2000).....	28
Figure 2.11	Mercedes-Benz '170V' front suspension with transverse leaf springs (1935) [1].....	30
Figure 2.12	Ford Escort rear suspension with a single transverse composite leaf [34] ...	30
Figure 2.13	Ford Focus rear suspension (1998) [1]	31
Figure 2.14	Canondale Scalpel rear suspension (http://www.cannondale.com/bikes/innovation/clinics/scalpel/scalpel_12.html)	32
Figure 2.15	Soft Ride seat suspension (http://www.softride.com)	32
Figure 3.1	Wheel control forces	41
Figure 3.2	Cantilever beam with applied control forces	43
Figure 3.3	Four bar fixed guided compliant parallel mechanism and pseudo rigid body model	47
Figure 4.1	Ford A-Arm suspension and representative planar four-bar mechanism [2].....	57
Figure 4.2	Compliant parallel 4-bar mechanisms with rigid coupler. The circled mechanisms have been implemented previously with transverse leaf springs.....	58
Figure 4.3	McPherson strut and representative four link planar mechanism.....	59
Figure 4.4	Trailing arm suspension and representative planar two link mechanism	60
Figure 4.5	Ford multi-link rear suspension	61
Figure 4.6	Spatial compliant mechanism	62
Figure 4.7	Watt and Roberts linkages	64
Figure 4.8	Folded beam linear motion mechanism	65
Figure 4.9	Three dimensional version of folded beam mechanism	66
Figure 4.10	Component of a compliant A-Arm mechanism	67

Figure 5.1	Mechanism concept configurations	71
Figure 6.1	Representation of FEA beam model	85
Figure 6.2	FEA force deflection prediction of compliant A-Arm and linear beam theory prediction of two cantilever beams acting in parallel	86
Figure 6.3	Deflection path of endpoint, C , and pseudo-rigid-link model of endpoint deflection	87
Figure 6.4	Pseudo-rigid link approximation of deflection path for a vertical load	88
Figure 6.5	Free-body diagram of compliant A-Arm mechanism	89
Figure 6.6	Deflections due to applied loads and redundant loads	93
Figure 6.7	Physical prototype specifications	96
Figure 6.8	Plastic test prototype results	97
Figure 6.9	Stress distribution at the base of the beam	100
Figure 6.10	Specific volume efficiency, η , at a maximum deflection: $\Theta = 0.8$ radians	104
Figure 6.11	Specific volume efficiency, η , as a function of Θ	105
Figure 6.12	Non-dimensionalized transverse load index, $(\alpha^2)_t$, versus Θ for α between 0 and 90 degrees	107
Figure 6.13	Linear curve fits for $b/h = 8$	108
Figure 6.14	Non-dimensionalized transverse load factor versus Θ for different values of b/h and $\alpha = 90$ degrees	108
Figure 6.15	$K_{\Theta c}$ data points	110
Figure 6.16	$K_{\Theta c}$ surface plot	110
Figure 6.17	2-D plots of $K_{\Theta c}$	111
Figure 6.18	Torsional spring constant, K , for $b/h = 20$ and $\alpha = 60$ degrees	114
Figure 6.19	Force deflection predictions from FEA model and PRBM at different b/h values and $\alpha = 90$ degrees	115
Figure 6.20	Maximum error at any give Θ between $(\alpha^2)_t$ predicted by pseudo-rigid-body model and FEA model	116
Figure 6.21	Double compliant A-Arm mechanism	118
Figure 6.22	Pseudo-rigid-body model of suspension compliant A-Arm at design load deflection, y , and at maximum deflection, $y + y_c$	119
Figure 6.23	Pseudo-rigid-body model predictions of mechanism load and spring rate	119
Figure 6.24	FEA beam model and pseudo-rigid-body model predictions	121
Figure 6.25	Compliant A-Arm geometry	122
Figure 6.26	FEA shell element model predictions	122
Figure 7.1	Compliant A-Arm FEA comparisons configuration	129
Figure 7.2	Compliant A-Arm design example configuration	129
Figure 7.3	Examples of compliant beams with varying cross-sections	131
Figure 7.4	Cross-Section orientation	132
Figure 7.5	Compliant double A-Arm suspension in parallel with extra coil spring	133
Figure A.1	Compliant A-Arm configuration	139
Figure A.2	Free-body diagram of compliant A-Arm mechanism	140
Figure A.3	Deflections due to applied loads and redundant loads	145

The purpose of this research is to investigate how the characteristics and design constraints of compliant mechanisms affect their use in suspension systems. This objective also includes the development of new compliant suspension mechanisms.

The primary function of a suspension system is to minimize acceleration inputs to a vehicle. Acceleration inputs may come from a variety of sources. The most prevalent source comes from irregularity of the surface over which the vehicle is travelling. Vertical compliance between the wheel and the vehicle body allows the wheel to traverse these irregularities while a spring or energy storage element temporarily stores and releases energy and thus insulates the vehicle body from acceleration peaks. The system also includes a damping element to ensure that oscillations induced in the system die quickly.

Suspension systems originally came to use in horse-drawn carriages. The word suspension originated from the original attempts of suspending the carriage body by leather straps from a framework connected to the wheels. These first attempts were

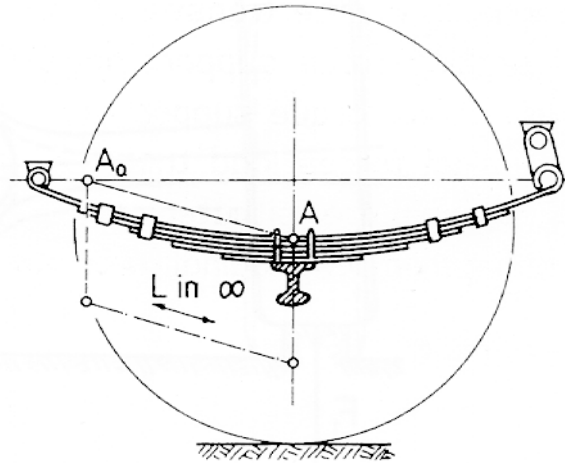


Figure 1.1 Traditional leaf spring suspension configuration [1]

replaced by systems using leaf springs very similar to that shown in Figure 1.1. The leaf spring became the first system used on the automobile. It is a very attractive design solution that is still popular today, especially in truck applications. It is simple and inexpensive because it combines the spring function with the wheel location function of the suspension. Eventually the automobile industry moved towards the use of kinematic suspension mechanisms to control wheel motion with an added spring element for energy storage. In essence, the two functions of wheel location and energy storage were separated.

A typical automobile suspension is shown in Figure 1.2 with a representative planar 4-bar mechanism. A kinematic 4-bar linkage controls the wheel motion while the coil spring provides energy storage. The use of kinematic linkages has significantly complicated the suspension system in comparison to the simplistic leaf spring design. This was

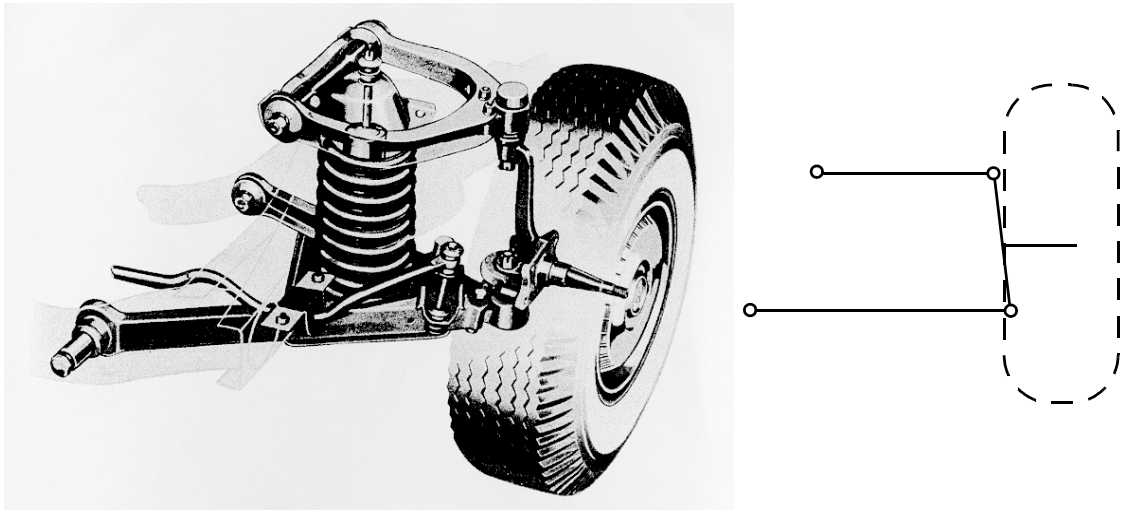


Figure 1.2 Kinematic 4-bar linkage suspension system [2]

done, however, for increased performance. The automobile introduced speeds and vehicle dynamics that necessitated the use of kinematic mechanisms to achieve exact and reproducible wheel motion that could not be produced by the simplistic leaf spring suspension [1]. The leaf spring also has the disadvantage of increased weight and space requirements.

Leaf springs are examples of compliant mechanisms. A compliant mechanism is a mechanism that gains at least a portion of its motion from the deflection of flexible members. The leaf spring mechanism shown in Figure 1.1 gains its motion from the motion of the flexible leaves. If the leaves are viewed as a rigid link, then the leaf spring becomes a structure with zero degrees of freedom. However, the leaves are flexible and the leaf spring behaves as a mechanism allowing vertical motion even though the leaves have no kinematic joints.

Compliant mechanisms have the advantage of reducing the number of joints and parts making them less expensive to make. They may also have superior performance

characteristics and be more durable. Compliant mechanisms also have the ability to store energy in the flexible members as in the leaf spring suspension example.

The recent research in the field of compliant mechanisms has led to the increased understanding of mechanisms that utilize flexible members. This includes modeling and synthesis techniques that greatly increase the speed and accuracy of the design process. This new knowledge serves as a proper basis to be able to understand and design new suspension mechanisms that integrate flexible members for motion and energy storage, just as the original leaf spring did, while still maintaining performance standards of kinematic mechanisms.

1.1 Thesis Objective

The objective of this research is to investigate how the characteristics and design constraints of compliant mechanisms affect their use in suspension systems. This research objective is three-fold:

1. Outline the important design constraints and functional requirements of implementing compliant mechanisms in suspension systems.
2. Identify suspension applications or mechanisms where compliant mechanism technology is suited best to perform.
3. Identify possible solutions within the design constraints that meet the functional requirements.

1.2 Research Justification

The justification for this research lies in the potential benefits of using compliant mechanisms in suspensions systems and in the general understanding of the design of a compliant suspension system.

1.2.1 Benefits of Compliant Mechanisms in Suspensions Systems

The use of compliant mechanisms has many advantages. The possible advantages of their use in suspension systems include:

- reduced number of joints
- reduced number of parts
- reduced wear
- energy storage in flexible members
- reduced manufacturing and assembly costs
- reduced weight
- reduced maintenance

There are also many potential design constraints associated with the use of compliant mechanism in suspensions. This thesis will help identify these constraints.

1.2.2 Contributions

The main contribution of this thesis is an understanding of the design characteristics and constraints of the use of compliant mechanisms in suspension systems. Suspension applications that are suited for compliant mechanisms are identified and possible design solutions are presented. The compliant A-Arm concept is presented and models are developed for design use. This work enables future designers to more successfully use compliant mechanisms and this new concept in suspension systems.

1.3 Thesis Outline

This section outlines the material presented in each chapter of the thesis and provides a general overview of the work.

In Chapter 2, general background information is presented about suspension systems and compliant mechanisms. An introduction to suspension systems and the important parameters or design factors that affect them is presented. The purpose of this section is to give the reader enough information to understand the workings of a suspension system but will not explain suspension systems in detail. Compliant mechanisms and some of the important concepts that will be important to this work will be introduced. This chapter will also overview some of the work that has been completed in the application of flexible members in suspension systems.

Chapter 3 presents the findings of the first objective of this thesis: Outline the important design constraints and functional requirements of implementing compliant mechanisms in suspension systems. Detailed explanations of these constraints and functional requirements are presented. Chapter 3 also presents the findings of the second objective of this thesis: Identify suspension applications or mechanisms where compliant mechanism technology is suited best to perform.

Chapter 4 presents some of the concepts explored as part of the third objective of this thesis: Identify possible solutions to the design constraints and functional requirements. These concepts are presented in detail.

Chapter 5 presents results from evaluation of the concepts presented in Chapter 4.

Chapter 6 presents further research on the compliant A-Arm concept. A pseudo-rigid-body model is presented and results from finite element models and physical prototypes of this concept are presented. A design example is also presented to demonstrate the use of such a concept in a suspension system.

Chapter 7 presents conclusions of this research and recommendations for future work in this area.

BACKGROUND & LITERATURE REVIEW

The purpose of this chapter is to provide background information about suspension systems and compliant mechanisms, and to review where flexible members have been integrated into suspension mechanisms. The background information is intended to give the reader enough information to understand the workings of a suspension system and characteristics of different systems. Background information of compliant mechanism topics relevant to this work is also included.

2.1 Suspension Systems

This section introduces suspension systems and the factors that influence their performance. Applications of suspension systems and examples of different systems and their characteristics are discussed.

2.1.1 Applications

The most prevalent and well known suspension application is the automobile, but there are many other land vehicles that require a suspension system. The requirements of

the suspension system depend on the vehicle application. For example, the requirements of a bicycle suspension will be much different than those of an automobile. Also, the requirements of a race car suspension will be much different than those of a normal passenger automobile. Chapter 3 describes these different requirements and identifies which applications match up well with the strengths and weaknesses of compliant mechanisms.

Possible applications are:

- Automobile (all highway type vehicles)
- All-Terrain-Vehicles
- Bicycles
- Motorcycles
- Snowmobiles
- "Light" utility vehicles
- Remote control cars
- Others

2.1.2 Functions of a Suspension System

This section outlines the necessary functions of a suspension system. The information presented in this section is most applicable to automobile suspension systems, but it may be extended to other vehicle applications. Gillespie [2] outlined the primary functions of a suspension system as:

- Provide vertical compliance so the wheels can follow the uneven road, isolating the chassis from roughness in the road.
- Maintain the wheels in the proper steer and camber attitudes to the road surface.
- React to the control forces produced by the tires—longitudinal (acceleration and braking) forces, lateral (cornering) forces, and braking and driving torques.
- Resist roll of the chassis.
- Keep the tires in contact with the road with minimal load variations.

2.1.3 Design Considerations

The functions listed above are directly connected to important design considerations and suspension properties that a designer must understand in order to successfully design a suspension system. The basic factors that affect suspension performance are discussed here.

2.1.3.1 Suspension System Dynamics

A suspension must allow some degree of vertical compliance between the wheel and the vehicle chassis. A spring element is inserted to insulate the vehicle chassis from acceleration peaks induced by the irregular road surface and a damping element is inserted to insure that oscillations induced in the system die quickly.

A typical 4-bar A-Arm or wishbone automotive suspension system is shown in Figure 2.1. The four-bar mechanism controls the kinematics or the motion of the system while the inserted spring and damper control the kinetics and dynamics of the system. A

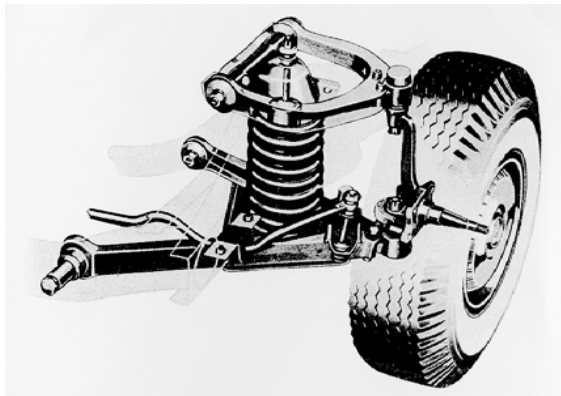


Figure 2.1 Kinematic 4-bar linkage suspension system [2]

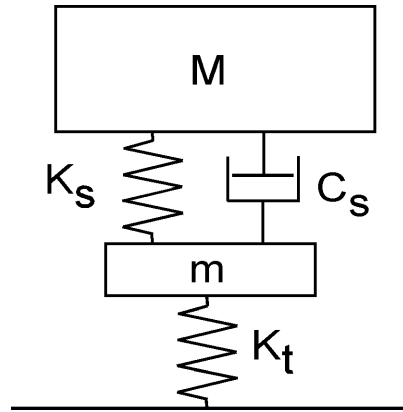


Figure 2.2 Quarter-car model two-mass system

suspension system is most simply modeled as a two mass system shown in Figure 2.2. This is typically referred to as a quarter-car model since it represents one wheel or one quarter of the vehicle. The unsprung mass, m , represents the masses of the wheel, wheel carrier and a portion of the suspension linkages. The sprung mass, M , represents the mass of the vehicle body. K_s and K_t represent the stiffness of the spring and tire and C_s the suspension damper. The damping properties of the tire are usually omitted from the model because their effect is negligible. The ride of the vehicle is of concern when examining suspension dynamics. The ride of a vehicle can be tied directly to the vehicle's natural frequency. It has been found that comfortable frequencies for humans fall in the range of 0.7 Hz to 2.0 Hz [1]. The natural frequency may be calculated by first determining the ride rate, RR :

$$RR = \frac{K_s K_t}{K_s + K_t} \quad (2.1)$$

RR is the effective spring rate of the two springs in series. Neglecting damping, the natural frequency, ω_o , may then be calculated by

$$\omega_o = \sqrt{\frac{RR}{M}} \quad (2.2)$$

or

$$f_n = \frac{1}{2\pi} \sqrt{\frac{RR}{M}} \quad (2.3)$$

If the stiffness of the tire is neglected, RR may be replaced with K_s in equations (2.2) and (2.3). It is also common to calculate the natural frequency from the static deflection of the system. If the tire spring rate K_t is large in comparison to the suspension spring rate K_s , then the static deflection, s_o , may be approximated by

$$s_o = \frac{Mg}{K_s} \quad (2.4)$$

The natural frequency or bounce frequency of the sprung mass, f_n , then becomes

$$f_n = \frac{1}{2\pi} \sqrt{\frac{g}{s_o}} \quad (2.5)$$

A ten inch static deflection corresponds to a natural frequency of 1 Hz, five inches is 1.4 Hz and 1 inch is 3.13 Hz. A comfortable ride of 1.5 to 1 Hz corresponds to a static deflection of 4 to 10 inches. A lower natural frequency and hence a higher static deflection is considered to be more comfortable and is often called a "soft" suspension. A soft suspension results in lower acceleration peaks transmitted to the vehicle from road irregularities. However, a softer suspension requires more travel or stroke to absorb the bumps in the

road. For example, Gillespie [2] reports that for a typical passenger car, 5 inches of stroke must be available in order to absorb a bump acceleration of one-half "g" without hitting the suspension stops.

The unsprung weight should also be kept to a minimum as it is easier to control a small moving mass than a larger one. This will result in lower force values transmitted to the vehicle body. A small unsprung mass will also be able follow the contours of the road better with a more uniform vertical force [3]. This translates into better handling properties. However, as the unsprung mass is reduced, the natural frequency, f_{hop} , of the unsprung mass increases. This is commonly labeled as the "hop" frequency to describe the hopping motion of the wheel:

$$f_{hop} = \frac{1}{2\pi} \sqrt{\frac{K_t + K_s}{m}} \quad (2.6)$$

A higher hop frequency increases the harshness of the ride. The typical ratio of sprung mass to unsprung mass is approximately 10 for passenger automobiles with a hop frequency around 10 Hz [4].

Although damping has not been mentioned previously, it plays a critical role in the dynamics of the suspension system. Damping normally comes from two sources: an installed hydraulic viscous damper and friction. Friction should be kept to a minimum as it increases the transmissibility of the forces and hence accelerations to the sprung vehicle mass.

A typical damping coefficient for a passenger vehicle falls between 0.2 and 0.4. There has always been a conflict between the "ride" characteristics and the "handling" characteristics of a vehicle. These characteristics are directly connected to the damping rate and the spring rate of the system or tuning of the suspension. Suspension performance tuning is not discussed in this thesis.

Other factors influence the ride of the vehicle. The pitch and roll frequency of the complete vehicle are usually on the same order of magnitude as the bounce frequency. These issues deal with a complete vehicle model and not the quarter car model discussed here. Vibrations and road noise that are transmitted to the chassis from the forces exerted at the wheel also reduce the comfort level of the passenger.

2.1.3.2 Motion Characteristics

A suspension mechanism is ideally a one degree of freedom mechanism that guides the wheel in a vertical direction. A result of using a kinematic linkage is translations and rotations of the wheel in other directions. These motions are normally unwanted because they adversely affect the performance of the suspension mechanism and the handling of the vehicle.

Scrub describes a translation of the wheel in the lateral direction, while the camber angle describes a rotation of the wheel about the longitudinal axis, as illustrated in Figure 2.3. Scrub and camber change cause scuffing of the tire and premature wear. A change in

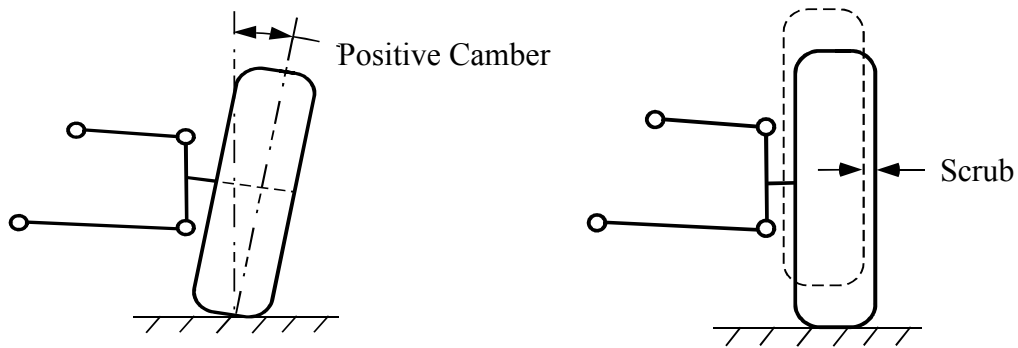


Figure 2.3 Camber and scrub

camber angle also changes how the tire interacts with the road because of the change in orientation of the tire and thus affects the handling of the vehicle.

Toe angle is the parameter that describes the steering angle of the wheel. This is illustrated in Figure 2.4 in a top view of the vehicle. Toe affects the directional control and stability of the vehicle or the understeer or oversteer tendency of the vehicle. These effects will be discussed in more detail in the following sections. An understeer vehicle's

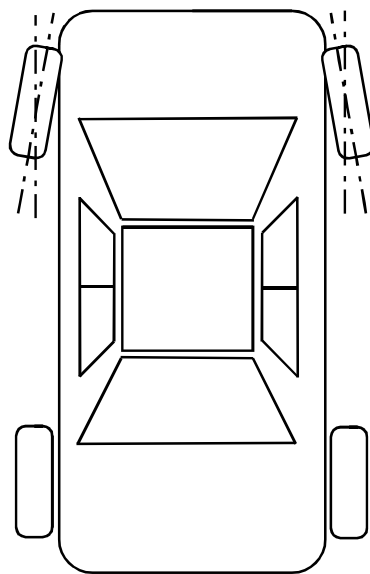


Figure 2.4 Toe angle

front tires slip before its rear tires in a cornering maneuver. This causes the vehicle to push towards the outside of the turn. The opposite is true of an oversteer vehicle and the vehicle slips on the rear tires first and tends to "spin out." Some degree of understeer is designed into normal vehicles because it is considered safer for the average driver.

2.1.3.3 Control Forces

Control forces refer to the forces developed at the tire that control the motion of the vehicle. Changes in velocity, either speed or direction, can be instigated by a force created between the tire and the ground. For example, to accelerate a vehicle in the forward motion, a force exerted by the tires to the ground in the opposite direction is generated. The most influential forces are illustrated in Figure 2.5.

These control forces are also directly tied to some overall dynamic properties of a vehicle. When a vehicle is accelerating, braking, or in a cornering maneuver, there is an associated load transfer from one wheel to another. An accelerating vehicle has a load

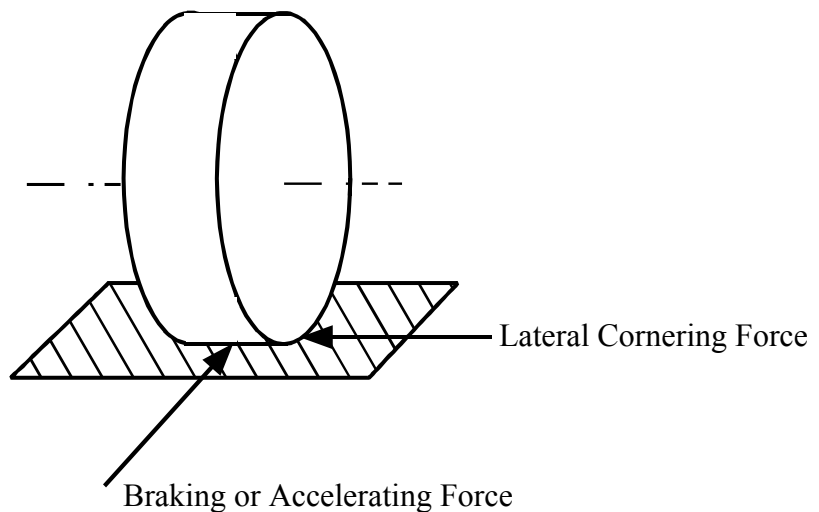


Figure 2.5 Control forces

transfer to the rear wheels. This load is transferred principally through the suspension, causing compression in the rear suspension. Load transferred to the rear must come from the front and causes a rebound in the front suspension. This combination pitches the vehicle rearwards and is often called "power squat." The reverse phenomenon occurs during braking and is termed "brake dive." Vehicle "roll" occurs during cornering maneuvers. The arrangement of the links of a suspension mechanism can be designed to reduce the affects of squat, dive, and roll. These arrangements are appropriately termed "anti-squat" and "anti-dive" geometries for the reduction of squat and dive. The location of the roll center of a suspension influences the roll property of the vehicle. The reader is referred to Gillespie [2] for more information on this topic.

The control forces at the wheel also may cause a change in position and orientation of the wheel not predicted by kinematic analysis of the mechanism, affecting the performance and handling of the suspension and the vehicle. These motions are a result of clearances in the mechanism joints or flexibility of the suspension links.

2.1.3.4 Elasto-kinematics

Elasto-kinematics deals with the use of bushings in the suspension joints. Bushings are normally made of rubber, but also can be polyurethanes, nylon, or even steel on steel. Soft bushings such as rubber allow considerable movement within the joint. This is undesirable because it allows the wheel to move in unwanted directions and affects the handling of the vehicle. However, soft bushings create a more favorable ride by better isolating the chassis from road noise, shocks, and vibrations. Hence, there is some conflict between ride and handling in the use of suspension bushings. Normal passenger vehi-

cles use softer bushings while high performance vehicles use hard bushings. Matschinsky [1] defines the term elasto-kinematics as:

"...conscious harmonization of the spring rates of the suspension joints (and possible elastic rates of any chassis elements) and of the spatial arrangement of the suspension links, with the aim of compensating the elastic displacements that occur under external loads, or even of converting them into wanted displacements."

A designer may use soft bushings for ride comfort that do not compromise handling characteristics with the correct combination of bushing elastic rates and suspension link arrangement. For example, it is advantageous for the wheel to have relative fore and aft motion to absorb some of the harshness from bumps in the road. This normally would cause undesirable toe angle changes and affect handling. The suspension links and bushings can be arranged and designed in such a way to allow this relative fore and aft motion while eliminating or designing a specific amount of toe change.

2.1.4 Classifications and Examples

Suspension systems for automobiles are normally divided into two categories:

- Solid Axle
- Independent

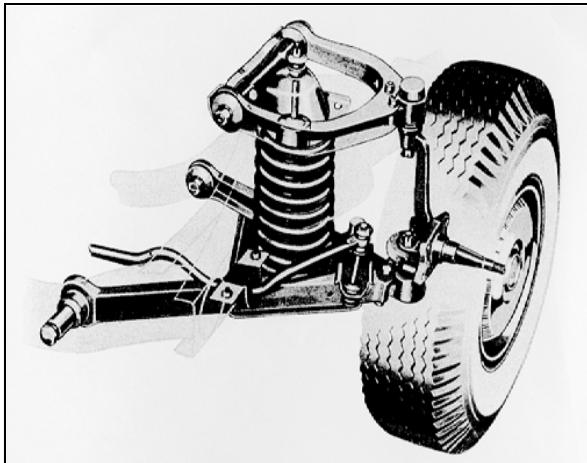
A solid axle suspension is one where the wheels on either side of the vehicle are connected by a rigid axle. Often this rigid beam is a drive axle itself. Independent suspensions use independent mechanisms on either side of the vehicle to control the wheel, allowing each

wheel to move independently of the other. The relative advantages and disadvantages are listed below:

	Solid Axle		Independent
Advantages		Advantages	
	<ul style="list-style-type: none"> • Inexpensive • No camber change in roll. 		<ul style="list-style-type: none"> • Independent action • Flexibility in design of geometry and hence motion characteristics
Disadvantages		Disadvantages	
	<ul style="list-style-type: none"> • Large unsprung weight • Wheel tramping and shimmy on steerable axles due to coupling of masses. • Space requirements • Coupling of wheels 		<ul style="list-style-type: none"> • Larger suspension deflections • Greater roll stiffness • Resistance to steering wobble and shimmy
			<ul style="list-style-type: none"> • Complex designs (part count)

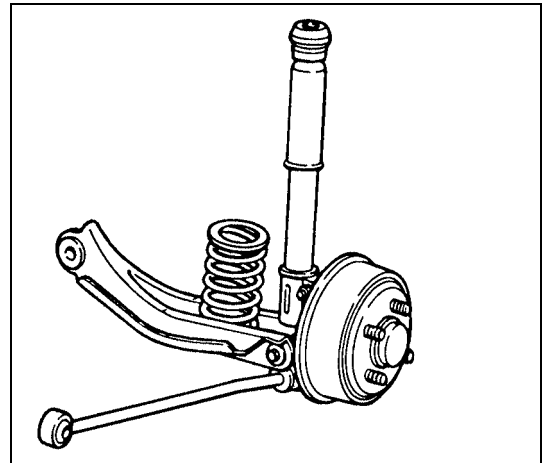
Suspensions mechanisms also can use different types of springs in the mechanism. The most common are the coil spring, torsion bar, pneumatic, and leaf spring. The choice of spring normally has little effect on suspension performance. The leaf spring used as the wheel location mechanism is an exception and will be discussed further in section 2.3.

Figures 2.6 and 2.7 show some common examples of both independent and solid-axle suspension types along with their relative characteristics.



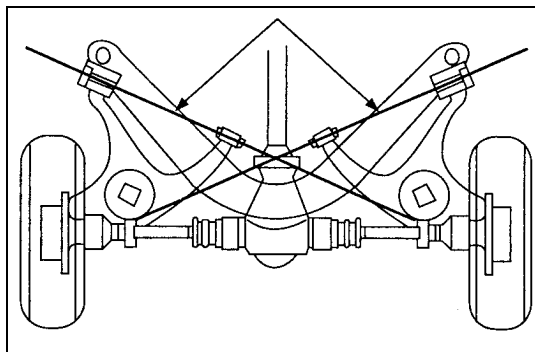
Double A-Arm or Wishbone

- Large range of kinematic possibilities to obtain desired performance
- Complexity and high cost potential for good designs.



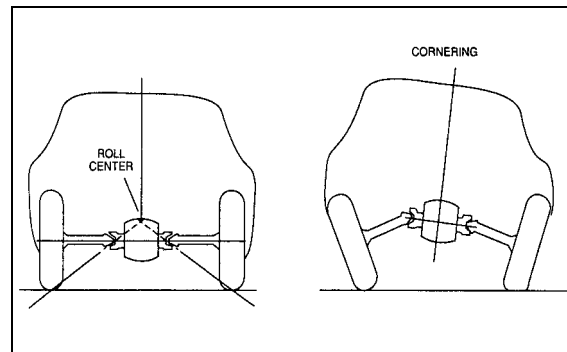
McPherson Strut

- Reduced space requirements
- Few parts and simplified assembly
- Less favorable kinematics
- High installed height (hood line)
- Friction in piston-rod and guide



Semi-trailing Arm (top view)

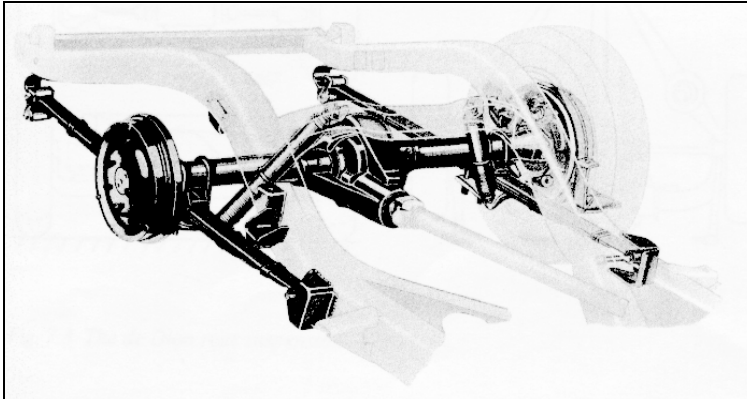
- Simple design
- Reduced space requirements
- Less favorable kinematics (camber and toe change)



Swing-axle

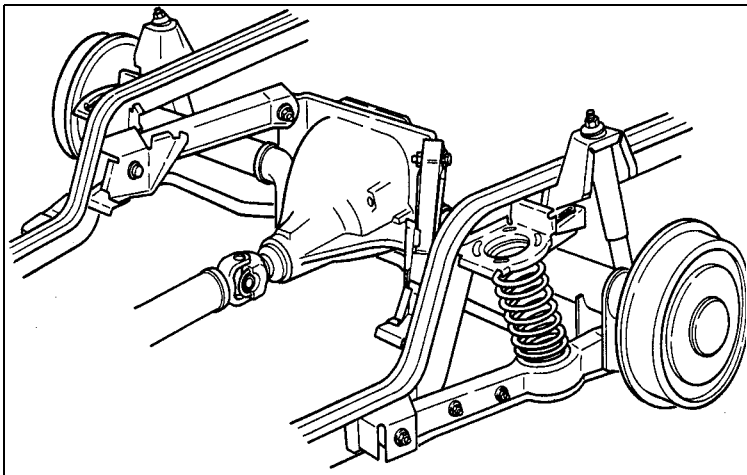
- Simple design
- Large camber change
- Vehicle jacking in cornering increases rollover possibility.

Figure 2.6 Common automobile independent suspensions [2]



Hotchkiss rear suspension

- Simple design
- Inexpensive
- Friction in multi-leaf designs
- Soft spring rate amplifies compliance in wind-up direction
- Longer leaves result in loss of side stability.



Four-link

- More control of suspension properties (roll center, anti-dive/squat, roll steer)
- Better ride properties
- More expensive

Figure 2.7 Common solid-axle automotive suspensions [2]

2.1.5 Current Suspension Research

Much of the current research in suspension systems may be found in SAE technical papers, particularly publications of yearly conferences in vehicle dynamics [5] and suspension and steering systems [6]. Other resources include *The Journal of Automobile Engineering* and *The International Journal of Vehicle Design*. Current and recent research in suspension systems include a wide array of subjects:

- Active suspension control [7-12]
- Materials and manufacturing techniques [13-16]

- New design, analysis, modeling and testing techniques for suspension improvements and optimization [17-21]
- Suspension component improvements [22-24]
- New suspension systems or mechanisms [25-27]

The papers referenced here are a sampling of recent research in the field of suspension systems. Active suspension control is a field of great interest with advances in vehicle ride and handling characteristics being the result. Other research is focused on how to improve current systems and their design and analysis for improved suspension performance. However, little work is being done or published in the field of new suspension systems or mechanisms. The approach taken in this research is to not improve current suspension mechanisms but to explore how compliant mechanisms could be used as new suspension mechanisms.

2.2 Compliant Mechanisms

A compliant mechanism is a mechanism that gains at least a portion of its motion from the deflection of flexible members. An example of a compliant mechanism used in suspensions is the familiar leaf spring.

There are several advantages associated with compliant mechanisms [28]:

- part count reduction
- simplified manufacturing processes
- increased precision
- increased reliability
- reduced wear
- reduced weight
- reduced maintenance

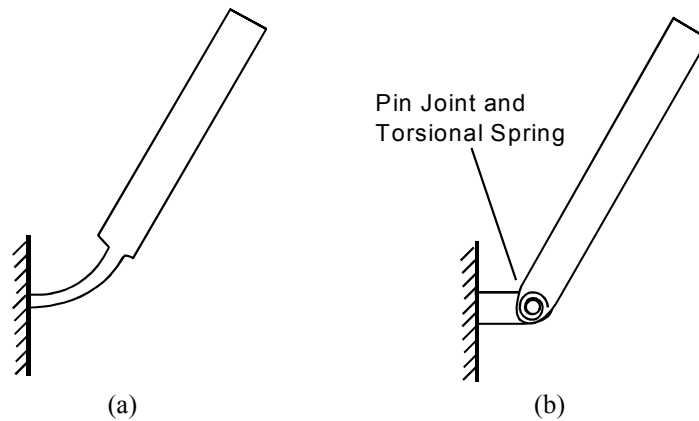


Figure 2.8 Example of how the pseudo-rigid-body model converts (a) a flexible segment into (b) a rigid-link mechanism

There are also several disadvantages associated with compliant mechanisms:

- difficulty of analysis and design
- potential for undesired energy storage in flexible segments
- design for fatigue more critical
- limited rotational ability of flexible links
- stress relaxation or creep

Compliant mechanisms used in suspensions take advantage of utilizing flexibility for motion and energy storage. This has the potential for reducing parts, cost, space and weight when compared to traditional mechanisms.

2.2.1 Pseudo-Rigid-Body-Model

The small-length flexural pivot pseudo-rigid-body model illustrated in Figure 2.8 has been developed to assist in the design and analysis of compliant mechanisms [28]. It is a method for the approximation of large deflections in compliant mechanisms. The method models flexible links as rigid links with accompanying torsional springs. The pin joints placed at proper locations make it possible to analyze the motion of the mechanism

using existing kinematic theory. The torsional springs are used to accurately estimate the force-deflection relationships.

2.2.2 Compliant Mechanism Synthesis

Rigid-body replacement synthesis uses the pseudo-rigid-body model to replace a rigid-body model. Since rigid-body kinematic equations are utilized for both models, they have equivalent motions. A compliant mechanism may then be created from the pseudo-rigid-body model. This technique is useful in designing suitable compliant mechanisms that have the same motion characteristics of a rigid-body mechanism and allows the use of existing kinematic theory in the synthesis of a compliant mechanism to perform a given rigid-body mechanism task.

2.2.3 Type Synthesis

Type synthesis is concerned with predicting "which combination of linkage topology and type of joints may be best suited to solve a particular task," [29]. Raghavan [30] used number synthesis, a type synthesis technique, to systematically explore the possible linkages of an independent suspension. This was done through the use of graph theory and the application of matrices to represent the structure of a rigid-body mechanism. Information regarding compliant segment types and the connectivity between segments may be added to the rigid-body matrix to represent the structure of a compliant mechanism [28]. This representation may also be used to systematically explore different compliant mechanism structures to perform a given task.

2.2.4 Vibration Analysis

Lyon et al. [31] investigated the first modal frequency of compliant mechanisms. It was found that the frequency predicted by the pseudo-rigid-body model agrees with experimental results.

2.3 Use of Compliant Mechanisms in Suspensions

This section will discuss examples of flexible members used in suspensions. Leaf springs are the most common example and some important design methods are discussed. Other examples are also presented.

2.3.1 Leaf Spring

Leaf springs were the suspension of choice in the early days of the automobile. They have the advantage of using the same mechanism to control the wheel and provide the necessary spring force. They are simple, inexpensive, and easy to manufacture. However, they have significant limitations in controlling wheel motion which affects the handling properties of the vehicle. The use of multiple leaves also causes interleaf friction which is detrimental to the dynamics of the system.

Because of the design of the typical leaf spring suspension, control forces at the wheel can have large effects on the movement of the wheel. For example, brake wind-up is a common condition where a braking force creates a moment at the point where the wheel attaches to the leaf spring causing the wheel to rotate. This same phenomenon may also occur under driving torques. This condition is magnified when the spring rate is soft-

ened. Leaf springs are also lengthened to achieve lower spring rates which compromises the side stability of the springs and wheel. These limitations in wheel control inspired the use of kinematic linkage mechanisms to better control the forces at the wheel and achieve exact reproducible motion.

The history of leaf spring use has yielded important knowledge in the design of a compliant mechanism used in a suspension as well as some design methods that are similar to those developed specifically for compliant mechanisms.

Compliant mechanisms have normally been designed to provide a desired motion function. Leaf springs also serve a motion function, however, their primary function is that of a spring. The spring serves to store energy and there is a limit on the amount of energy that may be stored before failure occurs. Bastow [32] reports that for a single leaf spring made of steel at a maximum stress of 100 ksi, 17 ft-lbf/lb of energy may be stored. In contrast, a helical spring of round bar section stores 66 ft-lbf/lb at the same stress level. The leaf spring is much heavier in mass than other types of springs for a specified amount of energy storage. This is a result of a smaller percentage of material being stressed to the maximum level in the single leaf than in the helical spring. The more material that is stressed to its maximum, the more energy is capable of being stored. A dimensionless variable called "specific volume efficiency", or η , compares this energy storage capability to that of a rod under tension where 100% of the material is stressed to the maximum and $\eta = 1$ [33]. A single leaf or cantilever beam has $\eta = 1/9$ while a helical spring or a torsion bar has $\eta \cong 1/3$. The efficiency of a leaf spring may be increased by properly stepped leaves creating a multi-leaf design. These stacked leaves enable the use of steel to provide

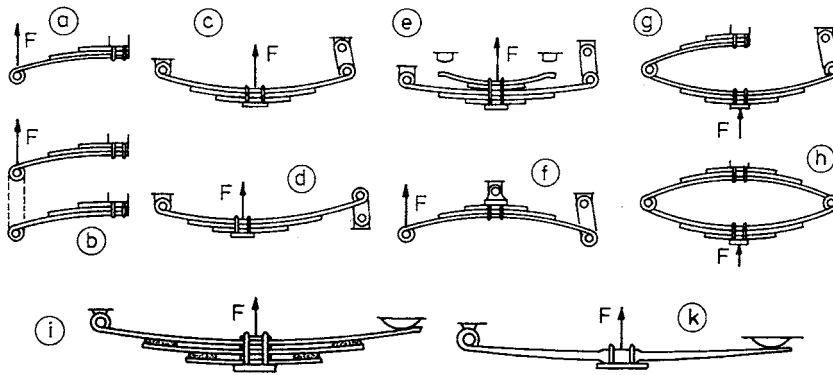


Figure 2.9 Leaf spring configurations [1]

the necessary spring constant and deflection in a constrained space within failure limits. Several different configurations of multi-leaf designs are shown in Figure 2.9. In the use of a single leaf, the shape may be optimized for a theoretical $\eta = 1/3$ [33]. These shapes are impractical, however, because of the lack of support material at the point of load application. Modified shapes must be used with support material at the load application points.

To calculate the motion of a leaf spring, designers have long been using the idea of a pseudo joint which is also used in the pseudo-rigid-body model in the design of compliant mechanisms. Figure 2.10 displays Matschinsky's effective kinematic lever radius of a leaf spring [1]. Several other works also refer to this concept [32][33]. The percentage of

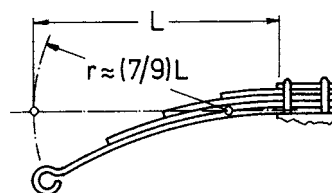


Figure 2.10 Kinematic lever radius of a leaf spring (Matschinsky, 2000)

length used for this kinematic link obviously depends on the leaf spring shape design. *The Manual on Design and Application of Leaf Springs* [33] reports for a cantilever beam this radius is approximately $0.83L$ which is very close to what Howell [28] reported as $0.85L$. Howell [28] reports that this value varies between 0.82 and 0.88 depending on the angle of applied loading, and hence the value of 0.83 reported by SAE [33] falls well within this range. SAE [33] also reports that this value ranges between 0.67 and 0.83 depending on the shape and stacking arrangement of multiple leaves.

2.3.2 Examples

Leaf springs are usually installed longitudinally or from the front to the rear of a vehicle as illustrated in Figure 2.7. They have also been implemented transversely from left to right. Figure 2.11 shows a transverse stacked leaf spring used on a Mercedes-Benz in the 1930's. The leaf springs serve both as the mechanism and the spring in this application. This concept has the drawbacks of increased weight and interleaf friction because of the multiple stacked leaves. More recent research has investigated using transverse leaves as both suspension links and springs with the use of composite materials [34][35][36]. A concept for the Ford Escort developed in 1986 is illustrated in Figure 2.12. The use of a single composite leaf has significantly reduced weight and eliminated interleaf friction. Lighter vehicles such as golf carts have been able to use a single transverse leaf made from steel that also serves both functions. Recent Chevrolet Corvette models have also used a single transverse composite leaf [37]. However, the leaf spring serves as a spring only and not as a suspension link. The main advantage of the Corvette design is the reduction in space requirements.

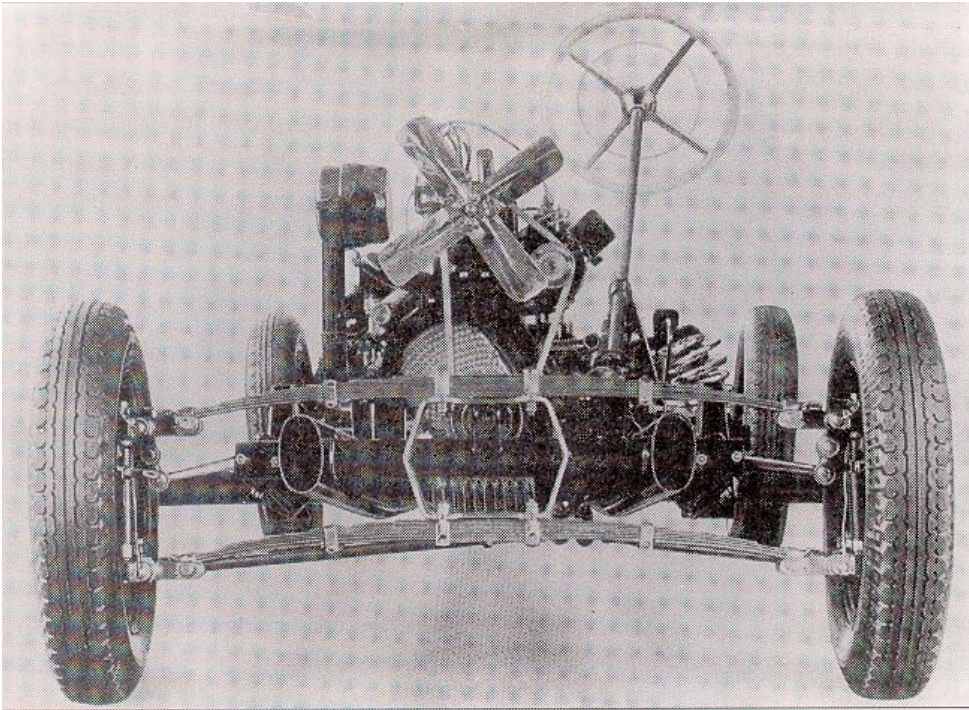


Figure 2.11 Mercedes-Benz '170V' front suspension with transverse leaf springs (1935) [1]

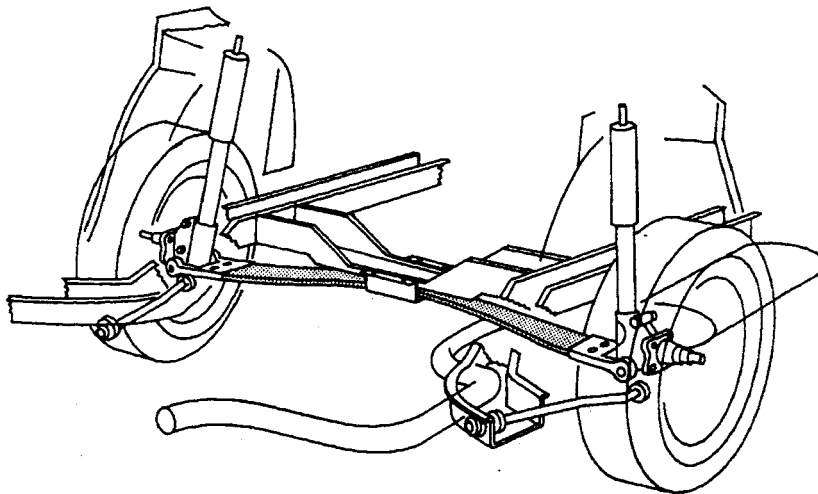


Figure 2.12 Ford Escort rear suspension with a single transverse composite leaf [34]

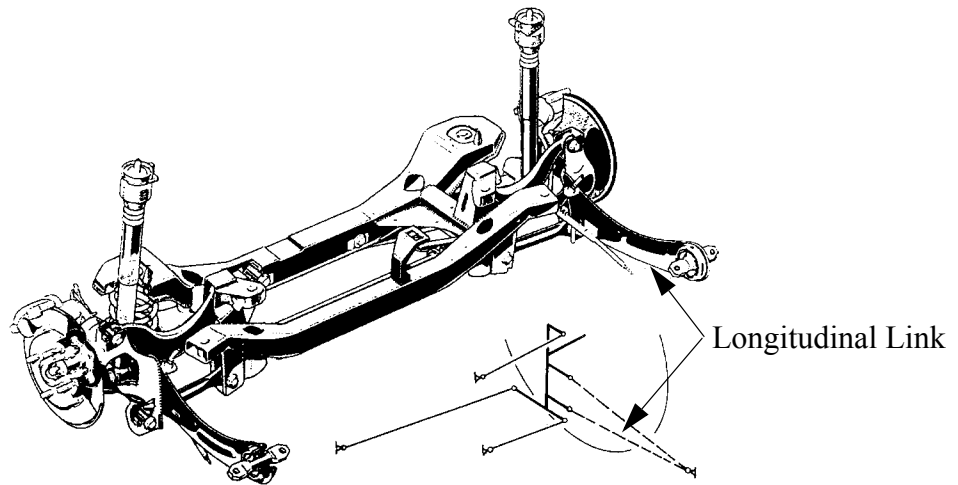


Figure 2.13 Ford Focus rear suspension (1998) [1]

2.3.3 Other Examples

Flexible members have been used elsewhere in suspension design. The Ford Focus uses a multi-link design for the rear suspension shown in Figure 2.13. Because the longitudinal link is fixed rigid to the wheel, it requires some lateral compliance or flexibility for the mechanism to achieve its motion.

An example outside the automotive world is a rear suspension design used on a Canondale mountain bike shown in Figure 2.14. The bottom member flexes to achieve the required motion. This also appears to be used primarily to replicate a joint and not for energy storage. Other bicycle companies have also developed suspensions that use flexible members to simulate a joint.

Soft Ride mounts the bicycle seat on a flexible cantilevered arm to give the seat a limited amount of travel and smooth out the bumps for the rider (Figure 2.15). This con-



Figure 2.14 Canondale Scalpel rear suspension (http://www.cannondale.com/bikes/innovation/clinics/scalpel/scalpel_12.html)



Figure 2.15 Soft Ride seat suspension (<http://www.softride.com>)

cept combines the suspension linkage function with the spring function. The suspension linkage or flexible member is connected directly to the seat and not to the wheel.

UNDERSTANDING THE DESIGN OF A COMPLIANT SUSPENSION SYSTEM

The functional requirements of a suspension system are demanding and warrant a discussion of how compliant mechanism characteristics and design constraints affect the fulfillment of these requirements. Favorable vehicle applications are also discussed relative to these findings.

3.1 Compliant Mechanisms and Suspension Functional Requirements

Compliant mechanism characteristics may be evaluated against suspension functional requirements to identify those characteristics that affect suspension performance. Industry experience with the use of leaf springs in vehicle suspension systems is also an aid to understanding which compliant mechanism characteristics and design constraints are important in the design of a suspension system.

Suspension functional requirements were explained in Chapter 2 and are listed here for reference. Specifically, a vehicle suspension system will:

- Provide vertical compliance so the wheels can follow the uneven road, isolating the chassis from roughness in the road.
- Maintain the wheels in the proper steer and camber attitudes to the road surface.
- React to the control forces produced by the tires—longitudinal (acceleration and braking) forces, lateral (cornering) forces, and braking and driving torques.
- Resist roll of the chassis.
- Keep the tires in contact with the road with minimal load variations.

Specific functional specifications common to suspension system design were also identified and related to the above functional requirements.

Compliant mechanism characteristics were also introduced in Chapter 2 and are listed here for reference.

- reduced weight
- increased precision
- energy storage
- limited motion
- motion dependent on input forces
- reduced friction
- reduced wear at joints
- reduced need for lubrication

Some of these characteristics including the latter three are part of the motivation to implement compliant mechanisms in suspension systems. Other characteristics may affect suspension performance depending on the compliant concept and concept implementation. Compliant mechanisms also have inherent failure constraints because of the deflection of flexible members and cyclic loading of these members. Fatigue, stress relaxation and creep all become more critical in the design of a compliant mechanism than in the design of a rigid link mechanism.

For each suspension functional specification, the compliant mechanism characteristics and design constraints that may affect the particular specification were identified as listed in Table 3.1. This table was reviewed to identify the areas where the characteristics of compliant mechanisms may affect the performance of a suspension mechanism.

TABLE 3.1 Identification of Suspension Functional Specifications, Compliant Mechanism Characteristics and Important Design Constraints

Functional Requirements	Functional Specifications	Compliant Mechanism Characteristics	Design Constraints
Vertical Compliance	Vertical Travel	Energy Storage Limited Motion	Fatigue Stress Relaxation or Creep
Maintain Steer and Camber Attitudes	Lateral force compliance steer Lateral force compliance camber Aligning torque compliance steer Braking force compliance steer Driving force compliance steer	Increased Precision Energy Storage Motion dependent on Input Forces	Fatigue
	Roll steer Roll camber Bump steer Bump camber	Increased Precision Motion dependent on Input Forces	
React to Control Forces	Lateral force compliance steer Lateral force compliance camber Braking force compliance steer Driving force compliance steer	Increased Precision Energy Storage Motion dependent on Input Forces	Fatigue
	Anti-squat Anti-dive	Limited Motion Motion dependent on Input Forces	
Resist Chassis Roll	Track width CG location		
	Roll center height	Limited Motion Motion dependent on Input Forces	
	Roll Stiffness	Energy Storage	
Keep tires in road contact with minimal load variation	Unsprung mass/Sprung mass ratio	Reduced weight	
	Wheel rate Energy storage capacity Spring rate curve Vertical travel	Energy storage Limited motion	Fatigue Stress Relaxation or Creep

3.2 Important Functional Requirements and Design Constraints of a Compliant Suspension System

A compliant suspension takes advantage of the energy storage and motion characteristics to achieve the vertical compliance and road holding capability of the wheel. A compliant suspension may also take advantage of the possibility of reduced weight for suspension dynamics and increased precision for wheel control. Excessive compliance or energy storage in the direction of control forces will adversely affect the motion of the wheel and the performance of the suspension system. The compliant mechanism characteristics that relate to chassis roll and the specifications: roll steer, bump steer, roll camber, bump camber, anti-squat, and anti-dive may have some effect. These specifications are not discussed further because they are more dependent on mechanism concept and configuration than compliant mechanism characteristics.

Fatigue is a concern in both the vertical motion of the mechanism and in the reaction to control forces. This design constraint and the control of wheel movement and attitude in reaction to control forces are discussed in more detail. How compliant beam geometry and mechanism configuration affect these properties are also discussed.

3.2.1 Fatigue

In a compliant suspension design, high stresses which lead to fatigue failure are of particular concern because of the heavy loads, large deflections, energy storage requirements, and other constraints of the suspension. Automobile leaf springs have long used multiple leaves to achieve the required motion and load carrying capacity and remain

within fatigue failure limits. Bastow [32] also cites one of the major disadvantages of transverse leaf springs is the impossibility of getting adequate up and down movements without thin leaves, high stresses or both.

3.2.1.1 The Effect of Suspension Functional Requirements on Beam Stress

A compliant suspension uses flexible members to achieve the motion and energy storage required to maintain contact between the tires and the road and cushion irregularities in the road. To illustrate how motion and energy storage affect the stress in a compliant beam, a cantilever beam is examined. This is a simplified example of a compliant suspension where the wheel is attached to the free end of the beam and the beam is fixed to the vehicle.

The maximum bending stress, σ , at the fixed end is given by

$$\sigma = \frac{6FL}{bh^2} \quad (3.1)$$

where F is the force applied to the free end and L , b , and h are the dimensions of the compliant beam. The linear spring rate, k_w , measured at the wheel is given by

$$k_w = \frac{3EI}{L^3} \quad (3.2)$$

where E is the modulus of elasticity of the material and I is the moment of inertia given by $I = bh^3/12$. Finally the energy storage capacity of the beam, U , may be written as

$$U = \frac{1}{2} \left(\frac{F^2}{k_w} \right) \quad (3.3)$$

Equations (3.1), (3.2), and (3.3) may be manipulated to yield σ in terms of E , h , L , U , and k_w :

$$\sigma = \frac{3\sqrt{2}}{2} \left(\frac{Eh}{L^2} \right) \sqrt{\frac{U}{k_w}} \quad (3.4)$$

In suspension design, it is desirable to reduce the wheel rate, k_w , and soften the suspension. This creates a more favorable ride by lowering the natural frequency and reduces the load variation at the wheel for better handling. It is also desirable to increase the amount of energy storage capacity, U , of a suspension. This allows the suspension to absorb larger bumps at higher speeds without fully compressing the suspension. However, Equation (3.4) shows that decreasing k_w and increasing U has the adverse effect of increasing the bending stress in the beam.

3.2.1.2 The Effect of Compliant Beam Properties on Beam Stress

Equation (3.4) shows that the stress in the beam may be reduced by decreasing E and h and increasing L . These parameters are all related to the base of the beam, b , and the spring rate, k_w , by the equality constraint in Equation (3.2). By substituting $I = bh^3/12$ and rearranging yields the following:

$$b = \frac{4k_w L^3}{Eh^3} \quad (3.5)$$

The modulus, E , is determined by the choice of material. Equation (3.4) and [28] affirm that the best material choice for a compliant mechanism is one where the ratio of yield strength or fatigue strength to modulus of elasticity (S_y/E) is a maximum.

Increasing the length of the beam is an effective measure for reducing bending stress. Designers have increased leaf spring lengths which has allowed them to soften spring rates while maintaining suitable stress levels. However, the length of any compliant beam in a suspension is limited by the space constraints of the vehicle. For a given material and beam length, the only way to decrease stress is decreasing the thickness, h , of the beam. To maintain spring rate and energy storage requirements, the base, b , of the beam must be increased. This measure is limited by available space for wide beams. This is one of the reasons leaf springs are stacked—stacking effectively increases the base of the compliant leaves without taking a large amount of space.

3.2.1.3 Constraint of Weight on Stress Reduction

Weight also becomes a constricting factor as the beams become larger to fulfill spring rate and energy storage requirements. The weight of the vehicle should be kept to a minimum and the unsprung weight should be kept to a minimum. Rearranging Equations (3.1), (3.2), and (3.3) and substituting $V = bhL$ for the volume of the beam yields the energy storage per unit volume for a beam in bending:

$$\frac{U}{V} = \left(\frac{1}{9}\right)\left(\frac{1}{2}\right)\left(\frac{\sigma^2}{E}\right) \quad (3.6)$$

The value $1/9$ is termed the specific volume efficiency, η , and compares the energy storage capacity per unit volume to that of a rod in tension. Thus, a beam in bending, $\eta = 1/9$, will have 9 times the volume of a rod in tension and therefore weigh 9 times more. A bar in torsion or a helical spring by contrast has a specific volume efficiency, η , equal to $1/3$. A beam of constant cross-section in bending will weigh approximately three times that of

a helical spring made of the same material for a given amount of energy storage. *The Manual on Design and Application of Leaf Springs* gives examples of how to increase η for a beam in bending by varying the cross-section along the length or by stacking leaves appropriately [33]. Equation (3.6) also reveals that reducing the stress increases the volume or weight of the beam. This weight disadvantage of a leaf spring is offset by the advantage that the leaves also serve as the wheel locating mechanism thus saving the weight of extra suspension links. A compliant suspension of another configuration may also have this advantage.

This weight disadvantage may also be reduced by material selection. Substituting $V = m/\rho$ in Equation (3.6) and rearranging gives

$$\frac{U}{m} = \eta \left(\frac{1}{2} \right) \left(\frac{\sigma^2}{E\rho} \right) \quad (3.7)$$

Composite materials use such as E-glass have been explored in the use of leaf springs for its weight saving potential. A composite material such as E-glass has a much lower density, ρ , and modulus of elasticity, E , than an alloy steel. This results in a large weight savings for composite leaf springs over steel leaf springs. Cost, however, limits the widespread use of this material in production vehicles.

3.2.2 Creep

Creep occurs as a compliant member is subjected to a load for long periods of time, such as in the case of a compliant suspension that must constantly support the weight of the vehicle. It is known that leaf springs sometimes sag or lose their spring over time as

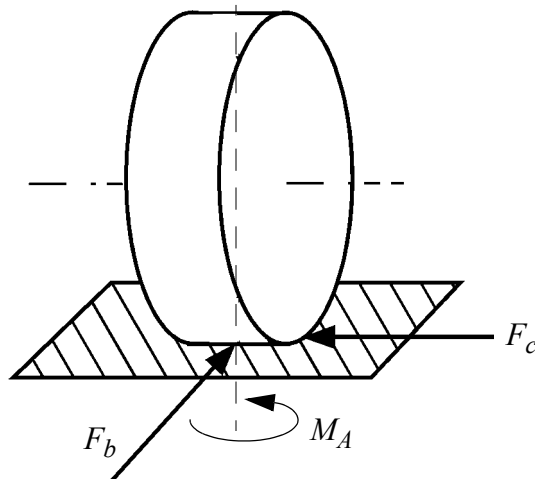


Figure 3.1 Wheel control forces

a result of creep. The design of a compliant suspension mechanism will have to ensure that the vehicle load will not cause significant creep in the compliant members.

3.2.3 Control Forces and Wheel Deflections

Vehicle handling characteristics are affected by the suspension system. The wheel rate and roll stiffness play an important role in vehicle handling. Two other important functions of a suspension system that affect vehicle handling are reacting to control forces and maintaining steer and camber attitudes of the wheel. The suspension mechanism directly controls the motion of the wheel both in translations and wheel attitude changes. Small wheel translations are often desired to isolate the chassis from vibrations, while angular wheel motions such as camber and toe affect handling and must be controlled properly by the suspension mechanism. A control force must exist between the wheel and ground to change the velocity of the vehicle. These forces are braking or accelerating, F_b , and cornering, F_c , forces as shown in Figure 3.1. These control forces also tend to cause

small wheel translations and attitude changes that are not in directions consistent with the natural motion of the suspension mechanism. Compliance of the suspension members and joints allow wheel movements in response to these control forces.

Table 3.1 identifies functional specifications that are measurements of steer and camber angles due to specific control forces. A lateral force or cornering force, F_c , may cause camber change and steer angle change of the wheel. Braking and driving forces, F_b , may also cause steer angle changes but do not usually result in a camber change in common suspension mechanisms. Aligning moment, M_A , describes the moment created about the vertical axis of the tire because of control forces that are offset from the vertical axis of the wheel or self-steering forces on the wheel.

Experience with compliant leaf springs illustrates some of the difficulties encountered from reacting to control forces and maintaining proper wheel attitude. In a suspension mechanism, wheel control forces can approach the magnitude of the vertical tire force in braking and cornering conditions. For example, cornering forces have been a problem with conventional leaf spring configurations shown in Figure 2.7. As the leaves have been made longer to soften spring rates, side stability has decreased.

A compliant suspension's resistance to control forces will depend on two main factors: compliant beam geometry and mechanism configuration. To illustrate the effect of compliant beam geometry, a cantilever beam is examined. Figure 3.2 shows a cantilever beam with appropriate loads applied assuming the beam is oriented laterally in the vehicle. Control forces at the wheel are resolved into forces and moments at the beam end. Com-

pliant beam geometry, length and cross-section will affect the beam's stiffness to the different loads (bending, axial, and torsion) that may be applied.

3.2.3.1 Braking Force

A braking force, F_b , will cause deflections in the x direction and a rotation about the z axis. For a suspension mechanism, small deflections in the x , longitudinal direction is desirable to alleviate bump harshness and isolate the vehicle from vibrations due to the dynamic rolling hardness of the tires. A Rotation about the z axis is a steer angle change which directly affects the steering and handling properties of the vehicle.

The stiffness of this beam in the direction of the braking force, F_b , is

$$k_b = \frac{3EI_z}{L^3} \quad (3.8)$$

where I_z is the moment of inertia about the z axis. The vertical stiffness or wheel rate, k_w , has the same form with the moment of inertia about the x axis. Since the width of a compliant beam is greater the thickness of the beam, the stiffness, k_b , will be much greater than

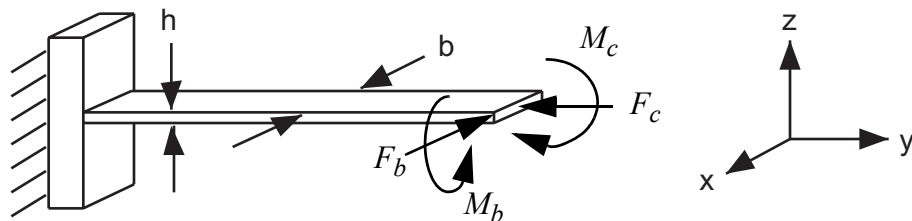


Figure 3.2 Cantilever beam with applied control forces

the wheel rate. The ratio of k_b to k_w is directly proportional to the ratio of I_z to I_x which is proportional the cross section of the beam by the following relationship:

$$\frac{k_b}{k_w} = \frac{I_z}{I_x} = \frac{(hb^3)/12}{(bh^3)/12} = \left(\frac{b}{h}\right)^2 \quad (3.9)$$

As the compliant beam becomes thinner and wider, its out-of-plane stiffness increases dramatically.

A beam width of 10 inches and a thickness of 0.24 inches, the stiffness ratio as described in Equation (3.9) is 1736. The wheel rate in this example is 75 lbs/in and the out of plane stiffness is 130,000 lbs/in. A maximum force of 750 lbs in the x direction will result in a deflection of 0.006 inches which is very stiff. More importantly this force creates a rotation about the vertical axis or steering angle. This angle, θ_z , is equal to

$$\theta_z = \frac{6F_b L^2}{Ehb^3} \quad (3.10)$$

In this example, the steering angle change is very small at 0.02 degrees. A steering angle on the order of one degree is significant for a vehicle suspension.

Bending stress results are also very favorable and the ratio of bending stress due to a braking force and bending stress due to a vertical force is

$$\frac{\sigma_b}{\sigma_w} = \frac{(Mb)/2I_z}{(Mh)/2I_x} = \left(\frac{h}{b}\right) \quad (3.11)$$

In this same example the stress due to a braking force is 2.4% of the stress due to the vertical force. The compliant beam naturally does very well in response to an out of plane

force, F_b . A very wide beam like this is also unrealistic because of space constraints and a stacked beam is more realistic. If the beam is divided into 5 pieces each 2 inches wide, the deflection will now equal 0.144 inches, a steering angle of 0.5 degrees, and a bending stress that is 12% of the stress due to the vertical force. Stacking increases the stress by a factor of the number of divisions and increases the deflections by this same factor squared. Overall, an out of plane force, F_b , does not cause significant deflection or stress results unless the beam is stacked to save space.

3.2.3.2 Braking Moment

The braking moment, M_b , results in the beam twisting about the y axis causing wheel wind up. Conventional leaf springs have this problem. This moment will cause the beam to twist with an angle, θ , of

$$\theta = \frac{M_b L}{JG} \quad (3.12)$$

where G is the shear modulus of elasticity and J is

$$J = \frac{bh^3}{3} \quad (3.13)$$

Since b is inversely proportional to h^3 by Equation (3.5), torsional stiffness, k_θ is only proportional to the constraints or L , k_w , and material constants, as

$$k_\theta = \frac{M_b}{\theta} = \frac{4}{3} k_w L^2 \frac{G}{E} \quad (3.14)$$

This assumes that end constraints do not prevent warping of the beam. Thus the cross section of the beam has no effect on the torsional stiffness of this beam. This relationship also reveals the result that lengthening the beam affects other beam geometry and allows a higher torsional stiffness. Shear stress in the beam due to a moment load is given by

$$\tau = \frac{3M_b E h}{4k_w L^3} \quad (3.15)$$

Thinner beams decrease the shear stress. Shear stress would not change with stacking.

3.2.3.3 Cornering Force and Moment

A cornering force, F_c , may cause deflections in the y direction or steering angle changes depending on the orientation of the compliant beam. In this example, these effects are negligible. The cornering moment, M_c , causes rotation about the x axis or wheel camber, θ , of

$$\theta = \frac{12M_c L}{E b h^3} \quad (3.16)$$

Typical maximum camber values are only a few degrees. A single cantilever beam, however, is a poor choice for controlling camber.

3.2.3.4 .Aligning Moment

An aligning moment, M_A , will cause a steer angle change of

$$\theta = \frac{12M_A L}{E h b^3} \quad (3.17)$$

Stacking will increase the rotation. Bending stress is also negligible.

3.2.3.5 The Effect of Compliant Mechanism Configuration on Wheel Deflections

A compliant suspension's resistance to control forces also relies heavily on the mechanism configuration. Mechanism configuration takes into account all other defining factors of the mechanism except compliant link cross-sectional properties. This includes:

- Number of links: compliant and rigid.
- Compliant link type or end conditions (pinned, fixed-fixed, etc.).
- Link configuration to achieve function, path, or motion of mechanism.
- Rigid and compliant link placement in mechanism.

The number of compliant links and their type will help define the cross-sectional properties. The link configuration will affect the amount of load carried in each link due to a control force on the mechanism.

To illustrate these principles, a pseudo-rigid four-bar compliant mechanism is examined as illustrated in Figure 3.3. Links 2 and 4 are compliant members and are fixed-guided links because both ends are fixed. If only links 2 and 4 are allowed to be compliant, there are also 15 different possible parallel-guiding mechanisms with different link end conditions (pinned or fixed). If only one link is compliant, the cross section of that link will be greater than that for two links that are compliant. This will be stiffer for out of

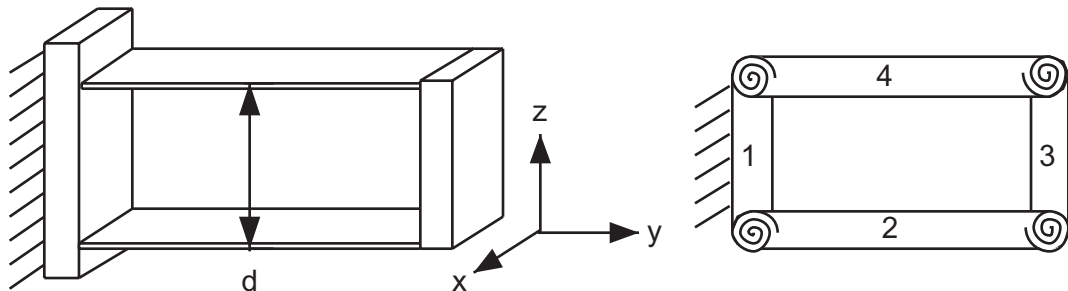


Figure 3.3 Four bar fixed guided compliant parallel mechanism and pseudo rigid body model

plane forces, braking force and moment and aligning moment, yet take up more space and may be a disadvantage because of the need of stacking. A fixed-fixed end condition for a compliant link will require a larger (b/h) ratio than one that is pinned to satisfy stress constraints. This will also be stiffer yet with the same disadvantage discussed above. The spacing, d , between parallel links will not change stiffness in the x direction but will increase rotational stiffness about the y axis. If links two and four are not parallel, there are many different possibilities of compliant link lengths and orientations that would change the stiffness of the mechanism in the out-of-plane direction. All of these factors are important in designing a mechanism that will be resistant to out of plane forces.

A compliant mechanism configuration such as a four-bar mechanism shown in Figure 3.3 is much stiffer in camber rotation due to a cornering force. The cornering force puts link 2 into compression and link 4 into tension and very small rotations result. Buckling would be a concern, however, if link 2 is a compliant segment.

The difficulty of wheel wind up for the conventional leaf spring design has also been mentioned. This is also an unwanted in-plane deflection. This results from the fact that the leaf spring's pseudo-rigid-body model is a five bar mechanism that has two degrees of freedom. A compliant suspension design must take this into account if the mechanism has two degrees of freedom in its pseudo rigid body model.

3.2.4 The Effect of Compliant Solutions on other Suspension Properties

Chapter 2 introduced some suspension properties related to suspension link geometry. These properties also affect the handling of the vehicle. Roll steer and camber, as

well as bump steer and camber, simply result from mechanism motion as one side of the suspension is compressed and the opposite side is extended as often happens in body roll or single wheel bump. Anti squat, anti dive, and anti roll are other kinematic properties that affect load transfer and handling. These properties must be taken into account as functional specifications that may limit the design possibilities of a compliant suspension configuration.

3.2.5 Other Considerations

There are many other factors that affect the performance and marketability of a suspension system. Among these are:

- cost and manufacturability
- space
- weight
- adjustability

Compliant mechanisms have the potential for saving on costs, but that may not be necessarily the case. Making a suspension adjustable with regards to spring rate is also a challenge.

Suspension mechanisms are often designed as spatial mechanisms to enable them to achieve their desired properties. A four-bar A-Arm suspension mechanism is a planar mechanism. The A-Arm design creates the stiffness necessary to react to control forces at the wheel. Spatial mechanisms use various links oriented in different directions to achieve the necessary stiffness and suspension properties. These mechanisms often require three degree-of-freedom joints and similar compliant mechanisms have not been developed yet.

Pseudo-rigid-body replacement synthesis of rigid-link suspension mechanisms for compliant concepts will be limited to those mechanisms with one degree-of-freedom rotational links.

As discussed in Chapter 2, current vehicle suspension mechanisms use elastic bushings for designed wheel control and for isolation of the chassis from high frequency vibration. Compliant mechanisms eliminate the need for joints and hence elastic bushings in a suspension mechanism. Other means such as a compliantly mounted subframe would need to be implemented to accomplish vibration isolation. Purposely designed wheel deflections will also be difficult to design as opposed to the design versatility of a multi-link suspension mechanism.

3.3 Design Conclusions

In summary, the use of compliant mechanisms in a suspension system presents significant design constraints and the need to fulfill important suspension functional requirements. These items are listed here in order of importance:

- Fatigue
- Reacting to control forces
- Maintaining proper wheel attitude
- Fulfilling other suspension geometry properties (anti-squat, dive, roll)
- Fulfilling space, weight, and cost restrictions

Fatigue failure is the most crucial factor. Energy storage requirements and space and weight constraints push stress levels to their limits. Control forces will add to the stress while potentially causing the wheel to move in unwanted directions compromising han-

dling capabilities. Other suspension geometry properties that affect load transfer and vehicle handling may also limit the design possibilities. Finally, other constraints such as space, weight, and cost will limit the implementation of a concept in actual practice.

3.4 Possible Vehicle Applications

Vehicle applications where these constraints and requirements are minimized in importance or severity are better suited for the implementation of a compliant suspension system. Equation (3.4) may be analyzed to determine the important factors that will minimize the stress of a compliant beam. Energy storage, U , wheel rate, k_w , and length, L , are the factors that depend on the vehicle application. In order to minimize stress, favorable applications must have:

- Low energy storage requirement
- High wheel rate
- Large space available for long compliant beams

Vehicle energy storage requirements generally reflect driving conditions and the severity of terrain for which the vehicle is designed. Rough terrain requires more energy storage which is accomplished by high wheel rates, large suspension travel, and suspension pre-load. Vehicles with low suspension travel are good candidates for a compliant suspension because they reflect lower energy-storage requirements. A lower weight vehicle generally will also require less energy storage.

Vehicles that have low wheel control forces when compared to their weight will minimize wheel deflections. Low vehicle handling requirements and vehicle speeds gen-

TABLE 3.2 Vehicle Application Information

Application	Vehicle Weight (lbs)	Wheel Rate (lbs/in)	Suspension Travel (in)	Available Space (ft)	Handling Req. L/M/H	Adjustability Req. L/M/H	Notes
Automobile	2000 - 4000	75 - 150	7 - 10	2	M - H	L	Some pre-load with bump stops
Motorcycle	200 - 400 (Dirt) 500 - 1000 (Cruiser)	50 - 75	10 - 12	1 (rear)	H	M	preload
Scooter	100 - 300	50 - 100	4	1 (rear)	L	L	
RC Car	3 - 4	1 - 2	1	1 - 2 inches	H (racing)	H (racing)	
Road Bike	200 - 250 (w/rider)	200	1 - 2	1 (rear)	L	L	
Mountain Bike	200 - 250 (w/rider)	100 - 200	2 - 6	1 (rear)	M	M	
Utility Vehicle	500 - 1000	50 - 100	3 - 10	1	L	L	Large load/vehicle variability
ATV	400 - 800	50 - 100	5 - 10	1	H	M	preload, progressive springing
Snowmobile	600 - 1000	100 - 200	10 - 13	Length of rear tread (3 ft)	H	M	preload, progressive springing

erally result in lower control forces. This will also result in lower compliant beam stresses. Vehicles with low handling requirements also do not require precise wheel control and wheel deflections become less of a concern. Other vehicle characteristics that are favorable for a compliant suspension system are low adjustability requirements and unconstrained suspension space for long compliant beams.

Table 3.2 lists general information about some vehicle applications and the design issues discussed above for comparison purposes. Individual specifications have a range of values to represent the different vehicle uses within each vehicle type.

Bicycles, scooters, and some utility type vehicles are favorable applications because of their low energy storage requirements and lower handling requirements. Some bicycles and utility vehicles, such as a golf cart, currently utilize a compliant suspension device. Chapter 2 depicts some of the different compliant suspension mechanisms used in the bicycle industry and the utility vehicle utilizes a single transverse leaf spring to act as a suspension arm and spring. These vehicles are of lower weight and generally are not subject to harsh terrain.

Recreational vehicles, such as ATVs or snowmobiles, also are lower weight than the automobile yet their energy storage requirements are comparable because of the types of terrain they are designed for. They also have high handling requirements and the suspension is more often adjusted to suit different riders. The snowmobile still may be a good possibility because of the large amount of space available in the rear suspension for long compliant beams.

CONCEPT EXPLORATION

Concept generation and exploration was not limited to any one single vehicle application. However, there is a distinct difference in suspension mechanisms for single-track vehicles (e.g. bicycles or motorcycles) and vehicles with two tracks (e.g. automobiles). The concepts explored in this research focus on two track vehicles, however the planar concepts may be implemented in a single-track vehicle.

A compliant suspension is one where the wheel gains at least a portion of its motion and energy storage through the use of flexible members other than a coil spring. There are many methods of achieving motion with flexible segments. These include small-length flexural pivots, flexible beams in bending, living hinges, torsional hinges, and others. Because of the high loads, high energy storage requirements, and weight and space constraints, only flexible beams in bending are explored. These beams must serve as both energy storage devices and links in connecting the wheel to the vehicle. This chapter details the methods of concept generation and concepts explored for a compliant suspension system.

4.1 Solution Objectives

The important objectives are to find concepts that fulfill the functional requirements of a suspension system and will:

- constrain motion to one-degree-of-freedom vertical motion with minimal movement in other directions in response to control forces
- maintain suitable stress levels for cyclic loading conditions while minimizing weight requirements
- fit within suitable space for possible applications

The process of concept generation and evaluation of concepts presented in this chapter focus on these objectives with emphasis on the first.

4.2 Rigid-Body Replacement Synthesis

Using rigid-body replacement synthesis of rigid-link suspension mechanisms, compliant concepts were developed that have the same motion characteristics as their rigid-link counterparts. Since the pseudo-rigid-body-model applies to planar compliant mechanisms, this method was constrained to those suspension mechanisms that are planar mechanisms. These include the double A-Arm or wishbone, McPherson strut, trailing arm, and swing-axle suspensions reviewed in Chapter 2. Because of the swing-axle suspension's known deficiencies of camber change and jacking, this concept was not explored. However, the cantilever beam example presented in Chapter 3 is a compliant counterpart to the simple swing-axle suspension.

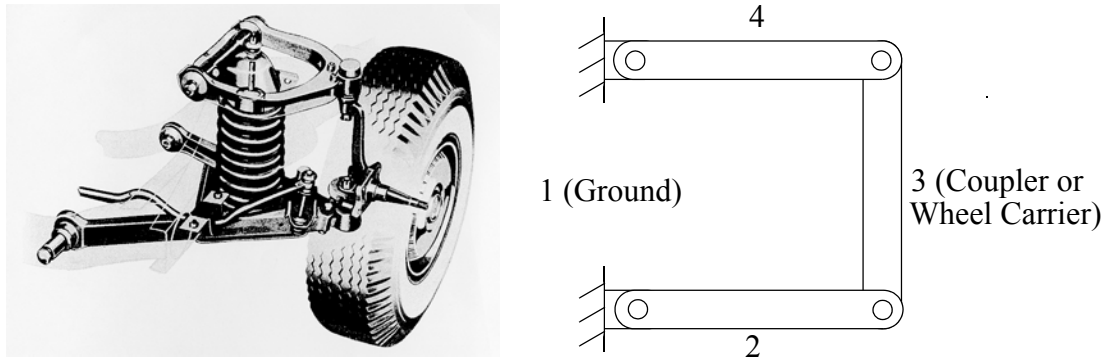


Figure 4.1 Ford A-Arm suspension and representative planar four-bar mechanism [2]

4.2.1 Double A-Arm 4-Bar Mechanism

The double A-Arm suspension is a planar four-bar mechanism as shown in Figure 4.1. The A-Arm or wishbone shape provides a very useful function in that it creates a redundant link that provides support in and out of the plane. Link 3, the coupler link, must be a rigid segment to function properly. This is also the wheel carrier in a suspension mechanism which also must be rigid to allow adequate attachment to the wheel. Only Links 2 and 4 may be compliant segments. There are fifteen different compliant mechanisms for a four-bar mechanism with these requirements as illustrated in Figure 4.2.

Of these configurations, three have been used in some form with a transverse leaf spring such as shown in Figure 2.11. These configurations are characterized by one or two compliant links fixed to the vehicle and pinned to the coupler link or wheel carrier. All the other configurations have either a fixed-guided compliant segment or a compliant segment that is fixed to the wheel carrier and pinned to the vehicle. These two characteristics both have disadvantages. A fixed-guided segment has the disadvantage of decreased thickness

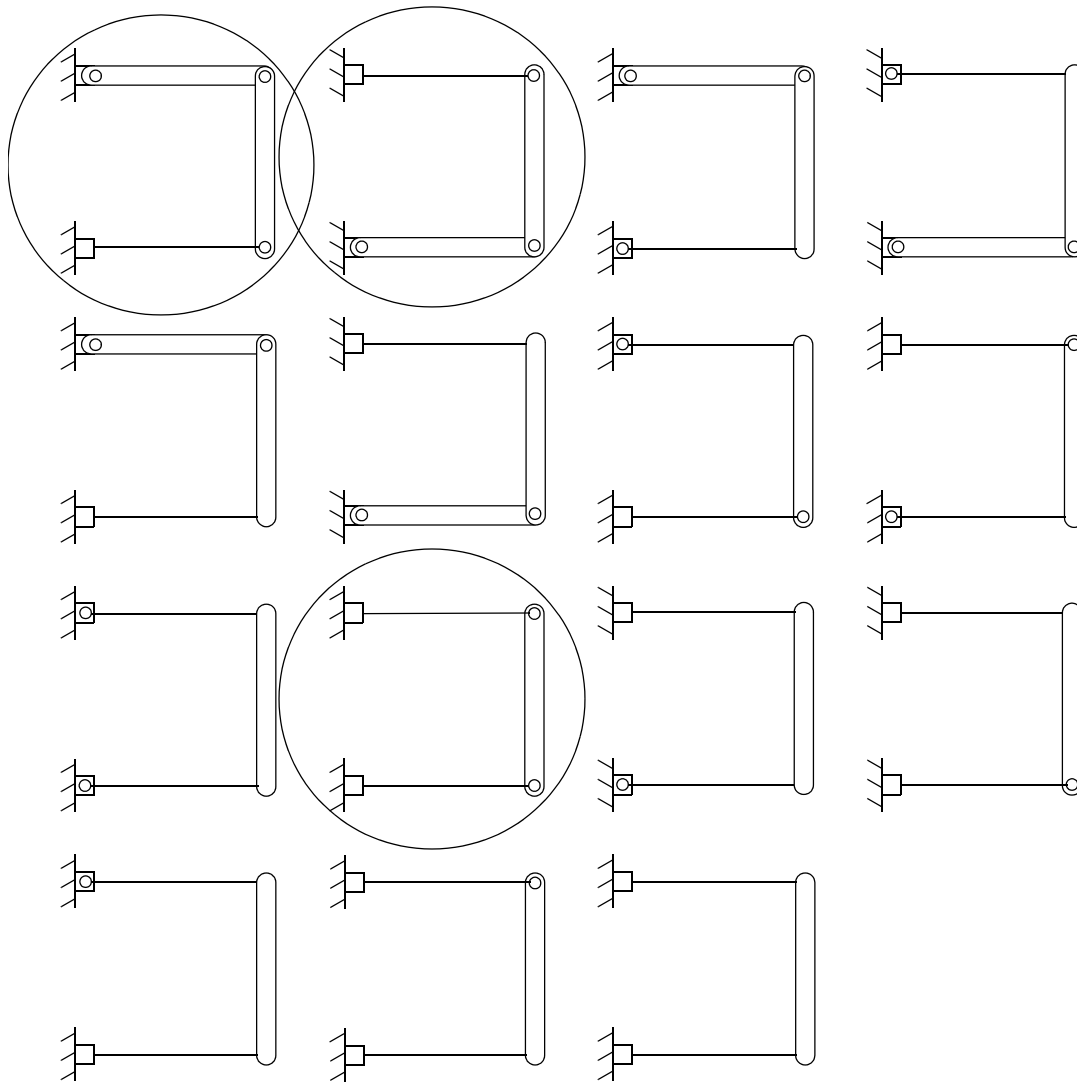


Figure 4.2 Compliant parallel 4-bar mechanisms with rigid coupler. The circled mechanisms have been implemented previously with transverse leaf springs

and increased width when compared to a cantilever beam with the same stiffness and stress requirements. A compliant segment that is fixed to the wheel carrier and pinned to the vehicle is more difficult to implement than one that is fixed to the vehicle and pinned to the wheel carrier, especially since a transverse leaf spring accomplishes the latter quite simply.

Bastow [32] explains one of the disadvantages of these 4-bar transverse leaf spring configurations is "...the stress caused by high fore and aft loading resulting from braking forces..." The use of a redundant link or transverse leaf would help alleviate this problem, however this has not been implemented because of space constraints within the vehicle and with the wheel carrier's attachment to the inside of the wheel.

4.2.2 McPherson Strut

The McPherson strut mechanism is a planar four-link mechanism as shown in Figure 4.3. The longitudinal rod pictured gives some out-of-plane support to the mechanism. The compliant counterparts to this mechanism are characterized by making Link 2 a compliant segment which results in three different mechanism configurations. The compliant segment may either be fixed at both ends creating a fix-guided segment or fixed at the vehicle and pinned at the wheel or vice versa. Because of the disadvantages of the fixed-guided segment and the segment fixed to the wheel, the best solution is a simple transverse leaf acting as the locating link. This concept has also been used and has the same disad-

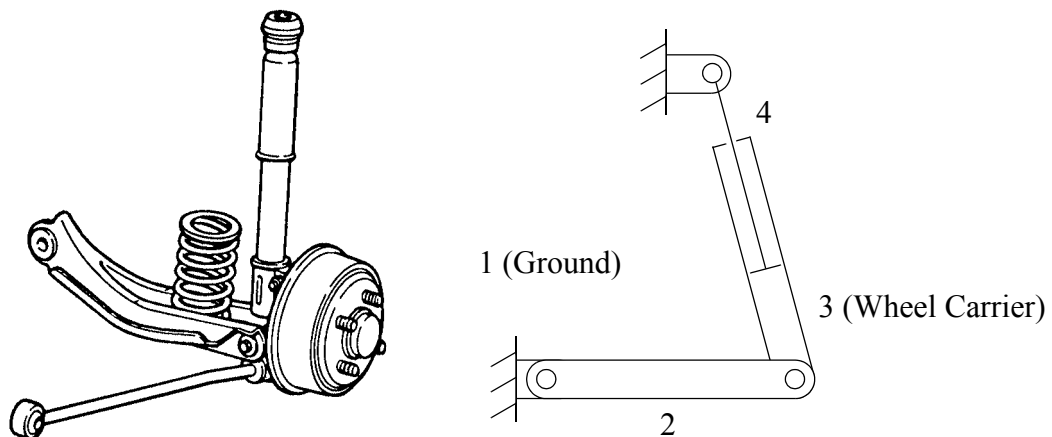


Figure 4.3 McPherson strut and representative four link planar mechanism

vantages as the transverse leaf concepts used in four-bar mechanisms. Again, a redundant link would be helpful but brings up problems with space constraints of the vehicle.

4.2.3 Trailing Arm

The trailing arm mechanism may either be a two link mechanism as shown in Figure 4.4 or a four-link mechanism such as the A-Arm mechanism that is oriented longitudinally in the vehicle. The trailing arm shown here is actually a semi-trailing arm because the axis of motion is not quite horizontal in the top view shown. This trailing arm also displays the A-Arm shape creating essentially a redundant link for support. The compliant counterparts to a four-link mechanism were discussed previously. The compliant counterpart to the two link mechanism shown in Figure 4.4 is the simple cantilever beam fixed to the vehicle. This concept has also been implemented in production as a trailing leaf spring. This concept has the disadvantages of poor response to a cornering force, added stress due to a cornering force, stress and packaging space problems associated with all leaf springs. A redundant trailing leaf would also be useful in this concept.

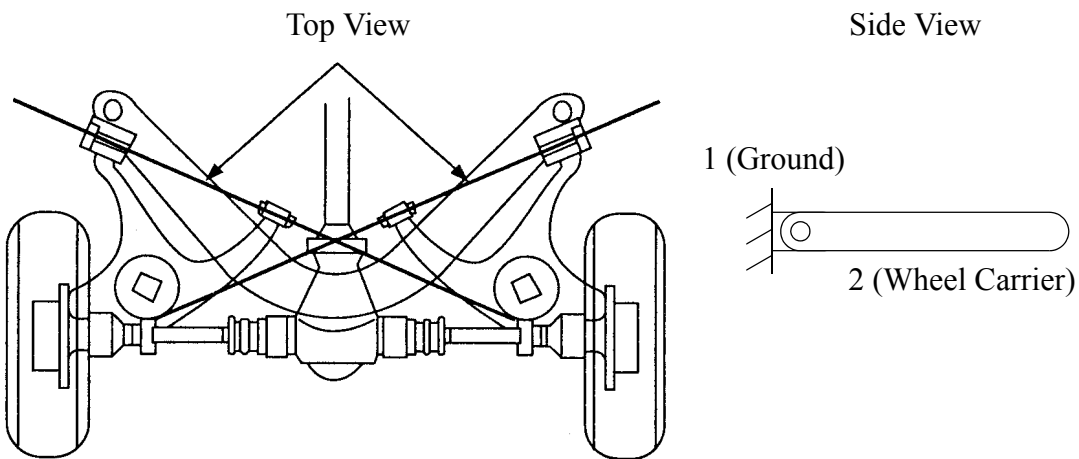


Figure 4.4 Trailing arm suspension and representative planar two link mechanism

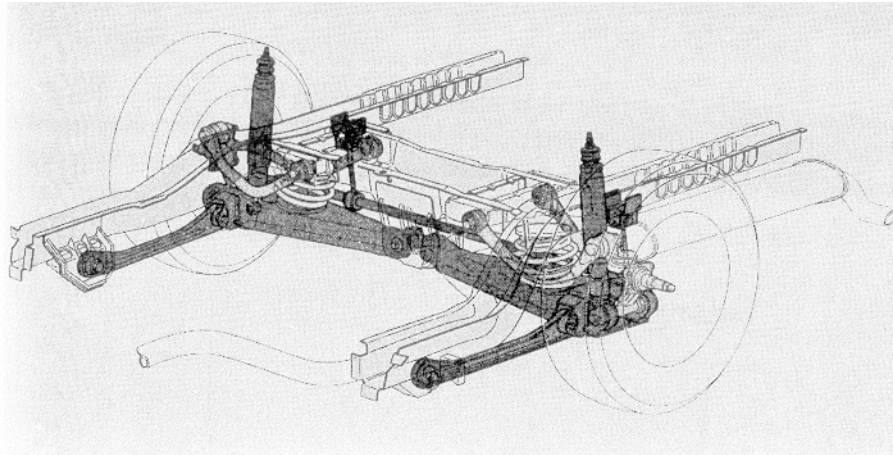


Figure 4.5 Ford multi-link rear suspension

4.2.4 Multi-link Mechanism

The multi-link mechanism is a more complicated mechanism. The multi-link rear suspension pictured in Figure 4.5 is a Ford Taurus/Sable suspension which uses four links to connect the wheel carrier to the vehicle. These link ends must have ball-joint connections to prevent binding the suspension or introducing extra bending moments in the links. Many variations of this configuration are possible using four or five links. A multi-link suspension has the advantage of its flexibility in controlling wheel motion, and with the use of elastic bushings, achieving desired wheel motions in response to control forces.

One of the advantages of the multi-link mechanism is that it is a spatial mechanism and locates the wheel to the vehicle with links oriented in different directions. This adds an element of control over wheel deflections that is not possible with a planar mechanism. A simple approach to spatially orienting compliant segments to locate the wheel in orthogonal directions is by connecting two cantilever beams to a coupler with pin joints as

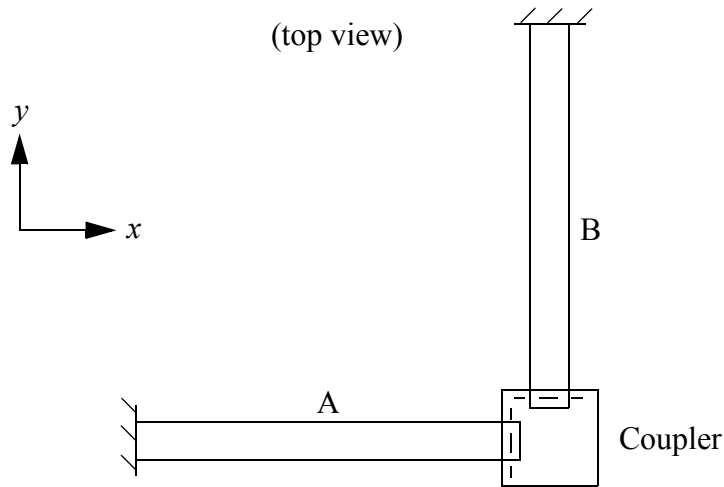


Figure 4.6 Spatial compliant mechanism

shown in Figure 4.6. Beam height or thickness is orthogonal to the page as is motion of the mechanism. The rigid-link equivalent to this mechanism has zero degrees of freedom. As the end of beam A moves out of the page, it also translates in the negative x direction. Translation in the negative x direction is constrained by beam B which binds the mechanism. This problem may be solved by connecting the end of the beams by a sliding pivot to the coupler. Other ways to solve the problem include using a sliding or rotating joint to connect the beams to ground. The disadvantage to these solutions is that the advantage of reduced part count and assembly time of compliant mechanisms is nullified by the need of extra complicated joints.

4.3 Other Mechanism Concepts

Other mechanism concepts exist that have not been used in a rigid-link suspension mechanism but may work well with a compliant mechanism. The conventional leaf spring

is an example of a compliant solution that does not have a rigid link equivalent mechanism that is used in a suspension.

4.3.1 Straight Line Mechanisms

A logical class of mechanisms to explore are those classified as straight-line mechanisms, because one of the main functional requirements of a suspension is vertical one-degree-of-freedom motion. A suspension mechanism need not have exact straight-line motion, but approximate straight-line motion is adequate as demonstrated by mechanisms just discussed. Versions of straight-line mechanisms have been used in locating some point of the suspension especially for lateral support and location of a rigid axle.

A simple radius rod also known as a panhard rod in the automotive industry is a crude approximation for straight-line motion. The swing-axle suspension is essentially a radius rod as is the simple trailing arm mechanism. The cantilever beam is the compliant equivalent and has already been discussed.

The Watt linkage and Roberts linkage shown in Figure 4.7 compensate for the error in a radius rod and provide more accurate straight line motion for point A of the mechanism. However, these are planar mechanisms and have no support in the out-of-plane direction. Compliant equivalents would have the same drawbacks as a conventional leaf spring or transverse leaf spring which has no out of plane support. There are other disadvantages to these mechanisms as well. The coupler link of the Watt linkage experiences large rotations which would result in large camber or wheel rotation depending on

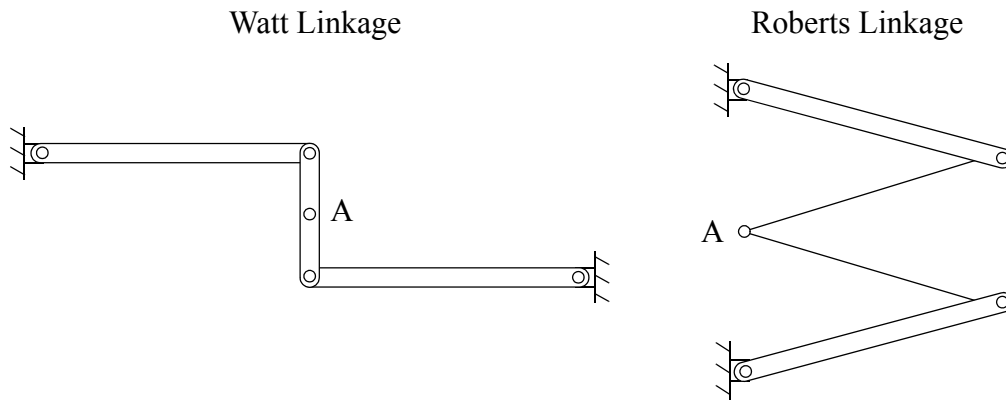


Figure 4.7 Watt and Roberts linkages

the orientation of the mechanism in the vehicle. The coupler link of the Roberts linkage is also unnecessarily large in concept, however, may be modified since precise straight line motion is not required. Examining the Roberts linkage further reveals that the mechanism is just a four bar mechanism with the coupler, link lengths, and configuration designed to give straight-line motion. Because exact straight-line motion is not required, the simple four-bar mechanism already discussed is sufficient. It is concluded that the rigid-link suspension mechanisms discussed previously offer more viable solutions for a compliant suspension than these straight-line mechanisms.

4.3.2 Compliant Linear Motion Mechanisms

Other compliant mechanisms have been designed to produce linear motion, particularly with microelectromechanical systems (MEMS). Perhaps the most common is the folded beam linear motion mechanism shown in Figure 4.8. The center shuttle translates in the vertical direction yet does not translate or rotate in other directions. Beams 1 and 2 create a fully compliant parallel-guiding mechanism between ground and the intermediate

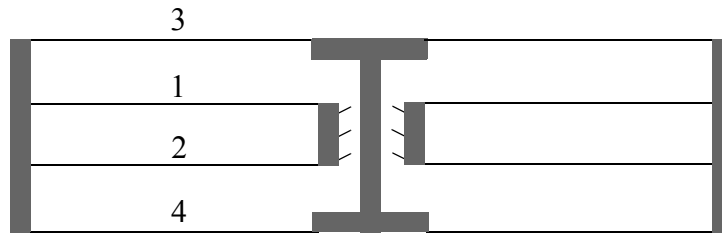


Figure 4.8 Folded beam linear motion mechanism

rigid link. Beams 3 and 4 create another fully compliant parallel-guiding mechanism between the intermediate rigid link and the center shuttle. Because the second parallel-guiding mechanism is folded back on the first, the center shuttle experiences no horizontal translation. This allows an identical mechanism to be attached to the other side of the center shuttle to support and align the center shuttle without causing any stress-stiffening effects. While this is a planar mechanism, this folded beam approach allows for an identical mechanism to be oriented orthogonal to the plane to yield additional support in this direction. The mechanism shown in Figure 4.9 in its deflected position is an example of this type of mechanism. The disadvantages of this type of mechanism include extra weight for the rigid segments and manufacturing and assembly complexity.

4.3.3 A-Arm Configuration

The spatial mechanism discussed as show in Figure 4.6 has the same advantage that the rigid link A-Arm mechanism has in providing support in the out-of-plane direction. This mechanism takes advantage of the axial stiffness of the flexible segments for out-of-plane support. One drawback to this mechanism is the need for some type of slid-

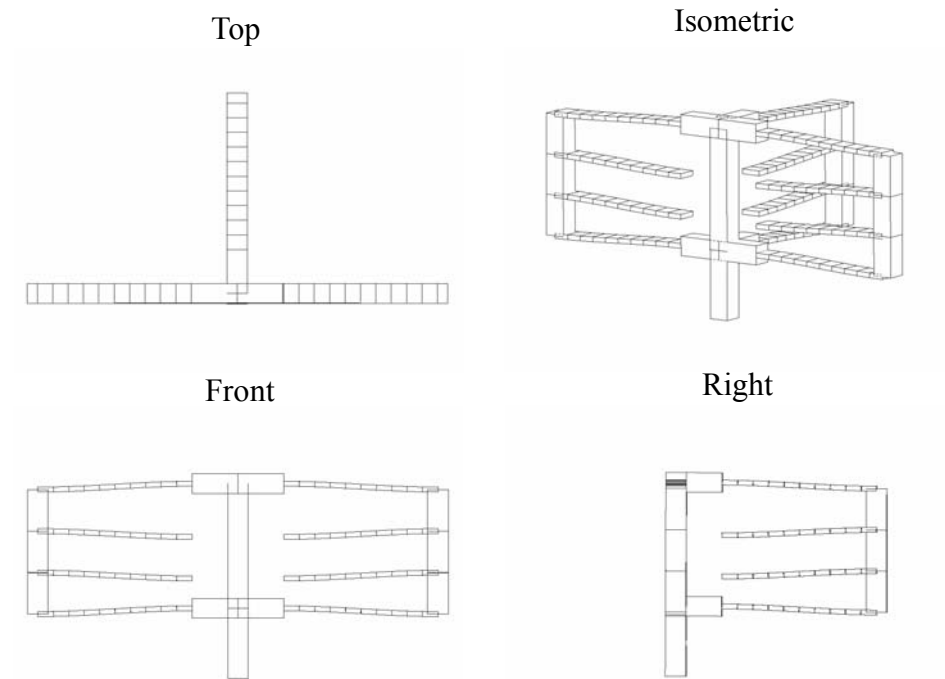


Figure 4.9 Three dimensional version of folded beam mechanism

ing and rotating joints to prevent undesired bending or twisting of the beams. If no extra joints are included as shown in Figure 4.10, the extra deflections create a stiffening effect. The end point of the mechanism will follow a path that is within the vertical plane indicated by the dashed line causing bending and torsion of the beams. This configuration takes advantage of the torsional flexibility and off-axis flexibility of the thin-walled beams to facilitate the motion of the end-point of the beams. This stiffens the structure, but may be acceptable provided the mechanism remains within failure limits and its energy storage specific volume efficiency compares favorably with a cantilever beam. The stress stiffening effect also is beneficial in creating a progressive rate spring. This type of mechanism does not have a simple model to predict stiffness or stress, and finite element analysis is

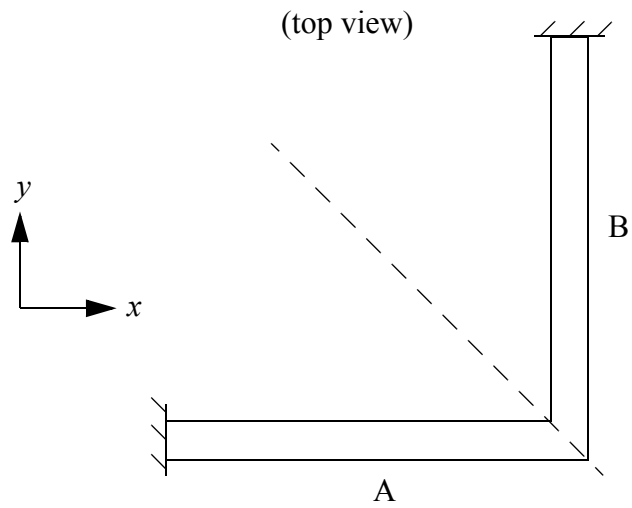


Figure 4.10 Component of a compliant A-Arm mechanism

used even in the initial design stages. This mechanism concept has many different configuration possibilities for a suspension mechanism where this A-Arm would act as one of the suspension linkages.

CONCEPT EVALUATION AND COMPARISONS

Evaluations of the concepts discussed in the previous chapter were based on the major design constraints and requirements presented in Chapter 3 and are identical to the concept solution objectives presented in the previous chapter.

5.1 Wheel Deflections and Control Forces

First, a compliant suspension will minimize deflections of the wheel in response to control forces. Comparisons of the performance of different concepts were made using a commercial finite element analysis program capable of nonlinear analysis. The following constraints were developed to compare different concepts on an equal basis:

- mechanisms have equal vertical stiffness, energy storage, and stress at maximum deflection
- compliant segments of different mechanisms have equal length

In this study, compliant segments have a length, L , of 2 inches and mechanisms have a spring rate of 2.7 lbs/in and a maximum stress of 1800 psi at 0.4 inches of deflection using polypropylene as the material. These particular specifications match a prototype of the

folded-beam mechanism for testing and verification purposes. However, they become less important when making comparisons between concepts with finite element analysis. Flexible beams were meshed with ten 3D elastic beam elements having beam width, b , and thickness, h . These elements have six degrees of freedom at each node with tension, compression, torsion, and bending capabilities. Rigid links or segments are modeled as perfectly rigid by using a high modulus of elasticity. All joints are ideal, experiencing no undesired rotations or deflections that would normally occur in a real joint because of clearances and bushing elasticity.

5.1.1 Concepts

The following concepts were evaluated and compared.

- Double transverse leaf spring
- Double transverse stacked leaf spring
- Conventional longitudinal leaf spring with rigid axle
- Conventional longitudinal stacked leaf spring with rigid axle
- Double transverse leaf spring with redundant transverse leaves
- Folded beam suspension
- Compliant A-Arm
- Compliant stacked A-Arm

These concepts are depicted in Figure 5.1. The double transverse leaf spring and conventional longitudinal leaf spring concepts are used as benchmarks. It is noted that the longitudinal leaf spring is not an independent suspension mechanism as the other concepts are. In this concept, the full axle or both sides of the suspension must be included in the analysis since one side lends support to the other and vice versa. Redundant transverse leaves refer to the extra transverse leaves which create redundant links for the mechanism. This

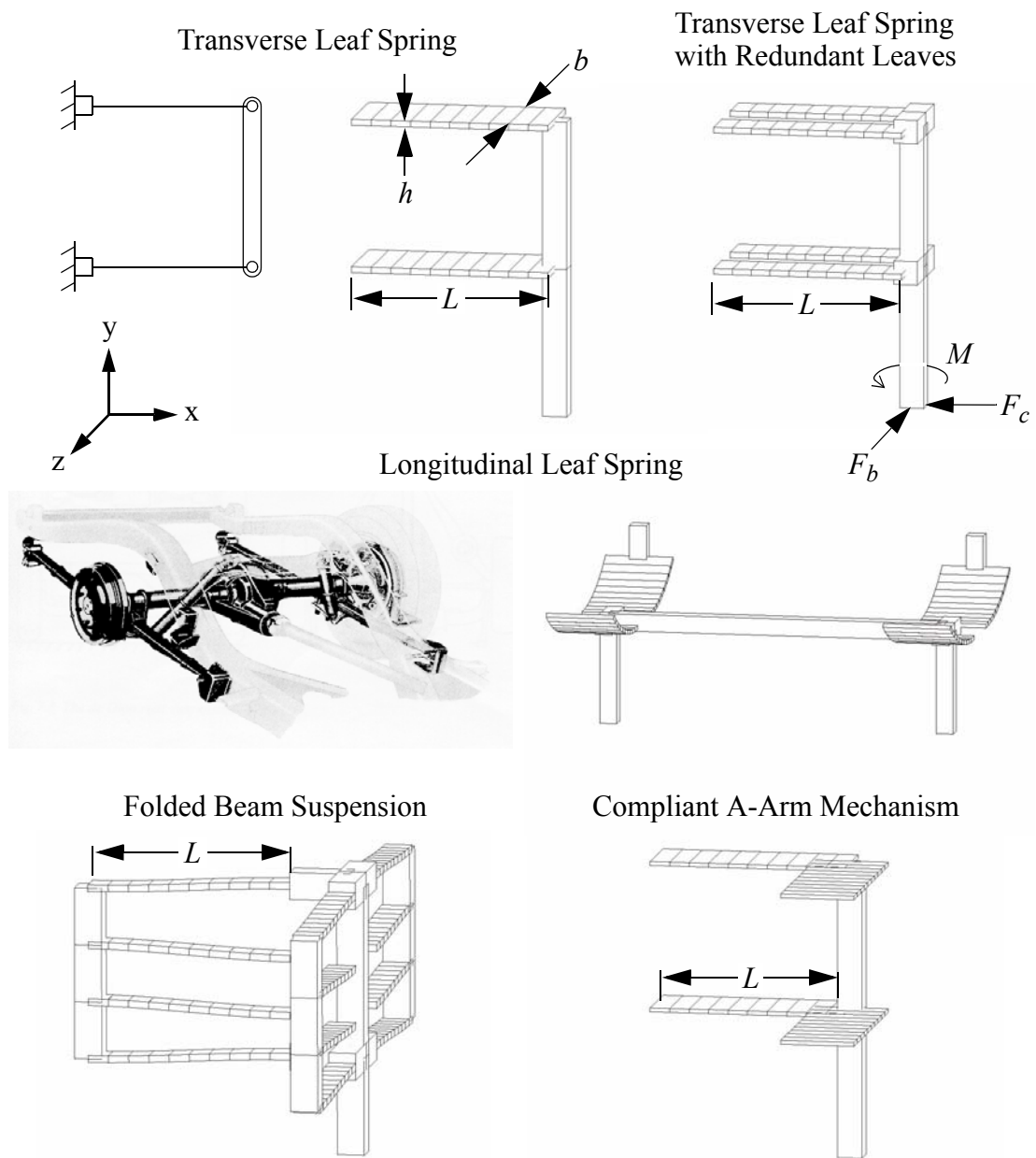


Figure 5.1 Mechanism concept configurations

adds out-of-plane support much like a rigid link A-Arm link. The transverse leaf concepts are fixed to the vehicle (ground) and pinned to the rigid wheel carrier. The longitudinal leaf spring is fixed in the middle to the wheel coupler and pinned to the vehicle and intermediate shackle link. The folded beam suspension has rigid connections with the center

shuttle acting as the wheel carrier and the compliant segments being fixed to ground as depicted in Figure 4.8. The compliant segments of the compliant A-Arm mechanism are fixed together as shown in Figure 4.10 creating the A-Arm shape. These A-Arms are pinned to the rigid wheel carrier creating a 4-bar mechanism. These concepts modeled with FEA software include a rigid beam that extends downward from the wheel carrier and represents the wheel. Loads were applied at the bottom of this rigid beam to simulate control forces.

Although the length of the compliant segments are equal for all of the mechanisms, their cross-sections are not equal because of the vertical stiffness and stress constraints.

Table 5.1 compares the different characteristics of the compliant segments of each of the

TABLE 5.1 Mechanism Concept Configuration Characteristics

Concept	L/b	b/h	Compliant Segment Type	No. of Compliant Segments
Transverse Leaf Spring	2	16.67	Fixed-pinned	2
Transverse Stacked Leaf Spring	8	4.16	Fixed-pinned	8
Longitudinal Leaf Spring	2	16.67	Fixed-pinned	2 (one side)
Longitudinal Stacked Leaf Spring	8	4.16	Fixed-pinned	8 (one side)
Transverse Leaf Spring with Redundant Leaves	4	8.33	Fixed-pinned	4
Folded Beam Suspension	12	2.77	Fixed-guided	12
Compliant A-Arm Mechanism	2.66	18.8	Fixed-pinned w/ stress stiffening effects	4 2 A-Arms
Compliant Stacked A-Arm Mechanism	8	6.25	Fixed-pinned w/ stress stiffening effects	12 6 A-Arms

mechanisms. Two dimensionless ratios are included. The L/b ratio describes the ratio of the beam length to its width. Higher values for L/b will conserve space as the compliant beams are not as wide. The aspect ratio, b/h , was introduced in Chapter 3 and compares the stiffness of the beam in different directions. A higher aspect ratio results in higher out-of-plane stiffness. Stacked leaf springs were included in these comparisons because the single leaf concepts have unrealistically low L/b ratios or wide compliant segments to satisfy the vertical stiffness and stress constraints. Stacked leaf springs take up less space and are also more characteristic of leaf spring suspension in past and current use. A "stacked leaf" version of the compliant A-Arm mechanism was added for comparison because the single leaf version also has a low L/b ratio.

5.1.2 Deflection Results

A braking force, F_b (z -direction), cornering force, F_c (x -direction), and steering moment, M , about the y -axis were applied separately to each mechanism in the FEA models. The magnitude of the braking and cornering forces is equal to the magnitude of the vertical force at the mechanism's maximum vertical deflection. Wheel attitude changes in response to these control forces are summarized in Table 5.2. Braking force compliance rotation is the amount of rotation about the wheel axis that occurs when a braking force is applied. The other measurements have similar definitions given by their names.

A physical prototype of the folded beam suspension was tested to validate these results. Mechanism stiffness in the direction of control forces were measured using a force transducer and linear positioner. The measured values for stiffness were 40% and

TABLE 5.2 Wheel Attitude Changes (radians)

Concept	Braking Force Compliance Rotation	Braking Force Compliance Steer	Lateral Cornering Force Compliance Camber	Steering Moment Compliance Steer
Transverse Leaf Spring	0.0016	0.0012	0.0004	0.0042
Transverse Stacked Leaf Spring	0.0206	0.0162	0.0004	0.0642
Longitudinal Leaf Spring	0.0831	0	0.0467	0.0003
Longitudinal Stacked Leaf Spring	0.0830	0	0.0641	0.0004
Transverse Leaf Spring with Redundant Leaves	0.0056	0.0004	0.0004	0.0014
Folded Beam Suspension	0.0075	0	0.0015	0.0255
Compliant A-Arm Mechanism	0.0007	0.0003	0.0007	0.0022
Compliant Stacked A-Arm Mechanism	0.0007	0.0001	0.0007	0.0164

56% greater than predicted for a cornering force and a braking force. This amount of error is large and raises questions of both the accuracy of the FEA predictions and the accuracy of the test setup. However, predicting trends was more important in this study. FEA predicts that the mechanism is 45% stiffer in response to a braking force than a cornering force. Test results show a 59% increase. This equates to only 10% error between prediction and test results of the ratio of braking force stiffness to cornering force stiffness. Since the results given in Table 5.2 differ by orders of magnitude, this level of accuracy in predicting trends is sufficient.

5.1.3 Discussion of Deflection Results

A braking force will cause wheel wind-up and to a lesser extent a change in steer angle. The results for the conventional longitudinal leaf spring demonstrate its known deficiency in controlling brake wind-up. The transverse leaf spring performs better than the longitudinal leaf spring, but not as well as the latter three concepts which provide more out-of-plane support. The ability to resist steering angle changes decreases greatly as the transverse leaf spring is stacked because it lowers the moment of inertia of the non-flexible axis of the compliant segments.

A lateral cornering force causes the greatest deflection in the longitudinal leaf spring in the form of camber change. The superior results of the other concepts may be explained by the fact that a cornering force is resisted by compliant segments placed in tension or compression resulting in low deflections. With the longitudinal leaf spring, however, the cornering force is resisted by torsion and vertical stiffness of the compliant leaves which results in higher deflections. Compliant beams are much stiffer in tension than in torsion or bending. This analysis, though, is based on the transverse concepts and the A-Arm concepts configured in an ideal position. If these mechanisms were deflected up or down, a lateral force would place some amount of bending load on the compliant segments resulting in larger deflections.

An applied steering moment may result from the offset of the braking or cornering force from the location at which it was applied in this analysis. For example, this analysis assumes the wheel extends down directly beneath the mechanism and is modeled with a

rigid beam. In reality, the wheel would extend outward from the vehicle and the mechanism. Therefore, a braking force on the wheel may be resolved into a force and a steering moment on the suspension mechanism. This analysis shows the largest steering angle change due to a steering moment occurs in the transverse stacked leaf spring. Since the compliant segments in this concept are placed under a pure moment, stacking increases the deflection because of the decrease in the moment of inertia of the non-flexible axis. The longitudinal leaf spring performs well because of the support on either side of the vehicle. The folded beam suspension is at a disadvantage because under this loading, the length of the compliant segments is effectively doubled, which results in increased deflections. The compliant A-Arm concept performs well, but stacking again reduces its performance.

5.1.4 Stress Results from Analysis of Control Forces

Stress is also important factor in evaluating the effect of control forces on these concepts. Table 5.3 gives approximations of bending and direct stress as given by FEA for each of the tests. These stresses are normalized by the maximum bending stress (1800 psi) due to the vertical force at maximum vertical deflection of the mechanism.

5.1.5 Discussion of Stress Results

Transverse leaf springs are known for the high stresses due to braking forces. This analysis also shows longitudinal leaf springs are also susceptible to high stresses from braking forces. The folded beam concept and A-Arm concept better support the load with

TABLE 5.3 Bending and Direct Stress due to Control Forces

Concept	Maximum Stress due to Braking Force	Maximum Stress due to Lateral Force	Maximum Stress due to Steering Moment
Transverse Leaf Spring	0.14	0	0.12
Transverse Stacked Leaf Spring	0.54	0	0.45
Longitudinal Leaf Spring	0.55	0.40	0
Longitudinal Stacked Leaf Spring	0.55	0.56	0
Transverse Leaf Spring with Redundant Leaves	0.24	0	0.06
Folded Beam Suspension	0.15	0.28	0.49
Compliant A-Arm Mechanism	0.04	0.04	0.16
Compliant Stacked A-Arm Mechanism	0.04	0.04	0.41

longitudinal links that are spaced vertically, resulting in tension and compression stresses in the compliant segments that are less than the bending stresses in the other concepts.

A lateral force also causes high stresses in the longitudinal leaf spring. Other Concepts have lower stresses for the same reasons discussed above.

The longitudinal leaf spring concepts have little to no stress due to a steering moment because of ideal configuration. The other concepts experience bending stresses under this loading condition and this bending stress will depend mainly on the moment of inertia of the compliant segments and to a lesser extent on the configuration.

5.1.6 Conclusions on Mechanism Response to Control Forces

The new concepts studied in this chapter offer greater stiffness in response to control forces because of the extra out-of-plane support added to originally planar mechanisms. Redundant leaves were added to the transverse leaf spring. An extra set of beams were added to the planar folded beam mechanism. Finally, transverse leaves were modified into compliant A-Arm type mechanisms. Stresses due to control forces were also lowered in these concepts.

5.2 Space and Weight Constraints on Stress Reduction

The specific volume efficiency, η , of these concepts except for the compliant A-Arm design is $1/9$. This efficiency may be improved by stacking or shaping the compliant segments. The specific volume efficiency of the compliant A-Arm concept, however, is less than $1/9$. Because of the deflection constraints of the compliant beams, stress-stiffening occurs and the location of the maximum stress becomes more localized. This reduces the specific volume efficiency. The overall weight of the compliant segments will therefore be greater than the other concepts.

The requirement of rigid segments in some concepts will also increase the required weight of the mechanism. The transverse and longitudinal leaf springs include the rigid wheel coupler. The redundant transverse leaf spring will require a larger wheel coupler. The folded beam suspension utilizes the greatest amount of rigid segments in both the wheel coupler, shuttle, and the intermediate rigid connecting segments. The A-Arm concept will also require a rigid segment for the wheel coupler.

One of the reasons the use of longitudinal leaf springs has continued is because of the efficiency and location of the space used. Leaf springs are stacked to reduce the necessity of wide beams. The longitudinal arrangement is also non-intrusive on constrained space within the vehicle. The transverse leaf spring, however, necessitates a large amount of space for the transverse leaves within the middle of the vehicle. On a front wheel drive vehicle, this space is occupied by powertrain components. Rigid-link suspension mechanisms have an advantage over transverse leaf springs in this regard because of the use of short links or struts to minimize overall package space of the suspension within the vehicle. Rear suspension space is not as limited but is still constrained by passenger, cargo, and possibly drivetrain space.

The compliant concepts in evaluation have increased space requirements when compared to leaf springs. The redundant transverse leaf spring utilizes excessive space within the vehicle and causes wheel attachment issues. Either spacing of the leaves must be reduced to fit within the wheel well or the lengths of the transverse leaves must be decreased so that attachment may be made outside of the wheel well. The folded beam suspension requires a large amount of space for the beams that extend fore and aft and into the vehicle. It also has the disadvantage of using fixed-guided compliant segments. These segments must be twice as wide yet thinner than a fixed-pinned segment with equal function specifications. In other concepts, most of the space needed to allow movement of the mechanism is close to the wheel. The rigid connecting beams of the folded beam suspension require a large amount of space for deflection of the mechanism. This will increase the overall package space of the mechanism. Lastly, the A-Arm concept in this configura-

tion requires transverse beams and longitudinal beams which is less space intensive than the other concepts. Other configurations of the A-Arm may be also developed to further reduce the space requirements of this concept.

5.3 Other Comparisons

Other factors to consider in the evaluation of these concepts include manufacturability and assembly issues. Leaf springs are relatively simple to manufacture and assemble in comparison to other suspension mechanisms. The folded beam suspension would require increased manufacturing and assembly complexity. This assumption is based on the number of separate compliant segments and their required connection to rigid components. It would, however, eliminate the need for any joints. The A-Arm concept would be competitive with the leaf spring in manufacture and assembly complexity. It would require two joints in this configuration.

5.4 Concept Evaluation Conclusions

The A-Arm concept performs well in controlling wheel deflections in response to control forces because of the out-of-plane stiffness given by the fore-aft bracing of the A-Arm configuration. Other concepts such as the folded beam mechanism and the transverse leaf spring with redundant leaves also perform well in comparison to the benchmark concepts because of out-of-plane stiffness. However, the compliant A-Arm has other advantages. The amount of space utilized is less than the new concepts considered and the potential cost of manufacture and assembly is the same as the benchmarks. The compliant

A-Arm's stiffness in response to control forces along with its advantages associated with space utilization and manufacturing costs make this concept the best candidate for further development.

The required weight for the compliant A-Arm needed to meet functional specifications will, however, be potentially greater due to the lower specific volume efficiency. This drawback may be decreased by a better understanding of the characteristics of the deflection, loading, and stress states of this mechanism. Utilizing this knowledge with optimizations techniques may result in compliant beam properties and configuration changes that will maximize the specific volume efficiency of the mechanism.

This chapter discusses the results of further analysis of the compliant A-Arm concept. A pseudo-rigid-body model is developed to model motion and stiffness characteristics based on FEA results. Test results are also given. A design example explains how a suspension might be configured and demonstrates how to use the pseudo-rigid-body model and FEA models to design a mechanism to meet suspension functional specifications.

6.1 Justification for Further Analysis

The compliant A-Arm concept shows many advantages in a suspension application when compared to other compliant concepts. These advantages are summarized below:

- Superior response to control forces: high stiffness and low stress
- Low space requirements
- Ease of manufacturing (similar to leaf spring)

High stiffness in response to control forces results in better handling characteristics. Low stress in response to control forces reduces the overall maximum stress for fatigue constraints. The A-Arm shape uses a small amount of space. The geometry of this shape gives a flexible design for fitting in constrained spaces. The basic A-Arm shape is also relatively simple to manufacture.

This concept also has natural progressive rate spring characteristics which is desirable for a suspension system. This characteristic is directly affected by the A-Arm shape and beam properties which reaffirms one of the design complexities of a compliant suspension. The suspension mechanism may not be designed independent of spring rate specifications. Further analysis is needed to better understand characteristics of this concept, simplify modeling techniques and improve the design.

6.2 Analysis with Beam Elements

Initial finite element analysis was completed using 3D line elements. This beam element is uniaxial and has tension, compression, torsion, bending, stress stiffening, and large deflection capabilities.

A representation of the FEA model of the mechanism is shown in Figure 6.1. Mechanism thickness and deflection are normal to the page. Each beam is divided into 10 elements creating 21 total nodes. The end nodes of each beam are coupled together. In one scenario, translations and rotations of the endpoints of the beams are coupled creating

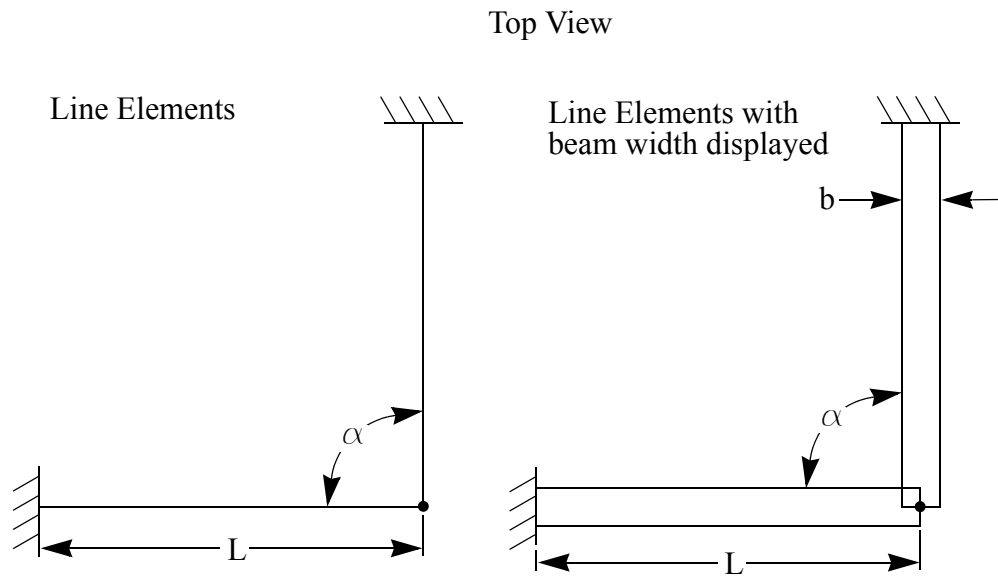


Figure 6.1 Representation of FEA beam model

a fixed joint between the beams. In the second scenario, these nodes are coupled in translations only allowing relative rotations creating a spherical joint. A spherical joint connection may relieve some of the stress stiffening effects created by fixing the beams together. This analysis used a length of 10 inches, a beam width of 1 inch, a thickness of 0.125 inches, an angle α of 90 degrees, a modulus of elasticity of 200,000 psi, and a Poisson's ratio of 0.4. A vertical displacement load of 4 inches was applied to the coupled node in a series of load steps with non-linear geometry effects applied. These specifications are used for later comparison with a physical test prototype.

6.2.1 Stiffness Results

Figure 6.2 displays force deflection results for the finite element results. These are compared with predictions from linear beam theory of two cantilever beams acting in par-

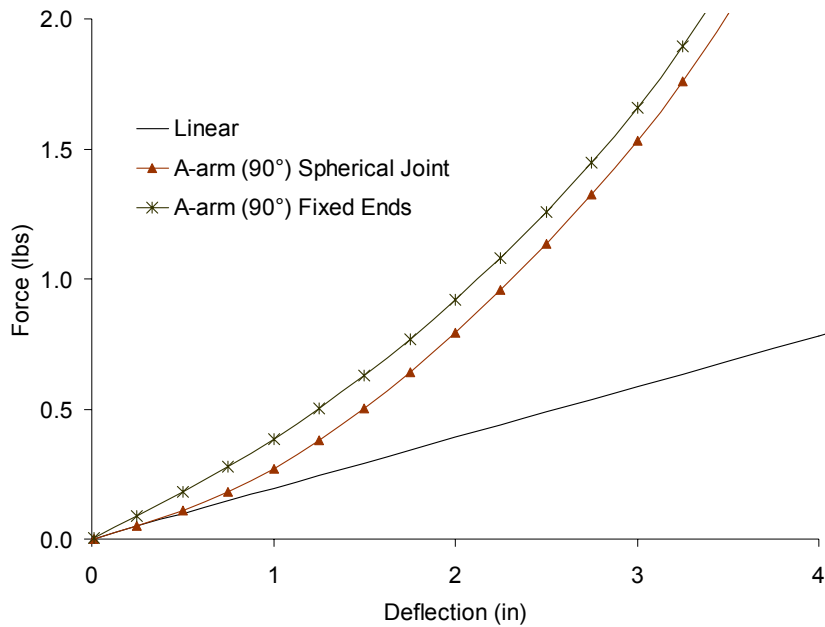


Figure 6.2 FEA force deflection prediction of compliant A-Arm and linear beam theory prediction of two cantilever beams acting in parallel

allel. Both A-Arm configurations have different stiffness characteristics than the cantilever beam model. The cantilever beam model has an initial stiffness of 0.195 lbs/in given by Equation (3.2). The A-Arm configuration connected by a spherical joint has an initial stiffness that is equal to the cantilever beam models, but diverges rapidly to a final stiffness of 1.5 lbs/in. The A-Arm configuration connected by a fixed joint has a higher initial stiffness of 0.35 lbs/in and also has non-linear force-deflection characteristics with a final stiffness of 1.5 lbs/in at a deflection of 4 inches.

6.2.2 Deflection Path

One of the key features of the pseudo-rigid-body model is the characteristic pivot that allows the designer to model the deflection with a rigid link and a pin joint. The

deflection of the compliant A-Arm design also shows this characteristic. The endpoint C shown in Figure 6.3 will follow a path that is contained in the vertical x' - y' plane. The distance from the coordinate axis origin to the endpoint, L' , is given by

$$L' = L \cos\left(\frac{\alpha}{2}\right) \quad (6.1)$$

The deflection of the endpoint of the beam may be modeled by a rigid link that moves in this plane and has a characteristic radius $\gamma L'$. The characteristic radius factor, γ , is found by maximizing the pseudo-rigid-body angle, Θ , subject to the constraint of a maximum error function of 1%. Since a closed form solution of the path of the mechanism is not known, finite element results of the beam model were used as the actual beam

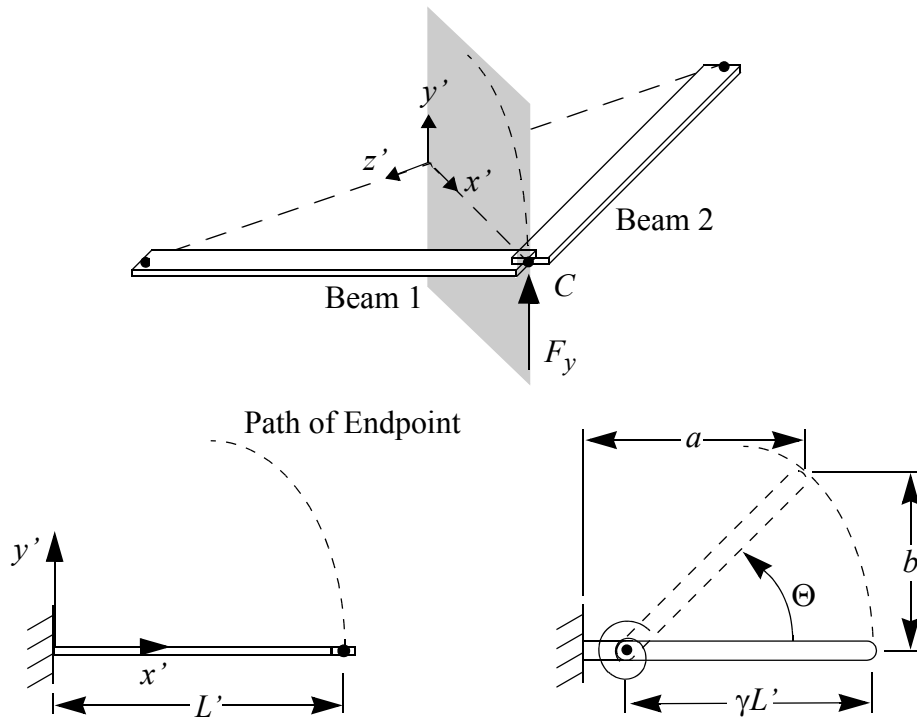


Figure 6.3 Deflection path of endpoint, C , and pseudo-rigid-link model of endpoint deflection

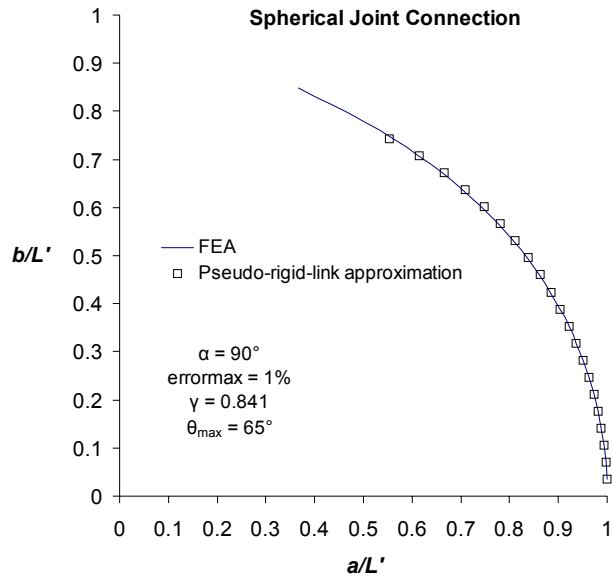


Figure 6.4 Pseudo-rigid link approximation of deflection path for a vertical load

path. Figure 6.4 shows the results for a vertical force, where the optimal γ is 0.841. The configuration with the fixed joint has an optimal γ of 0.863.

6.3 Linear Closed-Form Solution of Stiffness Results

The loading conditions of the beams that make up the A-Arm is important in understanding these non-linear stiffness characteristics and stress-stiffening effects. Figure 6.5 is a free-body diagram of this structure in the unique configuration where $\alpha = 90$ degrees. Because this structure is symmetric, it is useful to analyze this mechanism as one beam with half the load applied and appropriate reaction loads applied at the joint, C . R_{Ix} , R_{Iy} , and R_{Iz} are the reaction forces on Beam 1 in the x , y , and z directions respectively.

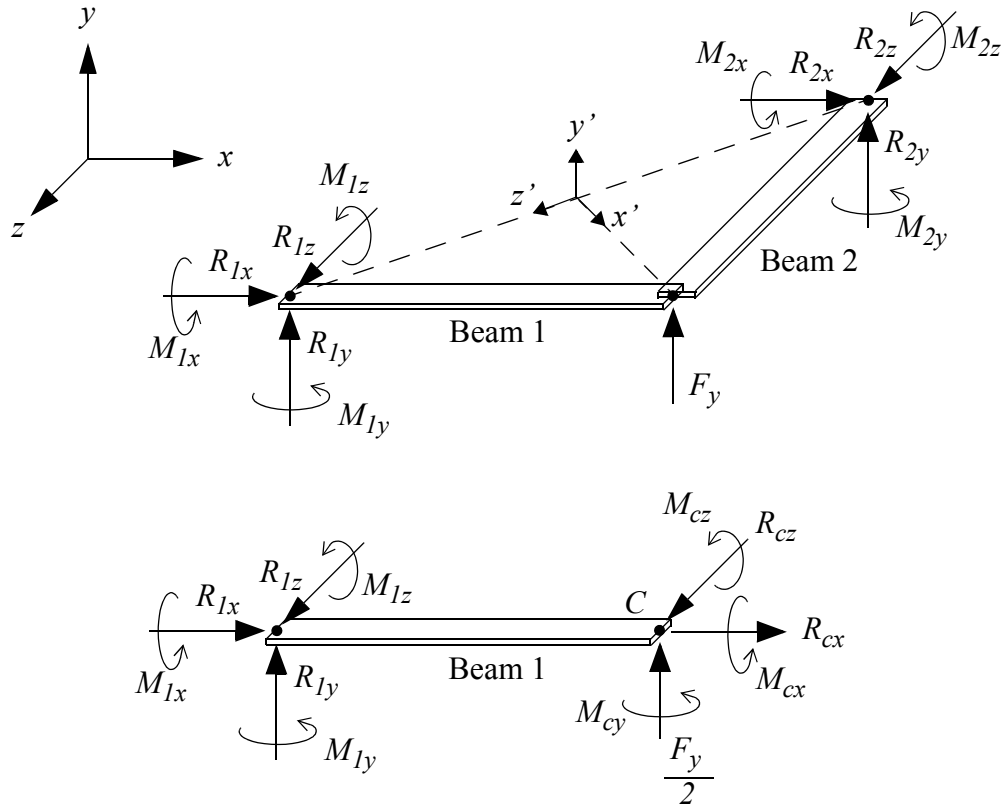


Figure 6.5 Free-body diagram of compliant A-Arm mechanism

M_{Ix} , M_{Iy} , and M_{Iz} are the reaction moments on Beam 1 about the x , y , and z axes respectively. Similarly labeled are the reaction forces and moments at the joint, C .

Using linear approximations, a load $F_y/2$ results in deflection of the end point of the Beam 1, C , in the y direction and rotation about the z -axis only. Similarly, this load results in deflections of the end point of Beam 2 in the y direction and rotation about the x -axis only. These linear assumptions yield

$$\delta_{cx} = \delta_{cz} = 0 \quad (6.2)$$

Because the motion of Beam 2 does not cause any linear deflection of Beam 1, the reaction forces at this connection must be equal to zero. Equilibrium arguments yield

$$R_{1x} = R_{cx} = R_{1z} = R_{cz} = 0 \quad (6.3)$$

With a spherical joint connecting Beam 1 to Beam 2, no moments are applied at C which cause no additional rotations of the end point, C :

$$\theta_{cx} = \theta_{cy} = 0 \quad (6.4)$$

$$M_{cx} = M_{cy} = M_{cz} = 0 \quad (6.5)$$

Equilibrium arguments yield

$$M_{1x} = M_{1y} = 0 \quad (6.6)$$

Because of the linear assumptions and the spherical joint connecting the two beams, this problem reduces to a simple cantilever beam with a vertical force applied. The reaction loads for Beams 1 and 2 are

$$R_{1y} = R_{2y} = -\frac{1}{2}F_y \quad (6.7)$$

$$M_{1z} = -M_{2x} = -\frac{1}{2}F_y L \quad (6.8)$$

The resulting stiffness, k , of the structure is

$$k = 2\left(\frac{3EI}{L^3}\right) \quad (6.9)$$

This is equal to two identical cantilever beams acting in parallel. FEA results shown in Figure 6.2 also show this mechanism to have an initial stiffness equal to two cantilever

beams in parallel. Further study reveals that these results remain valid as long as the joint connecting the two beams allows rotation about the x' -axis.

The analysis of this structure when the beams are fixed together is more complex. Equations (6.2) and (6.3) still hold because no displacements in the x or z direction occur. θ_{cy} and M_{cy} of equations (6.4) and (6.5) also still remain equal to zero. However, θ_{cx} and M_{cx} do not equal zero since the end point, C , is fixed to the end point of beam 2 which has a rotation about the x -axis when subjected to a vertical load. This rotation imparts a torsion load, M_{cx} , to beam 1 resulting in a rotation, θ_{cx} , of beam 1. Similarly, beam 1 imparts a torsion load, $-M_{cz}$ on beam 2. It is this torsion load on the beams that create an initially stiffer structure as shown in Figure 6.2.

The reaction loads, M_{Iy} and R_{Iy} in equations (6.6) and (6.7) are still valid. Summing moments about the x and z axes yield

$$M_{1x} + M_{cx} = 0 \quad (6.10)$$

$$M_{1z} + M_{cz} = -\frac{1}{2}F_y L \quad (6.11)$$

This structure is statically indeterminate to the second degree. The moments, M_{cx} and M_{cz} are chosen as the redundant reactions. By equating the rotations of the end point C of beams 1 and 2 due to the applied force, $F_y/2$, and the redundant reactions, the redundant

reactions may be solved. Each load is applied separately to each beam as shown in Figure 6.6. Compatibility equations and the principle of superposition are used to yield

$$(\theta_x)_1 + (\theta_x)_2 + (\theta_x)_3 = (\theta_x)_4 + (\theta_x)_5 + (\theta_x)_6 \quad (6.12)$$

$$(\theta_z)_1 + (\theta_z)_2 + (\theta_z)_3 = (\theta_z)_4 + (\theta_z)_5 + (\theta_z)_6 \quad (6.13)$$

where θ_x and θ_z are rotations about the x and z axes respectively. In terms of the applied loads given in Figure 6.6, these equations become

$$\frac{M_{cx}L}{GJ} = \frac{-\frac{1}{2}F_yL^2}{2EI} + \frac{-M_{cx}L}{EI} \quad (6.14)$$

$$\frac{\frac{1}{2}F_yL^2}{2EI} + \frac{M_{cz}L}{EI} = \frac{-M_{cz}L}{GJ} \quad (6.15)$$

Solving these equations for M_{cx} and M_{cz} yields

$$M_{cz} = M_{cx} = -\frac{1}{4}F_yL\left(\frac{GJ}{EI+GJ}\right) \quad (6.16)$$

Substituting Equation (6.16) into Equations (6.10) and (6.11) yield the reaction moments on beam 1:

$$M_{1x} = \frac{1}{4}F_yL\left(\frac{GJ}{EI+GJ}\right) \quad (6.17)$$

$$M_{1z} = \frac{1}{2}F_yL\left[\frac{1}{2}\left(\frac{GJ}{EI+GJ}\right) - 1\right] \quad (6.18)$$

Because torsion of the beams is also present, the cantilever beam linear stiffness relationship given in Equation (6.9) is not valid. Energy methods may be used to deter-

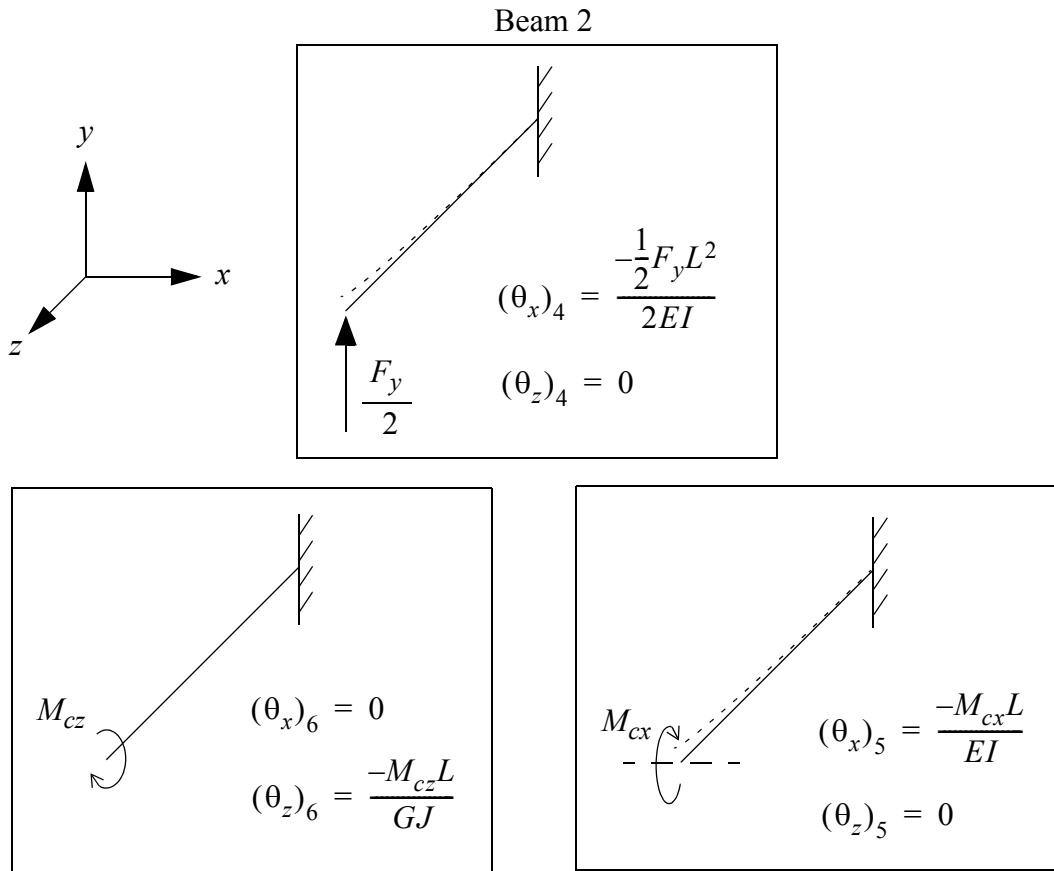
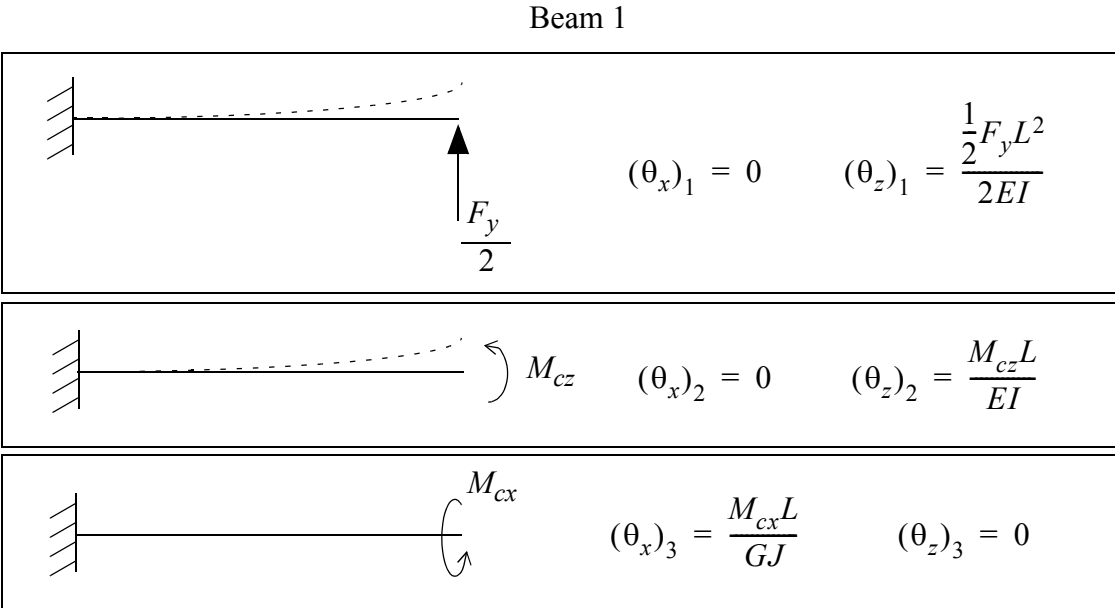


Figure 6.6 Deflections due to applied loads and redundant loads

mine the stiffness of this structure. Energy storage, U , may be expressed as a function of the internal moment and torsion of beam 1:

$$U = \frac{1}{2EI} \left[\int_0^L \left(M_{cz} + \frac{1}{2} F_y x \right)^2 dx \right] + \frac{1}{2GJ} \left[\int_0^L M_{cx}^2 dx \right] \quad (6.19)$$

Applying Castigliano's theorem gives us the deflection in the direction of the force $F_y/2$ by taking the partial derivative of the energy function with respect to the force $F_y/2$:

$$u_y = \frac{1}{EI} \left[\int_0^L \left(M_{cz} + \frac{1}{2} F_y x \right) \left(\frac{\partial \left(M_{cz} + \frac{1}{2} F_y x \right)}{\partial \left(\frac{1}{2} F_y \right)} \right) dx \right] + \frac{1}{GJ} \left[\int_0^L M_{cx} \frac{\partial M_{cx}}{\partial \left(\frac{1}{2} F_y \right)} dx \right] \quad (6.20)$$

Substituting Equation (6.16) into Equation (6.20) and solving yields

$$u_y = \frac{F_y L^3}{2EI} \left(\frac{1}{3} - \frac{1}{2} A + \frac{1}{4} A^2 \right) + \frac{F_y L^3}{2JG} \left(\frac{1}{4} A^2 \right) \quad (6.21)$$

where

$$A = \frac{GJ}{GJ + EI} \quad (6.22)$$

If the assumption that $b \gg h$ is made, then J for a thin walled section is $bh^3/3$ which is equivalent to $4I$. The shear modulus, G , may also be written in terms of E . Making these substitutions yields

$$A = \frac{2}{3 + \nu} \quad (6.23)$$

where ν is Poisson's ratio. The stiffness, k , of the mechanism is

$$k = \frac{2}{\frac{L^3}{2EI}\left(\frac{1}{3} - \frac{1}{2}A + \frac{1}{4}A^2\right) + \frac{L^3}{2JG}\left(\frac{1}{4}A^2\right)} \quad (6.24)$$

By assuming a Poisson's ratio of 0.3 and substituting Equation (6.23) into Equation (6.24), this equation simplifies to

$$k = 2\left(\frac{5.54EI}{L^3}\right) \quad (6.25)$$

This is nearly twice as stiff as the mechanism with the beams connected by a spherical joint or 2 cantilever beams acting in parallel. Equation (6.25) confirms the results given in Figure 6.2.

It should be noted that this solution is for the special case where α equals 90 degrees. When α is not equal to 90 degrees, the fixed joint case may be solved in the same manner, however the equations become very large with the addition of trigonometric terms to represent components of reaction loads and rotation angles.

6.4 Test Results

Two prototypes were made to compare with finite element analysis. The first prototype was made with polypropylene ($E = 200,000$ psi) and the second was made of steel ($E = 30$ Mpsi). The configuration of these prototypes are shown in Figure 6.7. The configuration of the physical prototype is slightly different because the beam elements as

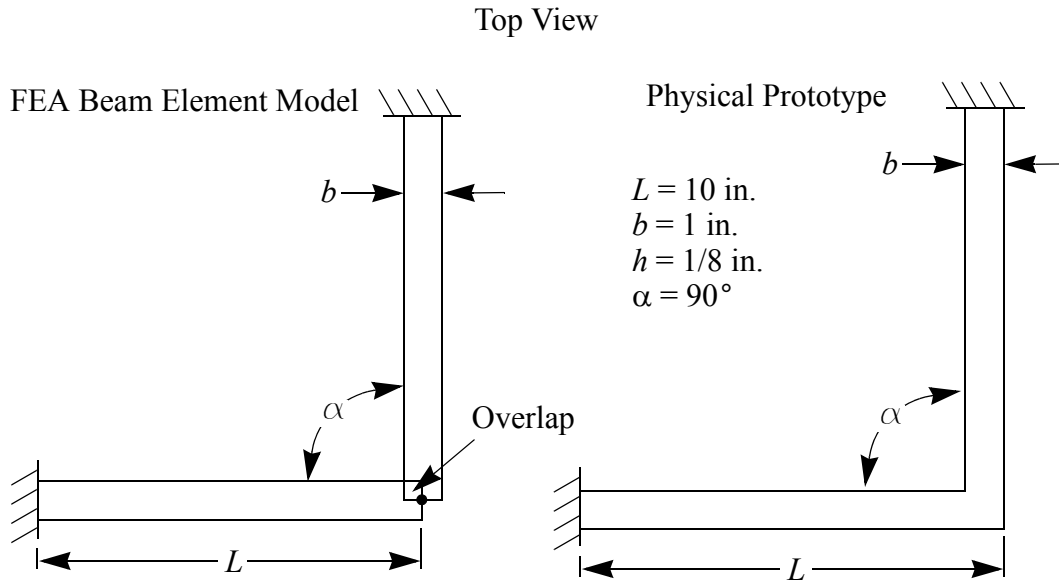


Figure 6.7 Physical prototype specifications

modeled in the FEA software causes an unrealistic overlap of material. An actual mechanism has a configuration more like that shown in Figure 6.7 and has dimensions as given in table x.x. Shell elements were used to more accurately model this configuration. Test data was gathered using a force transducer mounted on a linear positioning system. Data from three runs were averaged and the results are shown in Figure 6.8 with FEA shell element prediction results. The steel prototype has similar dimensions, however the actual width, b , is 1.02 inches and the actual height, h , is 0.022 inches. Test results for the steel prototype are also in close agreement with FEA predictions. These test results verify the

TABLE 6.1 Physical Test Prototype Specifications

Specification	Value
L	10 in.
b	1.0 in.
h	0.125 in.
α	90°

ability of the finite element model to predict stiffness in the non-linear deflection range and give confidence in using FEA for further studies in how this concept behaves.

6.5 Non-linear FEA Results

Linear deflections are characterized by the assumption that the path of the endpoint of the beam is a vertical translation only. For a single cantilever beam, large deflections result in a horizontal translation and non-linear stiffness characteristics. The path of the endpoint of a cantilever beam will trace an arc in the vertical plane through the beam axis. For the Compliant A-Arm mechanism, large deflections result in the path of the endpoint of the beam shown in Figure 6.3. Since this path does not match the natural path of the endpoint of a cantilever beam, a stress stiffening effect occurs as the second beam of the A-Arm design forces the first beam to follow this path and vice versa. This stress stiffening effect causes the non-linear stiffness results given in Figure 6.2. The reaction loads

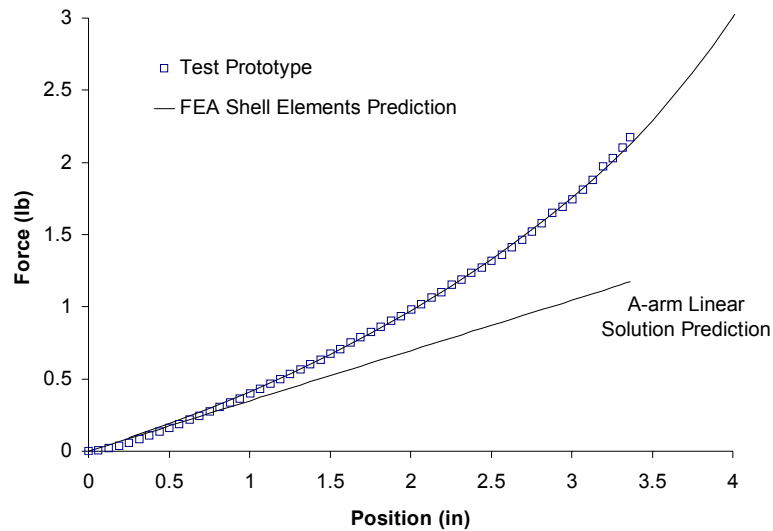


Figure 6.8 Plastic test prototype results

TABLE 6.2 Reaction Loads

Reaction Loads at Connection of Beam Ends (lbs, in-lbs)	Spherical Joint	Pin Joint x' axis	Fixed Connection
R_{Cx}	2.16	2.13	1.47
$F_y/2$	1.34	1.38	1.41
R_{Cz}	-2.16	-2.13	-1.47
M_{Cx}	0	0	-2.51
M_{Cy}	0	-2.30	0.32
M_{Cz}	0	0	-2.51
Reaction Loads at Fixed End of Beam 1 (lbs, in-lbs)	Spherical Joint	Pin Joint x' axis	Fixed Connection
R_{Ix}	-2.16	-2.13	-1.47
R_{Iy}	-1.34	-1.38	-1.41
R_{Iz}	2.16	2.13	1.47
M_{Ix}	7.14	7.01	6.86
M_{Iy}	-16.76	-14.31	-11.81
M_{Iz}	-3.23	-3.73	-4.18
Endpoint Deflection (in, radians)	Spherical Joint	Pin Joint x' axis	Fixed Connection
δ_x	-1.17	-1.09	-1.07
δ_y	4	4	4
δ_z	-1.17	-1.09	-1.04
θ_x	-0.35	-0.51	-0.56
θ_y	0.05	0	0
θ_z	0.65	0.60	0.56

and deflections of the endpoint, C , of the mechanism were analyzed to better understand this stress-stiffening effect. At a deflection of 4 inches in the y direction, the beam element model gives the results shown in Table 6.2 for reaction loads at the beam connection and at the fixed end of the beam. Table 6.2 also gives deflections of the endpoint of the beam.

6.5.1 Reaction Loads, Deflections, and Stress

In order for the end point of the beam to follow the path shown, the second beam imposes force loads, R_{cx} and R_{cz} , in the x and z direction for the different joint configurations. The fixed joint configuration also imposes additional moment loads on the end of the beam. Because of the deflection at the endpoint of the beam, the forces on the endpoint of the beam result in higher reaction moments at ground. M_{Ix} represents a torsion reaction. If $b > h$, M_{Iz} represents a bending moment reaction about the beam's flexible axis and M_{Iy} represents a bending moment reaction about the beam's stiff axis. The spherical joint connection experiences higher reaction forces, R_{cx} and R_{cz} , at the joint and also slightly higher reaction moments, M_{Ix} and M_{Iy} , at ground. The beams experience a complex loading condition of bending about both axes and torsion of the beam. The motion of the beam is somewhat facilitated by twisting of the beam.

It is reasonable to assume the largest stress in the beams occurs at the fixed portion of the beam where it is attached to ground. Stress may be directly calculated from the internal forces, moments and torsion of the beam. Finite element results verify that the maximum forces, moments and torsion occur at ground. Maximum axial stress at ground, σ_x , is calculated from bending stress:

$$\sigma_x = \frac{6M_{Iz}}{bh^2} + \frac{6M_{Iy}}{b^2h} \quad (6.26)$$

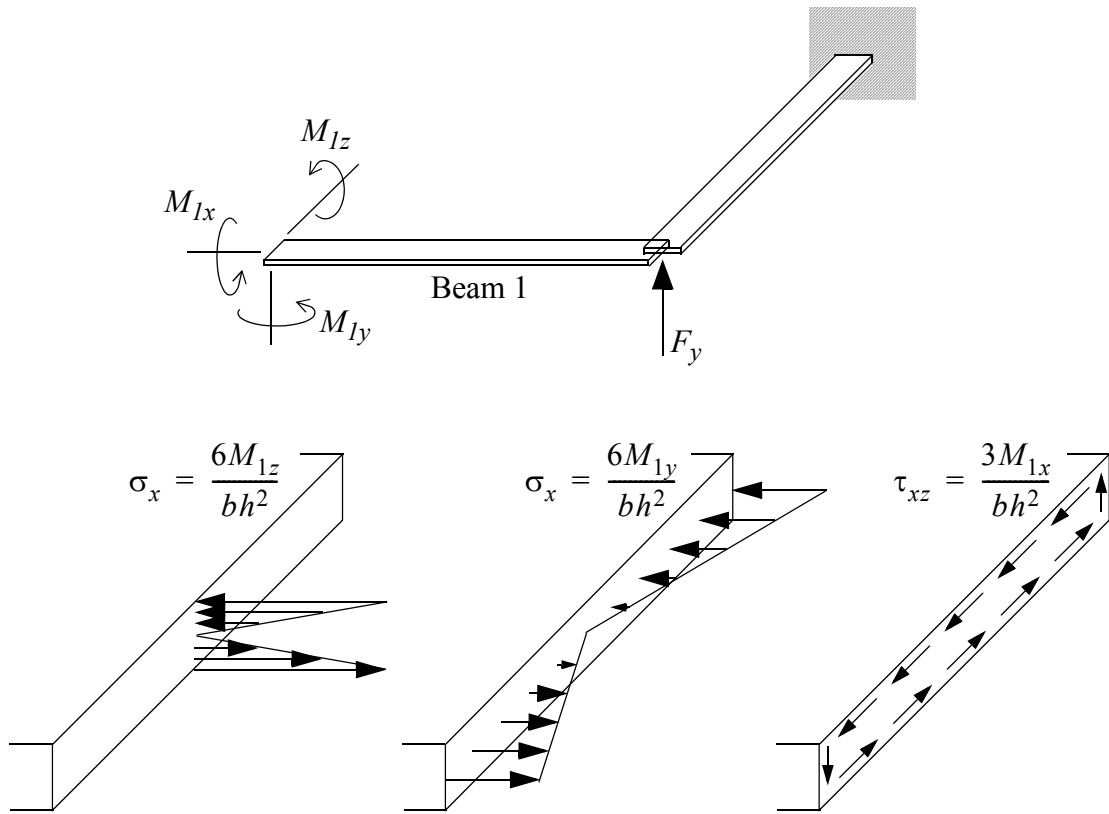


Figure 6.9 Stress distribution at the base of the beam

Stress due to axial loads may be neglected. Shear stress at the fixed portion of the beam, τ_{xy} , is calculated from torsional shear stress of a thin-walled open section as

$$\tau_{xz} = \frac{3M_{1x}}{bh^2} \quad (6.27)$$

This assumes the beam is allowed to warp at this connection and that $b \gg h$. Direct shear may also be neglected. The stress distribution at this location is shown in Figure 6.9. The von Mises stress for this two-dimensional stress state is given by:

$$\sigma' = \sqrt{\sigma_x^2 + 3\tau_{xy}^2} \quad (6.28)$$

The maximum von Mises stress for these results are 3,133, 3,150, and 3,150 psi respectively. This maximum stress will be located at the bottom outside corner of the base of the beam. In reality, torsional shear stress, τ_{xy} , is only at a maximum at the outer fibers at the midpoint of the width of the beam. The shear stress falls off to zero at the corner. This estimation of the von Mises equivalent stress is conservative because it over predicts the stress state at this location. If warping of the beam is restrained at this location, shear stress may be neglected, but high axial reaction forces develop in the region of the corners to restrain the warping. These high axial forces would result in a higher stresses than for the case above.

The specific volume efficiency, η , compares the energy storage per unit volume at a given stress to the energy storage capacity of a rod in tension. The specific volume efficiency may be calculated as

$$\eta = 2\left(\frac{U}{V}\right)\left(\frac{E}{\sigma'_{max}{}^2}\right) \quad (6.29)$$

where σ'_{max} is the maximum von Mises stress. The specific volume efficiency for the configurations given in Table 6.2 at a deflection of 4 inches are 1/16.5, 1/15.3, 1/14.5 respectively. These configurations have similar stress levels at this deflection, yet the energy storage in the fixed joint configuration is greater because of a higher initial stiffness which results in a higher specific volume efficiency.

6.6 Non-Linear Stiffness and Stress Predictions

A closed-form linear solution was given for stiffness. A mathematical model does not yet exist to predict stiffness in the non-linear range. The force-deflection prediction and reaction forces are also needed to predict stresses. Finite element analysis is needed to predict the stiffness and stress for non-linear deflections.

A parameter study was completed to study how the parameters listed above affect the characteristics of the mechanism. It was decided to study the fixed joint configuration because this configuration has a higher specific volume efficiency and does not include unnecessary joints. The effect of the physical parameters on the following mechanism characteristics were studied:

- stiffness k
- force-deflection curve
- maximum von Mises stress σ'_{max}
- energy storage U
- specific volume efficiency η
- degree of stiffness non-linearity

The FEA beam model explained previously was used for this analysis. Twenty load steps were applied with the final vertical deflection load being 75% of L' . This results in an equivalent pseudo-rigid-body angle, Θ , of 62 degrees as shown in Figure 6.3 for all configurations of α and L . The stiffness, k , is calculated with a backwards difference numerical derivative. Energy storage, U , is calculated by the trapezoidal area approximation numerical integration technique. Since only comparisons are made, these simple numeri-

cal techniques are adequate. Of particular interest is the specific volume efficiency, η , because it is desirable to find those designs that increase the specific volume efficiency.

The degree of stiffness non-linearity may be measured for comparison purposes by the ratio of the final stiffness at a given deflection, k_f , to the initial linear stiffness, k_i . For the fixed configuration example shown in Figure 6.2, at a deflection of 4 inches this ratio, k_f , is 4.3. Another measure of the non-linear stiffness characteristic is the ratio of energy storage of the mechanism at a given deflection to the energy storage at that deflection predicted by a linear stiffness relationship at the initial stiffness, k_i . For the fixed configuration example shown in Figure 7.2, at a deflection of 4 inches this ratio is 1.53.

A full factorial design of experiments study was performed with the FEA beam model. Young's modulus, E , was set to be 200,000 psi, and Poisson's ratio, ν , was set to be 0.4. The variables: b , h , L , and α ; were allowed to vary between: 5 and 15 inches for L , 0.5 and 3 inches for b , 0.05 and 0.3 inches for h , and 0 and 90 degrees for α . Equations (6.25) and (6.27) assume $b \gg h$. Since b/h has a minimum value of 1 in this study, the value for J and τ_{xy} is calculated by those formulas given in [39].

The important findings of this study are determining the importance of certain factors and finding the trends. The length, L , has little effect on the specific volume efficiency. The angle between the beams, α , has the largest effect and tends to decrease the specific volume efficiency. The beam width and height, b and h , also have a significant effect. A wide and thin beam will increase specific volume efficiency. The interaction

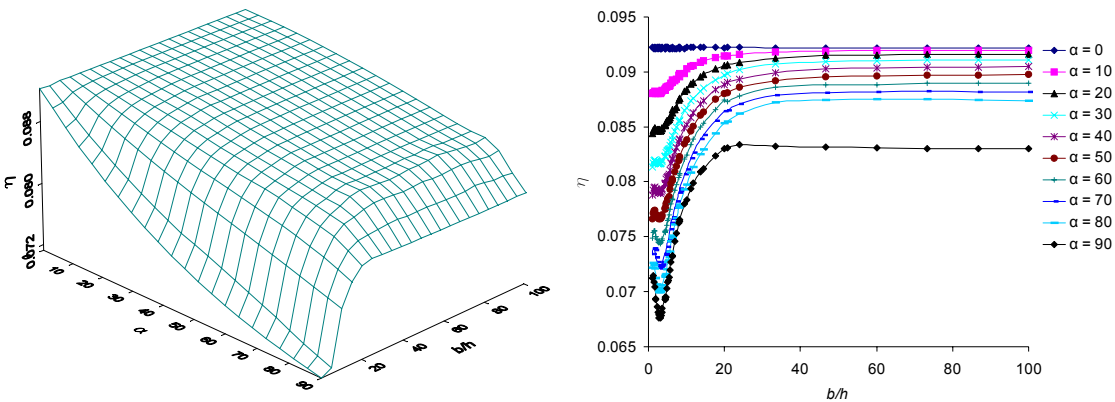


Figure 6.10 Specific volume efficiency, η , at a maximum deflection:
 $\Theta = 0.8$ radians

between b , h , and α is also significant as b and h have little to no effect at low values of α and have the most effect at high values of α .

A further design of experiments was completed with only the variables α , b , and h . The specific volume efficiency was computed at a deflection of $\Theta = 0.79$ radians (45 degrees) and is plotted as a function of the aspect ratio, b/h , and A-Arm angle, α shown in Figure 6.10. The specific volume efficiency decreases as α increases, and decreases as the aspect ratio decreases and sharply decreases as the aspect ratio falls below 10. This data is useful for understanding the trends of how η changes with different configurations.

The specific volume efficiency also changes as the deflection in the A-Arm changes. Figure 6.11 shows η as a function of the deflection, Θ , for various configurations. This shows a general decrease in η as deflection increases for the different configurations. However, the curves are not similar as the aspect ratio changes. Hence, the

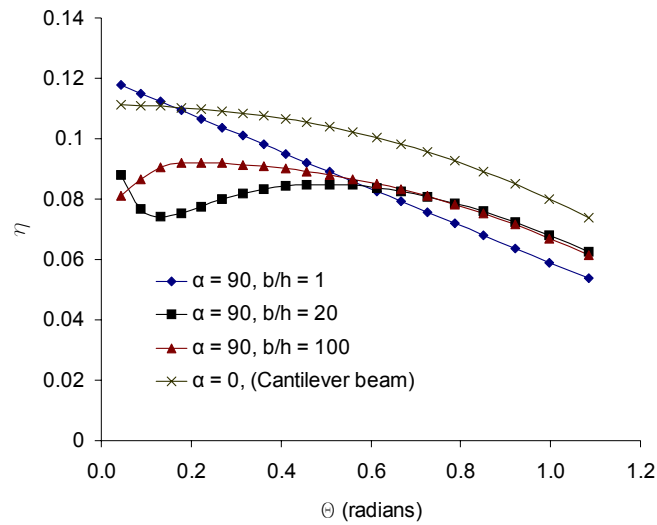


Figure 6.11 Specific volume efficiency, η , as a function of Θ

specific volume efficiency of any one design depends on the configuration and the deflection at maximum stress.

Results for the effect on k_r are similar. L has little to no effect, while α has the most effect and k_r increases as α increases. The parameters b and h also have a significant effect. Increasing b and decreasing h tends to increase k_r . These results are important in developing a suitable model to predict the force deflection curve of a given design. Only α , b , and h have an effect on the non-linear behavior of this curve.

6.6.1 Pseudo-Rigid-Body Model

The pseudo-rigid-body model of a cantilever beam models the deflection of the end of a cantilever beam with a pseudo-rigid link and the stiffness with a linear torsional

spring placed at the pseudo-joint. The torsional spring constant for a cantilever beam is based on a linear approximation of the non-dimensionalized transverse load index, $(\alpha^2)_t$:

$$(\alpha^2)_t = \frac{F_t L^2}{EI} = K_{\Theta} \Theta \quad (6.30)$$

where K_{Θ} is the linear approximation of $(\alpha^2)_t$ as a function of the pseudo-rigid-body angle, Θ . F_t is the transverse load or the load component that is normal to the pseudo-rigid link. A similar non-dimensionalized transverse load index is given for the compliant A-Arm design and is based on the linear stiffness solution:

$$(\alpha^2)_t = \frac{F_t (L')^2 \left(\frac{M}{EI} + \frac{N}{JG} \right)}{\left(\cos\left(\frac{\alpha}{2}\right) \right)^3} \quad (6.31)$$

where for $\alpha = 90^\circ$, M and N are

$$M = \frac{1}{3} - \frac{1}{2}A + \frac{1}{4}A^2 \quad (6.32)$$

$$N = \frac{1}{4}A^2 \quad (6.33)$$

where A is given by Equation (6.22). Note that M and N are non-dimensional variables representing the two terms within the parantheses in Equation (6.21) respectively. When α is not equal to 90 degrees, these two terms are also functions of α and are given in the appendix. Figure 6.12 plots this non-dimensionalized transverse load index, $(\alpha^2)_t$, versus the pseudo-rigid-body angle, Θ , for a vertical load at the tip of the A-Arm with α between

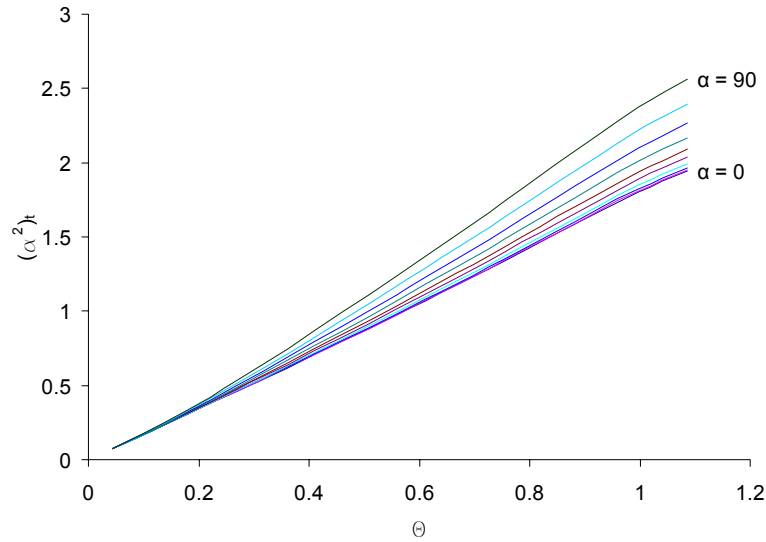


Figure 6.12 Non-dimensionalized transverse load index, $(\alpha^2)_t$, versus Θ for α between 0 and 90 degrees

0 and 90 degrees and the specifications given in Table 6.1. The selection of the terms in Equation (6.31) makes the initial slope of each line identical and is equal to the value of K_Θ , 1.76, for a cantilever beam. This value is different than 2.65 reported in [28] for a cantilever beam because of the different factors present in Equation (6.31) for the compliant A-Arm than in Equation (6.30) for a cantilever beam.

At larger values of α , the line transitions from an initial slope of 1.76 to a second line that is linear but with an increased slope. Figure 6.13 shows an example of two different linear curve fits when b/h is equal to 8. It also is noted that the slopes of these lines are functions of α and the cross-section of the beam represented by the dimensionless coefficient, b/h , as demonstrated in Figure 6.14. These curves may also be characterized with

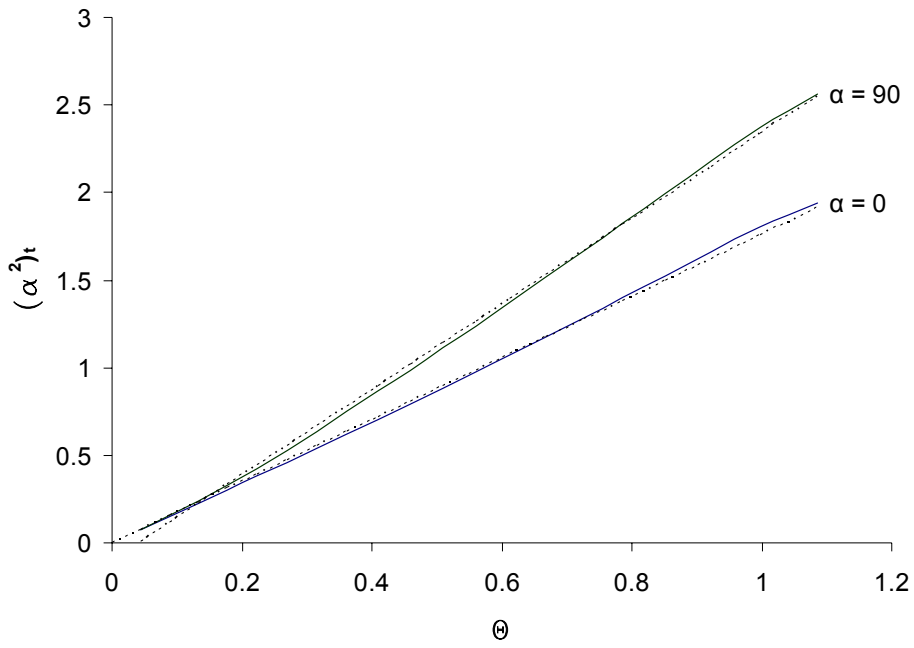


Figure 6.13 Linear curve fits for $b/h = 8$

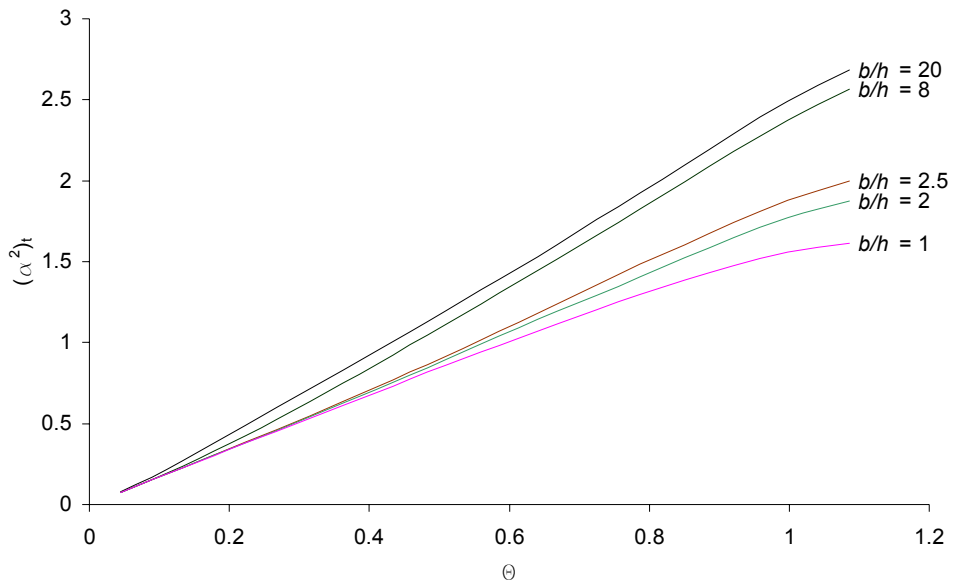


Figure 6.14 Non-dimensionalized transverse load factor versus Θ for different values of b/h and $\alpha = 90$ degrees

an initial linear fit that transitions to a second linear fit. The equations describing the two curve fits in Figure 6.13 are

$$(\alpha^2)_t = K_{\Theta} \Theta \quad \Theta < \phi \quad (6.34)$$

$$(\alpha^2)_t = (K_{\Theta} + K_{\Theta c}) \Theta - K_{\Theta c} \phi \quad \Theta > \phi \quad (6.35)$$

where ϕ is the value at which the curve makes the transition from the initial slope, K_{Θ} , to a final slope, $K_{\Theta} + K_{\Theta c}$. Setting $\phi = 0.15$ radians yields good linear fits for different values of α and b/h , especially at higher values of α and b/h where $K_{\Theta c}$ is the largest. The initial stiffness coefficient, K_{Θ} , is equal to 1.76. The stiffness coefficient correction, $K_{\Theta c}$, is a function of α and b/h .

A design of experiments of the FEA beam model was run at various values of α and b/h . Linear regression was used based on Equation (6.35) to determine $K_{\Theta c}$ for each configuration. Since the curves in Figure 6.14 show deviation from linearity as Θ approaches 1 radian and higher, linear regression was used to fit only the data points from $\Theta = \phi$ (0.15 radians) to $\Theta = 0.79$ radians (45 degrees). The A-Arm angle, α , was allowed to vary between 0 and 90 degrees and the ratio b/h , was allowed to vary between 1 and 100. The values for $K_{\Theta c}$ are shown in Figure 6.15 as a plot of data points and in Figure 6.16 as a surface plot. These two plots give a good representation of the effect that the two parameters, α and b/h , have on the stiffness coefficient. At higher values of b/h ($b/h > 10$), b/h has little effect while increasing α increases $K_{\Theta c}$ at these higher values. At lower values for b/h ($b/h < 10$), b/h and α have strong effects and a strong interaction effect. At

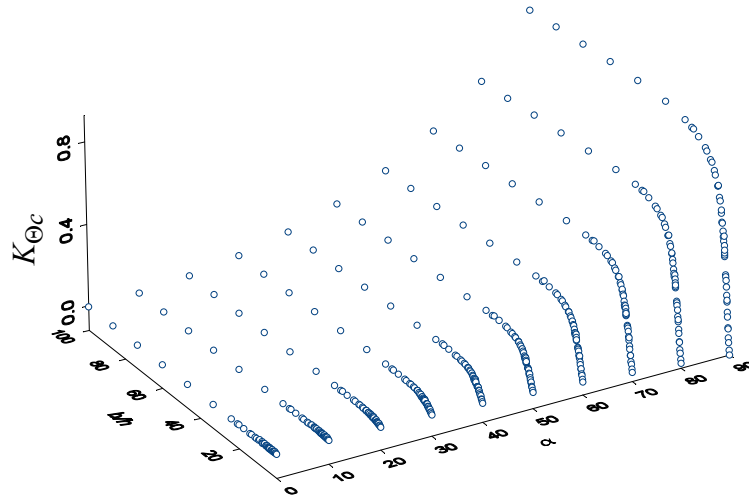


Figure 6.15 $K_{\Theta c}$ data points

low values of α , b/h has no effect while at high values of α , b/h has an effect of increasing $K_{\Theta c}$. Figure 6.17 presents other graphs that depict these trends in 2 dimensional plots. Since an accurate fit of the surface shown in Figure 6.16 is complex and difficult to create, the plots shown in Figure 6.17 are more useful in determining the stiffness coefficient for design purposes.

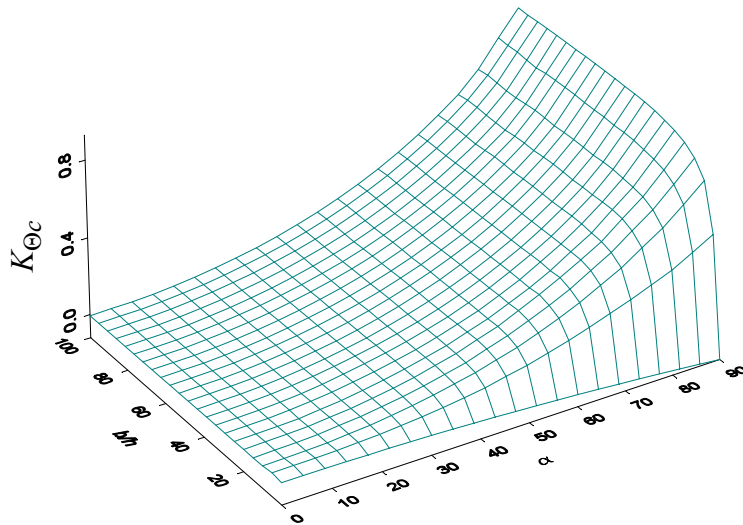


Figure 6.16 $K_{\Theta c}$ surface plot

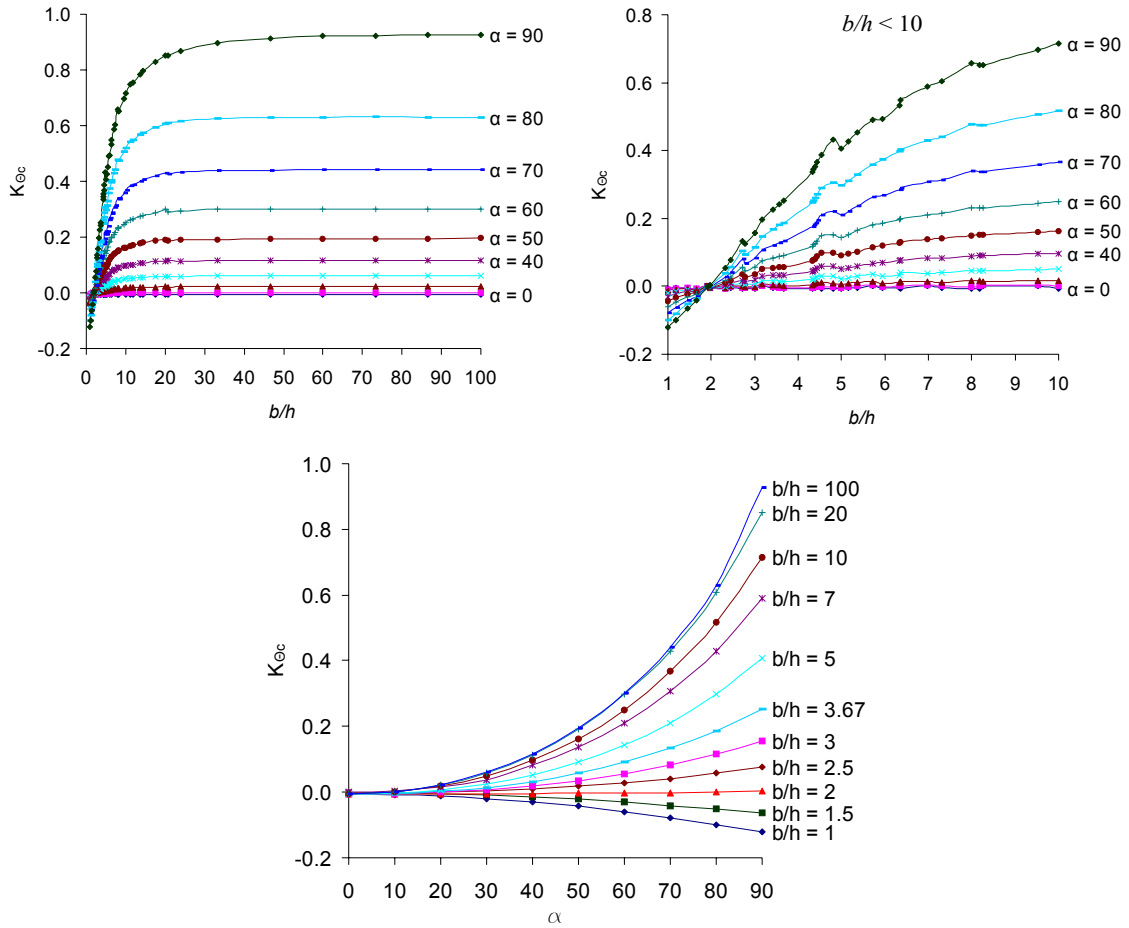


Figure 6.17 2-D plots of K_{Θ_c} .

From these plots, it can be seen that b/h has little to no effect at $b/h > 20$. This range can be characterized by a curve fit which is more useful for design than the plots:

$$\begin{aligned}
 K_{\Theta_c} = & -2.1969 \times 10^{-3} \alpha + 2.1054 \times 10^{-4} \alpha^2 \\
 & -2.9769 \times 10^{-6} \alpha^3 + 2.4182 \times 10^{-8} \alpha^4; \\
 & b/h \geq 20
 \end{aligned}
 \tag{6.36}$$

The data points for $b/h < 10$ are not very smooth. This may be explained by the presence of a lurking variable not present in the model above. The data suggests that the parameters b/L and/or h/L may have some small effect which causes the choppy data shown. How-

ever, this effect is negligible in comparison to the parameters present in the model. These data curves may be smoothed for use in design.

The plot shown in the upper right hand corner of Figure 6.17 shows that the different curves all converge to one point at $b/h = 1.9$. For this value of b/h , any value of α will result in the stiffness coefficient correction term, $K_{\Theta c} = 0$. This unique point is significant because it results in a simple linear fit of the non-dimensionalized transverse load index, $(\alpha^2)_t$. Equation (6.35) for $\Theta > \phi$ reduces to Equation (6.34) for all Θ . This results in a torsional spring constant, K , for the pseudo-rigid-body model that is not a function of Θ . This is a simplification of the torsional spring constant for the general compliant A-Arm pseudo-rigid-body model which is derived in the following pages.

The trends explained and shown here for the stiffness coefficient correction term, $K_{\Theta c}$, should not be confused with the effect that the parameters α and b/h have on the overall stiffness of the A-Arm. The stiffness of the A-Arm may be calculated by the torsional spring torque, T , given by

$$T = K\Theta \quad (6.37)$$

This torque may also be expressed as a function of the transverse load, F_t , multiplied by the moment arm:

$$T = F_t \gamma L' \quad (6.38)$$

Combining Equations (6.37) and (6.38) and solving for F_t yields

$$F_t = \frac{K\Theta}{\gamma L'} \quad (6.39)$$

Substituting Equation (6.39) into Equation (6.31) yields

$$(\alpha^2)_t = \frac{K\Theta L' \left(\frac{M}{EI} + \frac{N}{JG} \right)}{\gamma \left(\cos\left(\frac{\alpha}{2}\right) \right)^3} \quad (6.40)$$

Substituting Equation (6.40) into Equations (6.34) and (6.35) gives

$$\frac{K\Theta L' \left(\frac{M}{EI} + \frac{N}{JG} \right)}{\gamma \left(\cos\left(\frac{\alpha}{2}\right) \right)^3} = K_{\Theta} \Theta \quad \Theta < \phi \quad (6.41)$$

$$\frac{K\Theta L' \left(\frac{M}{EI} + \frac{N}{JG} \right)}{\gamma \left(\cos\left(\frac{\alpha}{2}\right) \right)^3} = (K_{\Theta} + K_{\Theta c}) \Theta - K_{\Theta c} \phi \quad \Theta > \phi \quad (6.42)$$

Solving for the torsional spring constant, K , and simplifying yields

$$K = \frac{\left(\cos\left(\frac{\alpha}{2}\right) \right)^3}{L' \left(\frac{M}{EI} + \frac{N}{JG} \right)} \gamma K_{\Theta} \quad \Theta < \phi \quad (6.43)$$

$$K = \frac{\left(\cos\left(\frac{\alpha}{2}\right) \right)^3}{L' \left(\frac{M}{EI} + \frac{N}{JG} \right)} \gamma \left(K_{\Theta} + K_{\Theta c} - \frac{K_{\Theta c} \phi}{\Theta} \right) \quad \Theta > \phi \quad (6.44)$$

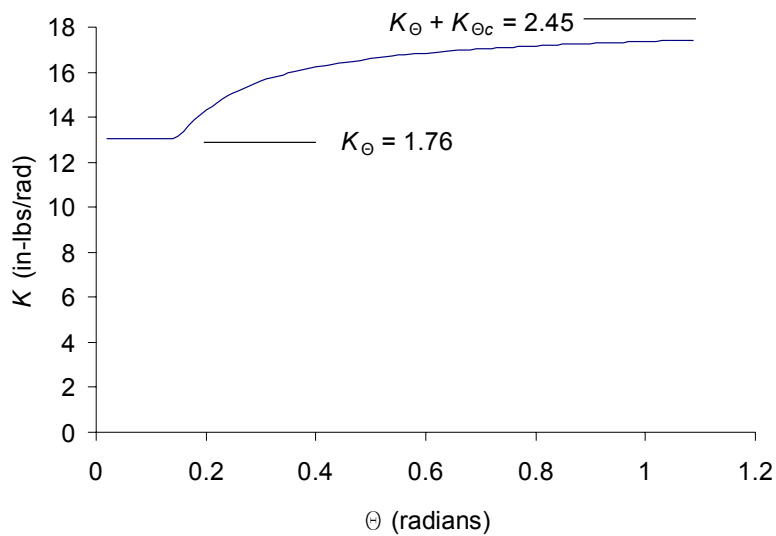


Figure 6.18 Torsional spring constant, K , for $b/h = 20$ and $\alpha = 60$ degrees

When $\Theta < \phi$, the torsional spring has constant stiffness, K . This is not the case for Equation (6.42) where $\Theta > \phi$. The right side of this equation is the second linear fit of $(\alpha^2)_t$ which is shifted vertically downwards by the constant term, $K_{\Theta c}\phi$. This creates a term in Equation (6.44) that is inversely proportional to Θ . The torsional spring, K , is not constant as it is in the pseudo-rigid-body model for a cantilever beam, but is a function of Θ , as demonstrated in Figure 6.18 for $b/h = 20$ and $\alpha = 60$ degrees. The stiffness coefficient correction, $K_{\Theta c}$, is actually a representation of the increase or decrease of the initial stiffness of the mechanism as it is deflected and not a representation of relative stiffness of different configurations. The relative stiffness of different configurations may be compared using Equation (6.43).

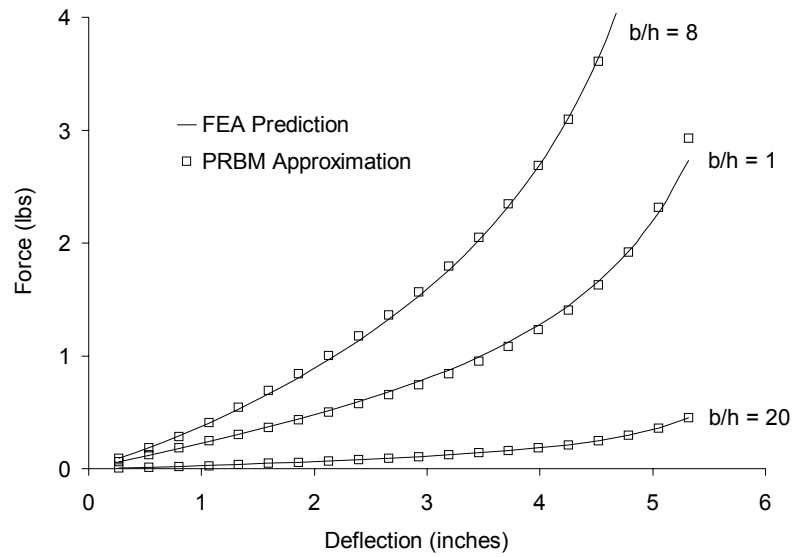


Figure 6.19 Force deflection predictions from FEA model and PRBM at different b/h values and $\alpha = 90$ degrees

The torsional spring constant, K , given by Equations (6.43) and (6.44) may be substituted into Equation (6.39) to predict the force-deflection relationship of the mechanism. Figure 6.19 compares the force-deflection predictions using this model and predictions using FEA for different b/h values and $\alpha = 90$ degrees.

6.6.1.1 Pseudo-Rigid-Body Model Stiffness Error

The error in this model may be characterized by comparing $(\alpha^2)_t$, predicted by the model in Equations (6.34) and (6.35) and $(\alpha^2)_t$ calculated from force data output by FEA as shown in Figure 6.13. The maximum error at any given Θ for the configurations explored is 25%. However, this error is highly localized in the transition phase from the first linear fit to the second linear fit of $(\alpha^2)_t$. Outside of this region, the error between the linear fits given by the pseudo-rigid-body model and the FEA prediction of $(\alpha^2)_t$ is generally only 3-

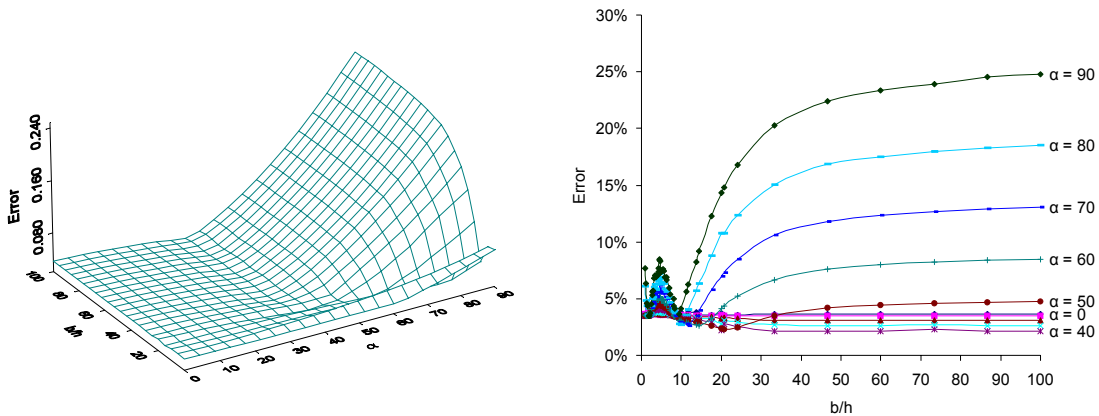


Figure 6.20 Maximum error at any give Θ between $(\alpha^2)_t$ predicted by pseudo-rigid-body model and FEA model

5%. The maximum error generally increases at higher values of α and b/h as shown by the surface plot shown in Figure 6.20. Optimization could be performed to determine a better value for ϕ , which would minimize this error.

6.6.1.2 Pseudo-Rigid-Body Model Conclusions

The pseudo-rigid-body model developed here models the motion and stiffness of the compliant A-Arm as a rigid link with a torsional spring at the pseudo joint. This assumes that the free end of the A-Arm is free to rotate. This necessitates the use of a pin joint placed at the tip of the A-Arm whose axis is parallel to the z' axis of the A-Arm. This allows the compliant A-Arm to be used for any fixed-pinned segment in a 2-dimensional compliant mechanism, especially where out-of plane stiffness is needed.

The developed model is more complex than the pseudo-rigid-body model for a cantilever beam in modeling stiffness. However, once coded this model is a useful initial design tool for deflection and stiffness predictions. The user should understand the nature

of the error as shown in Figure 6.20. This model also assumes an idealized beam model as shown in Figure 6.1 which only approximates an actual configuration as shown in Figure 6.7. After the initial design it is recommended to do finite element analysis for further force-deflection and stress predictions. The model given also does not help in making stress predictions because the reaction loads at the base of the beam are not known. This can make initial design work with the pseudo-rigid-body model difficult as it is desirable to know the stress state of the mechanism while developing a suitable force-deflection curve for the suspension.

6.7 Compliant A-Arm Suspension Design

This section illustrates the use of the pseudo-rigid-body model developed previously and finite element tools for the design of a suspension system utilizing compliant A-Arms. The compliant A-Arm may be used as a control arm in the suspension mechanism much like the rigid link A-Arms are used in the double A-Arm suspension. It may replace any of the fixed-pinned segments shown in Figure 4.2 for a four-bar mechanism or replace the lower arm of the McPherson strut mechanism shown in Figure 4.3. A spherical joint placed at the tip of the A-Arm allows it to replace two links in a spatial mechanism such as the bottom two links shown of the spatial mechanism shown in Figure 4.5.

As an example, a four-bar mechanism with two fixed-pinned segments, as shown in Figure 6.21, is chosen as a suspension mechanism. This mechanism uses two compliant A-Arms as a lower and upper control arm pinned to the wheel carrier or coupler link.

Design specifications are given for a possible suspension for a light golf cart type vehicle.

The suspension has the following specifications at each wheel:

- Wheel rate $k = 100$ lbs/in
- Design load $P = 200$ lbs
- Clearance at design load $y_c = 2.5$ inches
- Maximum length, $L' = 12$ inches
- Maximum stress at full deflection, $S_{max} = 200$ ksi

Since this configuration uses two parallel A-Arms, the deflection of one A-Arm will be equal to the deflection of the other. This simplifies the modeling of this mechanism as two compliant A-Arms acting as springs in parallel. If the arms were not parallel, a method such as virtual work could be used to determine force-deflection results for this mechanism. It is also assumed that these two A-Arms are identical. This further simplifies the modeling to one compliant A-Arm with

- Spring rate, $k_1 = k_2 = 50$ lbs/in
- Design load, $P_1 = P_2 = 100$ lbs
- Clearance at design load, $y_c = 2.5$ inches
- Maximum length, $L' = 12$ inches
- Maximum stress, $S_{max} = 200$ ksi

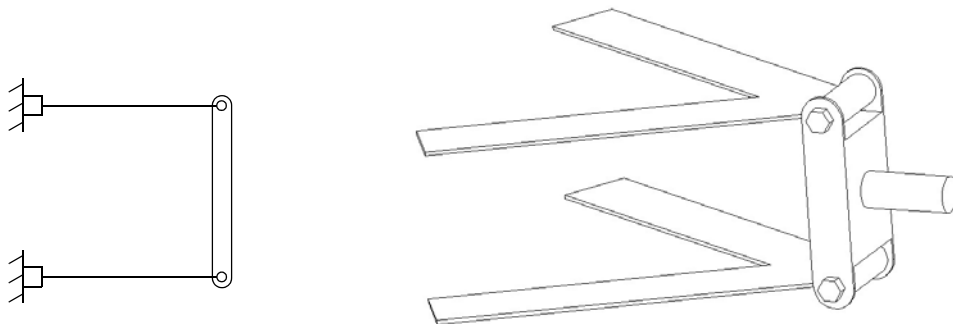


Figure 6.21 Double compliant A-Arm mechanism

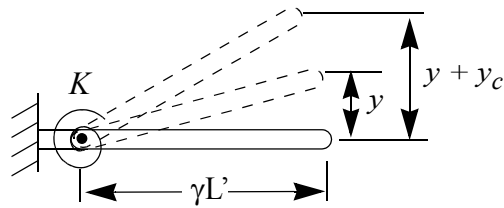


Figure 6.22 Pseudo-rigid-body model of suspension compliant A-Arm at design load deflection, y , and at maximum deflection, $y + y_c$.

The two arms acting together will give the necessary spring rate, $k_1 + k_2 = k$, and load, $P_1 + P_2 = P$. The pseudo-rigid-body model displayed in Figure 6.22 with torsional spring, K , given by Equations (6.43) and (6.44) is used to model the force-deflection relationship of this A-Arm. It is useful to code this model in a spreadsheet or other program to yield a force-deflection curve. The spring rate may also be plotted on the same graph shown in Figure 6.23. This shows the initial deflection, y , at the design load, P . The maximum deflection is equal to the initial deflection, y , plus the clearance at design load, y_c . Since α , b , and h are the remaining design variables and there are only two constraint equations,

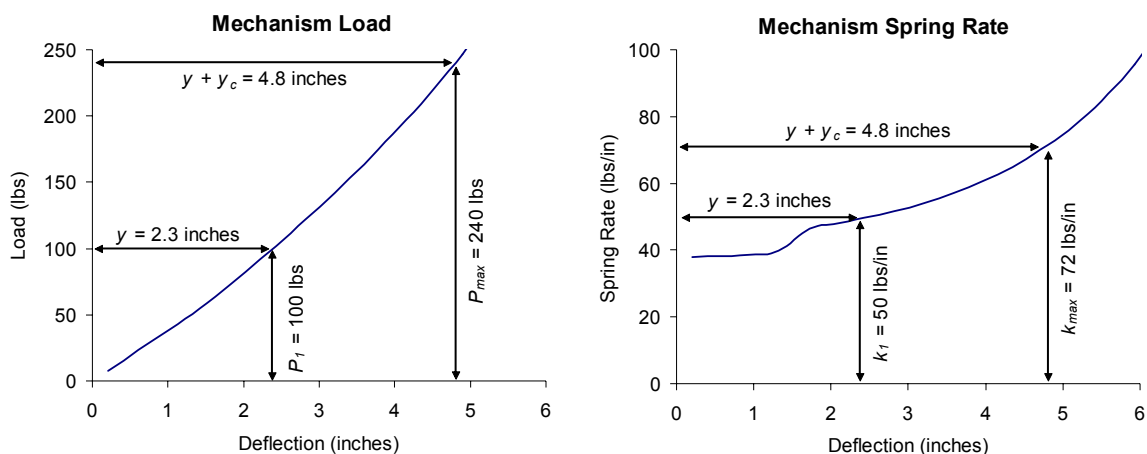


Figure 6.23 Pseudo-rigid-body model predictions of mechanism load and spring rate

spring rate and maximum stress, there are potentially many solutions to the above design specifications. The initial selection of α limits the solutions to a single point design, although the process is still iterative to find values for b and h . The following procedure may be used to converge upon a solution. Values for the example problem are also given.

1. Select α to fit vehicle space requirements (note: increasing α generally increases the value of $K_{\Theta c}$ which represents the degree to which the torsional spring constant K , increases as the A-Arm is deflected.)
 - $\alpha = 60$ degrees
2. Select values for b and h that meet the spring rate at a given design load specifications given.
 - $b = 2.5$ inches
 - $h = 0.125$ inches
3. Adjust the value for $K_{\Theta c}$ shown in the charts in Figure 6.15.
 - $K_{\Theta c} = 0.3$
4. Repeat steps 2 and 3 and if necessary 1, to meet spring rate at design load specifications. Stress cannot be determined at this stage as reaction loads are not known. Maximum stress may be estimated by placing half of the maximum load at the maximum deflection on the end of a cantilever beam with the same b , h , and L specifications for the A-Arm. This is a conservative prediction as it overpredicts the stress predicted by FEA. This overprediction generally increases as α increases and rises to as much as twice the stress predicted by FEA.
5. Run FEA beam model to check force-deflection curve and determine stress state at maximum deflection.

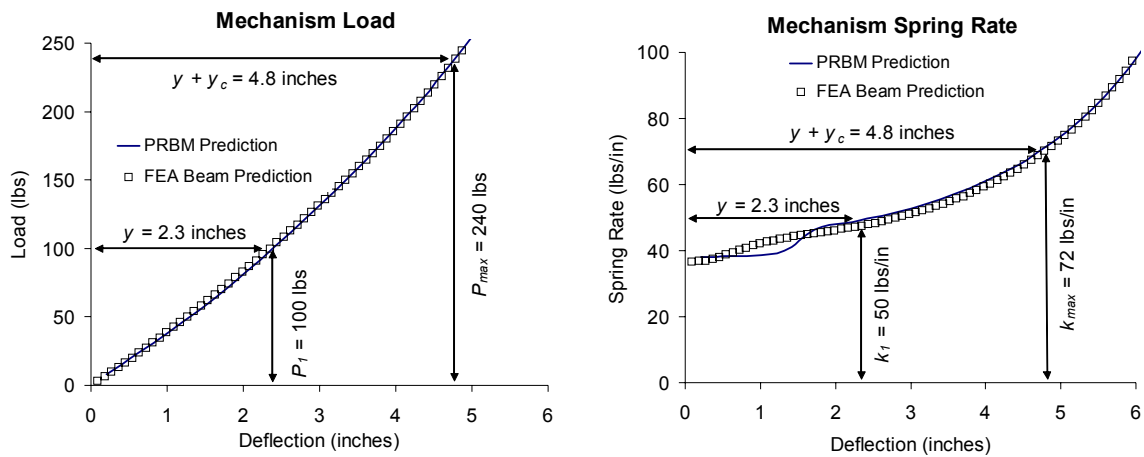


Figure 6.24 FEA beam model and pseudo-rigid-body model predictions

- FEA beam model outputs a force deflection curve shown in Figure 6.24.
- The maximum stress may be found at a maximum deflection of 4.8 inches. This is found by adding y_c , 2.5 inches, to the deflection at design load P , 2.3 inches:

$$2.3 + 2.5 = 4.8 \text{ inches} \quad (6.45)$$

The von mises stress state may be found by determining the reaction moments at the base of the beam and applying Equations (6.26), (6.27), and (6.28). ($M_x = 907$ in-lbs, $M_y = 1231$ in-lbs, $M_z = 962$ inch-lbs)

$$\sigma' = 196.1 \text{ ksi} \quad (6.46)$$

6. Repeat steps 1-5 as necessary to meet stiffness and stress requirements.

Increasing b while decreasing h will maintain stiffness and lower maximum stress.

7. Run FEA shell element model that accurately models A-Arm geometry when manufactured. The geometry shown in Figure 6.25 was chosen to allow attachment of a

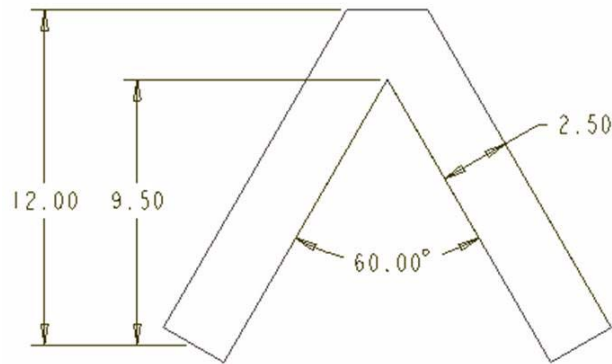


Figure 6.25 Compliant A-Arm geometry

joint to the tip of the A-Arm. Shell element force-deflection results are shown in Figure 6.26.

8. Adjust values of b , h , and α to give spring rate at design load specifications for actual geometry in shell element model.

This process may require many iterations because the initial stress data is not known, error exists in the pseudo-rigid-body model, and these models are only an approx-

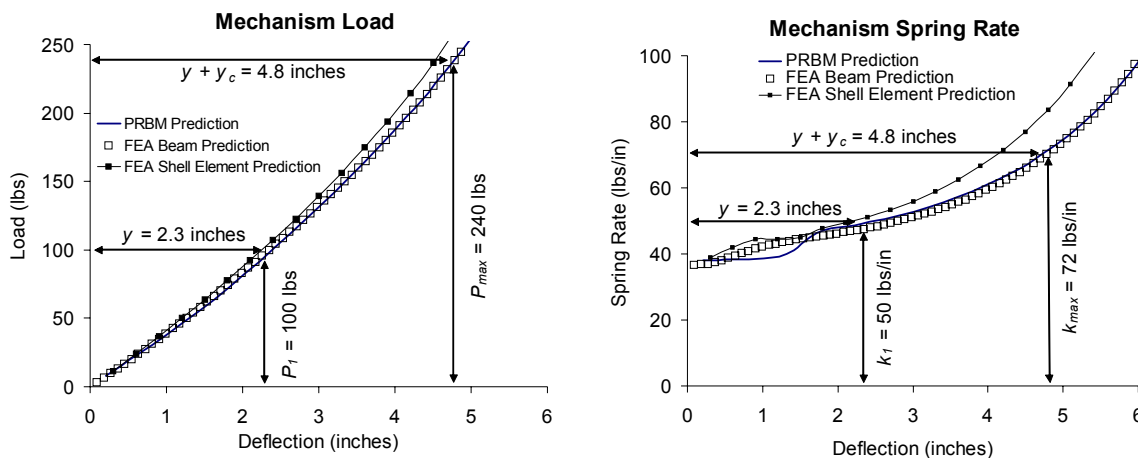


Figure 6.26 FEA shell element model predictions

imation of actual A-Arm geometry. Although these errors exist, the models developed are a useful tool for the design of a compliant A-Arm used in a suspension.

6.8 Conclusion

In conclusion, the characteristics of the compliant A-Arm have been explored. This configuration experiences a non-linear force-deflection relationship with a rising spring rate characteristic. A pseudo-rigid-body model has been developed to approximate deflection and stiffness characteristics. In particular, the endpoint of the beam follows a path whose curve is a constant radius allowing the use of a pseudo-rigid link for deflection approximations. Stiffness may also be modeled by a torsional spring that is not constant but a function of the pseudo-rigid-body angle, Θ . Finite element models and test results have verified this pseudo-rigid-body model. The specific volume efficiency, η , has also been estimated for various geometries.

The compliant A-Arm has shown to be a suitable concept for use in a suspension system. It performs well in response to control forces and its space utilization and potential manufacturing costs are less than other concepts. A proper understanding of its motion, stiffness and stress characteristics have been explored for further development of this concept.

CONCLUSIONS AND FUTURE WORK

This thesis has explored the use of compliant mechanisms in vehicle suspension systems, specifically where a compliant mechanism acts as part of the wheel locating mechanism and as the energy storage element. A compliant mechanism has the potential of reducing part count, joints, and manufacturing and assembly costs of a suspension system. The reduction in joints also reduces wear and the possibility of replacing suspension parts over the life of the vehicle. This chapter outlines the important findings of this research and future work that may be completed in developing compliant suspension systems.

7.1 Conclusions

The first objective of this thesis was to outline the important design constraints and functional requirements of implementing compliant mechanisms in a suspension system. Compliant mechanism characteristics and design constraints were evaluated against suspension functional requirements to help achieve this objective. Fatigue failure has been found to be a limiting design constraint. This design constraint competes with weight and

space constraints. Efforts to decrease stress in a compliant beam of constant cross-section by modifying beam geometry results in longer or wider yet thinner beams. This increases both the space and weight of the mechanism. Methods used in leaf spring mechanisms such as stacking and/or using beams of varying cross-section help to reduce the space and weight of the mechanism.

Controlling wheel motion in response to control forces has also been shown to be an important functional requirement for a compliant suspension system. It has been shown that planar compliant mechanisms such as leaf springs behave poorly in this regard. A compliant suspension mechanism that provides support normal to the plane of motion and is stiff in all directions (rotations and translations) other than the intended vertical motion of the mechanism would improve the performance of compliant leaf spring suspension mechanisms.

The second objective of this thesis was to identify suspension applications or mechanisms where compliant mechanism technology is best suited to perform. Based on the constraints of fatigue, weight and space and the need to control the wheel in response to control forces, the vehicle applications best suited for the use of compliant suspension systems are those that are low weight, have low energy storage requirements, and do not require precise vehicle handling characteristics. Examples of vehicles that fit these requirements include utility type vehicles and bicycles. There are manufacturers of both of these vehicle types that use some form of a compliant mechanism in the suspension system.

The third objective of this thesis was to identify possible solutions within the design constraints that meet the functional requirements. New compliant suspension concepts have been explored that support the wheel in 3-dimensions to minimize undesired wheel motions. Mechanism stiffness and stress due to control forces were compared to leaf spring mechanisms. These new concepts demonstrate increased stiffness and decreased stress due to control forces. Of these concepts, the compliant A-Arm proves to be the most promising candidate for future development. It has added advantages of lower space requirements, lower number of extra joints and rigid links, and simpler design for manufacture and assembly. This A-Arm configuration exhibits the same kinematic properties of a rigid-link A-Arm and also the added benefit of out-of-plane support.

The stiffness, stress, and kinematic characteristics of the compliant A-Arm configuration have been explored. This configuration has a non-linear force-deflection curve that is facilitated by the stress-stiffening effects of large deflections. In large deflections, the beams of the A-Arm experiences bending about both axes and torsion. This concentrates the maximum stress in one corner at the base of the beam which has the adverse effect of decreasing the specific volume efficiency of the mechanism.

A closed-form linear stiffness solution and a pseudo-rigid-body model has also been developed to aid in the initial design of the compliant A-Arm in a suspension system. Finite element analysis predicts that the endpoint of the beam follows a path whose curve is a constant radius which allows the use of a pseudo-rigid link for deflection approximations. Stiffness may also be modeled by a torsional spring that is not constant but a function of the pseudo-rigid-body angle, Θ . This pseudo-rigid-body model along with FEA

prove to be useful in the initial design stages of a suspension system using the compliant A-Arm.

The compliant A-Arm was shown to be a suitable concept for use in a suspension system. It performs well in response to control forces and its space utilization and potential manufacturing costs are less than other concepts. A proper understanding of its motion, stiffness and stress characteristics have been explored for further development of this concept.

7.2 Future Work

The Compliant A-Arm configuration is in the conceptual stage and early development stages. A test mechanism has been tested to verify finite element stiffness results. However, it would be very beneficial to make a practical prototype of a suspension mechanism that uses this concept and implement it in a vehicle to demonstrate its viability. There are also many different items to consider for future development and improvement.

7.2.1 Suspension A-Arm Mechanism Configurations

This A-Arm configuration, when configured in a mechanism such as the double A-Arm mechanism shown in Figure 7.1, performs well in controlling wheel motion in response to control forces. This is only one mechanism configuration where both A-Arms are parallel with $\alpha = 90$ degrees and one beam of the A-Arm is oriented longitudinally in the vehicle or parallel to the braking-force direction. Another possible configuration is the

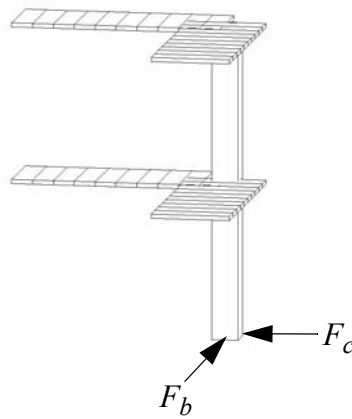


Figure 7.1 Compliant A-Arm FEA comparisons configuration

one used in the design example in Chapter 7 and shown in Figure 7.2. This mechanism configuration is also a double A-Arm design with parallel arms yet the beams are only at an angle of 60 degrees and the beams are oriented differently in the vehicle. It is recommended that different configurations of the compliant A-Arm concept in a suspension mechanism be explored to give optimum wheel control. Different mechanisms may be explored beyond the double A-Arm and McPherson strut mechanism for the use of this concept. Specifically, examples of multi-link mechanisms show many different possibilities for the implementation of this concept in a suspension mechanism.

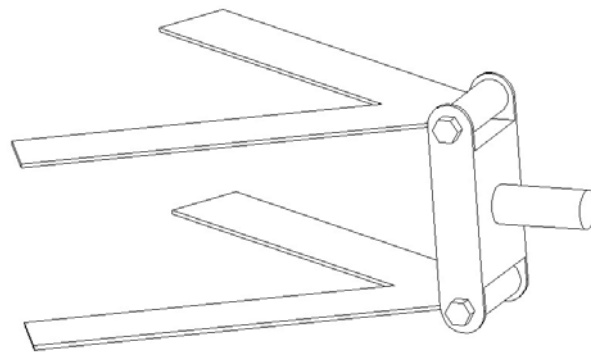


Figure 7.2 Compliant A-Arm design example configuration

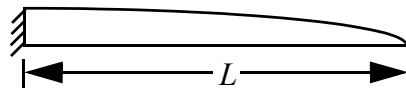
One of the advantages of rigid link suspension systems, and especially the multi-link suspension mechanism, is their use of elastic bushings. Elastokinematics or the design of the suspension mechanism in cooperation with the elastic bushings gives great flexibility and advantage in designing for desired and undesired wheel movements in response to control forces. A superior design in terms of vibration control, ride comfort, and vehicle handling may be achieved with proper design of suspension linkage placement and elastic bushing stiffness. The compliant A-Arm configuration reduces joints and hence this advantage of elastic bushings. A compliantly mounted subframe to which the suspension mechanism is attached is an example of a technique that may be used with the compliant suspension to attain the same effect of elastic bushings. It is also possible to have some type of elastic material between the ends of the A-Arm and where they would mount to the vehicle to achieve the same effects of elasto-kinematics.

7.2.2 Techniques for Decreasing Stress and Weight

Many of the techniques used by leaf springs to decrease stress and weight are also areas to research for the compliant A-Arm. These techniques include stacking leaves and/or varying the cross-section along the length as shown in Figure 7.3. More detailed explanations of stacking and varying the cross-section may be found in *The Manual on Design and Application of Leaf Springs* [33].

This research has also assumed a rectangular shaped cross-section. Since the beams of the compliant A-Arm experience more than bending about one axis, this rectan-

Varying Beam Thickness Along Length



Varying Beam Width Along Length

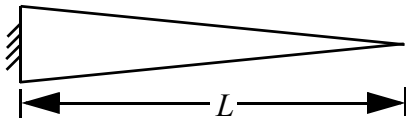


Figure 7.3 Examples of compliant beams with varying cross-sections

gular shape may not be the optimum shape for stress considerations. An oval or a cross-section of another shape may be a better shape for minimizing stress and weight.

The rectangular cross-sections used for the A-Arm beams are also assumed to be oriented parallel to the plane of the A-Arm mechanism. The cross-section orientation may be changed as shown in Figure 7.4 to allow the end-point of each beam to follow the path of the end-point of the mechanism better. This may help reduce the stress by reducing the extra bending moment and torsion load on the beams.

7.2.3 Proper Ground Clearance

Leaf springs also use an elliptic configuration or initially curved beams to give added ground clearance to the vehicle. This would also be very beneficial for the compliant A-Arm concept. It is recommended that the characteristics of this concept with initially curved beams be explored also.

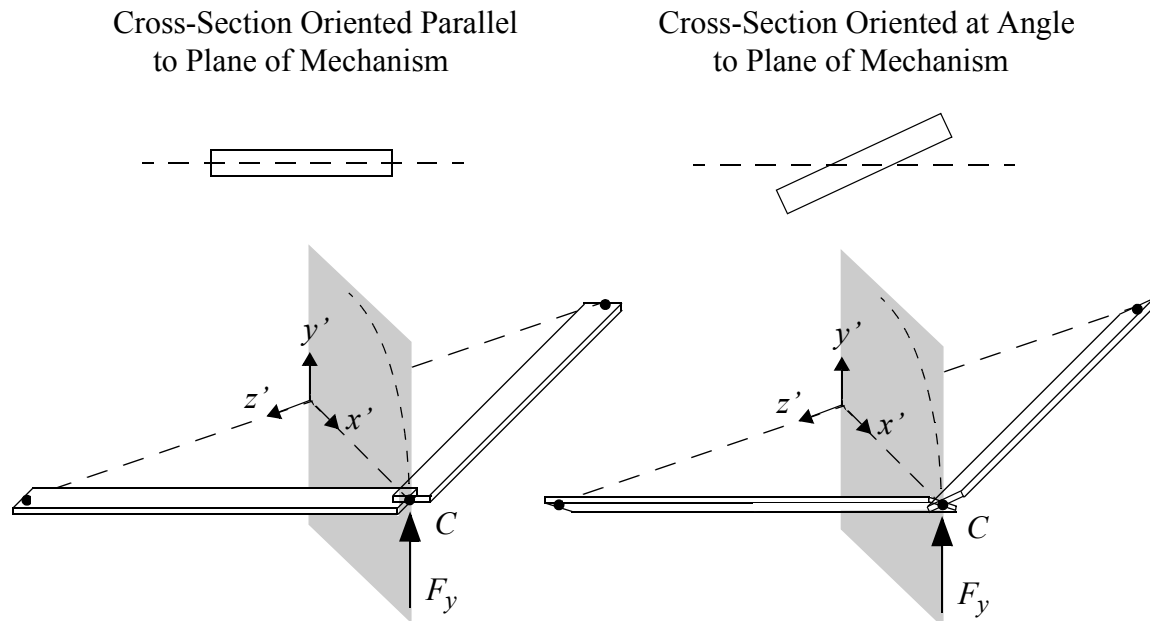
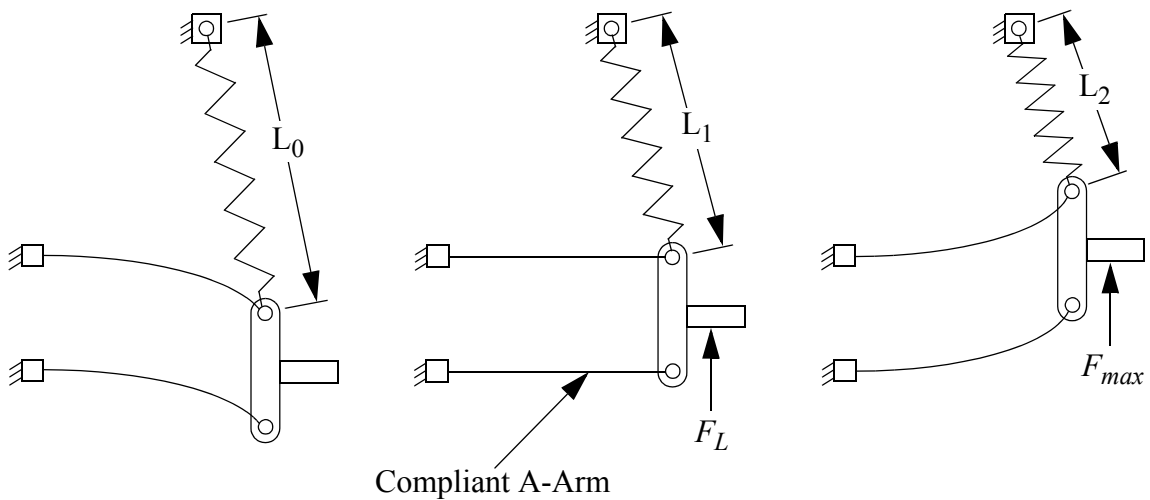


Figure 7.4 Cross-Section orientation

7.2.4 Compliant Suspension Used in Parallel with Extra Energy Storage Device

Compliant suspensions as explored in this work assumes that the compliant members are the only energy storage device. This is cost effective since it eliminates the need for an extra energy storage element. In this type of design, however, fatigue failure may limit the possibilities of the design of a compliant suspension in many vehicle applications where the energy storage requirements are high and available space is low. This is the case in vehicles such as automobiles and especially recreational vehicles. If an extra energy storage element such as a coil spring is introduced, it may act in parallel with the compliant A-Arm as illustrated in Figure 7.5. In this way the load is shared by the compliant A-Arm and spring. This will lessen the stress on the compliant A-Arm and improve



L_0 = undeflected length of coil spring
 L_1 = spring length at design load, F_L
 L_2 = spring length at maximum load, F_{max} , or maximum deflection

Figure 7.5 Compliant double A-Arm suspension in parallel with extra coil spring

the fatigue life characteristics. Cost reduction advantages still exist because of the elimination of joints by the compliant members even though a spring has been added. This particular example demonstrates how the system may be designed so that at design load, F_L , the compliant A-Arms are undeflected and all the load is carried in the coil spring. When the vehicle is unloaded, the coil spring will actually force the compliant A-Arm downwards, and when the vehicle is loaded more, the compliant A-Arm shares the load with the coil spring. In this design the compliant A-Arm will then be unloaded the majority of the time at design load and will only be deflected as the wheel moves up and down during vehicle usage.

REFERENCES

- [1] Matschinsky, W., 2000, *Road Vehicle Suspensions*, Professional Engineering Publishing Limited, London.
- [2] Gillespie, T., 1992, *Fundamentals of Vehicle Dynamics*, Society of Automotive Engineers, Warrendale, PA.
- [3] Dixon, J., 1996, *Tires, Suspension and Handling*, Society of Automotive Engineers, Warrendale, PA.
- [4] Barak, P., 1991, "Magic Numbers in Design of Suspension for Passenger Cars," SAE Paper no. 911921.
- [5] *Vehicle Dynamics and Simulation 2003*, 2003, Society of Automotive Engineers, Warrendale, PA.
- [6] *Steering and Suspension Technology Symposium 2002*, 2002, Society of Automotive Engineers, Warrendale, PA.
- [7] Williams, R. A., "Automotive Active Suspensions Part 1: Basic Principles," *Journal of Automobile Engineering*, Vol. 211, n. 6, 1997, pp. 415-426.
- [8] Williams, R. A., "Automotive Active Suspensions Part 2: Practical Considerations," *Journal of Automobile Engineering*, Vol. 211, n. 6, 1997, pp. 427-444.
- [9] Schuetze, K., Buckner, G., Beno, J. H., 1999, "Intelligent Estimation of System Parameters for Active Vehicle Suspension Control," SAE Paper no. 1999-01-0729.
- [10] Motta, D. S., Zampieri, D. E., Pereira, A. K. A., 2000, "Optimization of a Vehicle Suspension Using a Semi-Active Damper," SAE Paper no. 2000-01-3304.

- [11] Jawad, B. A., Todd, J., DiGrande, J., 2002, "Effectively Approaching and Designing a Suspension With Active Damping," SAE Paper no. 2002-01-3285
- [12] Yang, H., Liu, L. Y., 2003, "A Robust Active Suspension Controller With Rollover Prevention," SAE Paper no. 2003-01-0959.
- [13] Hasegawa, K., Okura, S., Imaizumi, T., 2002, "New Technology of Manufacturing for Coil Springs Used in Automotive Suspensions," SAE Paper no. 2002-01-0318.
- [14] Mokhtar, M. O. A., Azzam, B. S. N., Naga, S. A. R., 2001, "Composite C-Springs," SAE Paper no. 2001-01-2710
- [15] Niwa, T., Hiramatsu, N., Kazi, K., Mochizuki, M., Kachi, H., 2000, "Development in Polymer-Based Bearing Material for Automotive Shock Absorbers," SAE Paper no. 2000-01-0097.
- [16] Yoneguchi, A., Schaad, J., Kurebayashi, Y., Itoh, Y., 2000, "Development of New High Strength Spring Steel and Its Application to Automotive Coil Spring," SAE Paper no. 2000-01-0098.
- [17] Chandrasekaran, A. K., Rizzoni, G., Soliman, A., Josephson, J., Carrol, M., 2002, "Design Optimization of heavy Vehicles By Dynamic Simulations," SAE Paper no. 2002-01-3061.
- [18] Rae, W. J., Kasprzak, E. M., 2002, "Kinematics of a Double A-Arm Suspension Using Euler Orientation Variables," SAE Paper no. 2002-01-0279.
- [19] Ward, D., Hanke, O., Bertram, T., Hiller, M., Bardini, R., 2001, "A Generic Suspension Model for Middle Class Passenger Vehicles," SAE Paper no. 2001-01-1280.
- [20] Krishna, M. M. R., Kroppe, W. J., Anderson, S. V., 2000, "Flexibility Effects of Control Arms and Knuckle on Suspension - A Finite Element Versus Rigid Body Comparative Analysis," SAE Paper no. 2000-01-3446.
- [21] Soares, E. J., Carvalho, D. M. D., Onusic, H., Barreiro, J. A., Ferraro, L. C., 1999, "Development of a Test Bench for Static and Dynamic Tests of a Leaf Spring for the Suspension of Commercial Vehicles," SAE Paper no. 1999-01-2990.

- [22] Gummadi, L. N. B., Lin, S., Cai, H., Fan, X., Cao, K., 2003, "Bushings Characteristics of Stabilizer Bars," SAE Paper no. 2003-01-0239.
- [23] Krishna, M. M. R., 2001, "Design of An Upper-Control Arm Using Shape Optimization," SAE Paper no. 2001-01-2711.
- [24] Shuster, M., Maughan, G., Arnold, R., 1999, "Development of a Maintenance Free Self-Lubricating Ball Joint," SAE Paper no. 1999-01-0036.
- [25] Dudding, A. T., Wilson, W., 2000, "Development of a New Front Air Suspension and Steer Axle System for On-Highway Commercial Vehicles," SAE Paper no. 2000-01-3449.
- [26] Kasahara, T., Morioka, N., Satou, M., Yagi, T., Muraoka, K., 2000, "Development of a New Multi-Link Suspension," SAE Paper no. 2000-01-0092.
- [27] Sampson, N., 1999, "ULSAS - Improving Performance Through Lightweight Automotive Suspension Systems - Phase 1 - Benchmarking and Initial Design Concepts," SAE Paper no. 1999-01-1311.
- [28] Howell, L.L., 2001, *Compliant Mechanisms*, John Wiley & Sons, New York.
- [29] Erdman, A.G., Sandor, G.N., 1997, *Mechanism Design: Analysis and Synthesis*, Prentice Hall, New Jersey.
- [30] Raghavan, M., 1991, "An Atlas of Linkages for Independent Suspensions," SAE Paper no. 911925.
- [31] Lyons, S. M., Erickson, P. A., Evans, M. S., Howell, L. L., "Prediction of the First Modal Frequency of Compliant Mechanisms Using the Pseudo-Rigid-Body Model," *Journal of Mechanical Design*, Vol. 121, June 1999, pp 309-313.
- [32] Bastow, D., Howard, G., 1993, *Car Suspension and Handling*, Pentech Press Limited, London.
- [33] *The Manual on Design and Application of Leaf Springs*, 1982, Society of Automotive Engineers, Warrendale, PA.
- [34] Morris, C. J., "Composite Integrated Rear Suspension," *Composite Structures*, Vol. 5, 1986, pp 233-242.

- [35] Kuch, I., Delonge-Immik, G., 1991, "Development of FRP Rear Axle Components," SAE Paper no. 910888.
- [36] Kirkham, B. E., Sullivan, L. S., Bauerle, R. E., 1982, "Development of the Liteflex Suspension Leaf Spring," SAE Paper no. 820160.
- [37] Schmid, H. A., Ryan, J. P., Fuja, S. P., "Design Synthesis of Suspension Architecture for the 1997 Chevrolet Corvette," SAE Paper no. 970092.
- [38] Reimpell, J.C., Stoll, H., 1996, *The Automotive Chassis: Engineering Principles*, Society of Automotive Engineers, Warrendale, PA.
- [39] Young, W. C., 1989, *Roark's Formulas for Stress and Strain*, McGraw-Hill, Inc, New York.

LINEAR CLOSED FORM SOLUTION OF COMPLIANT A-ARM

The compliant A-Arm has a top view as shown in Figure A.1. To analyze this mechanism, a free-body diagram is used as shown in Figure A.2. Because this structure is symmetric, it is useful to analyze this mechanism as one beam with half the load applied and appropriate reaction loads applied at the joint, C . R_{Ix} , R_{Iy} , and R_{Iz} are the reaction forces on Beam 1 in the x , y , and z directions respectively. M_{Ix} , M_{Iy} , and M_{Iz} are the reaction moments on Beam 1 about the x , y , and z axes respectively. Similarly labeled are the

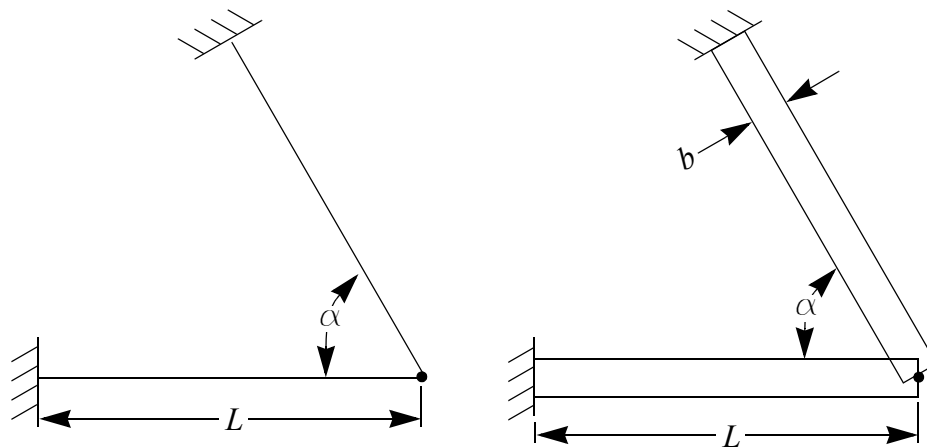


Figure A.1 Compliant A-Arm configuration

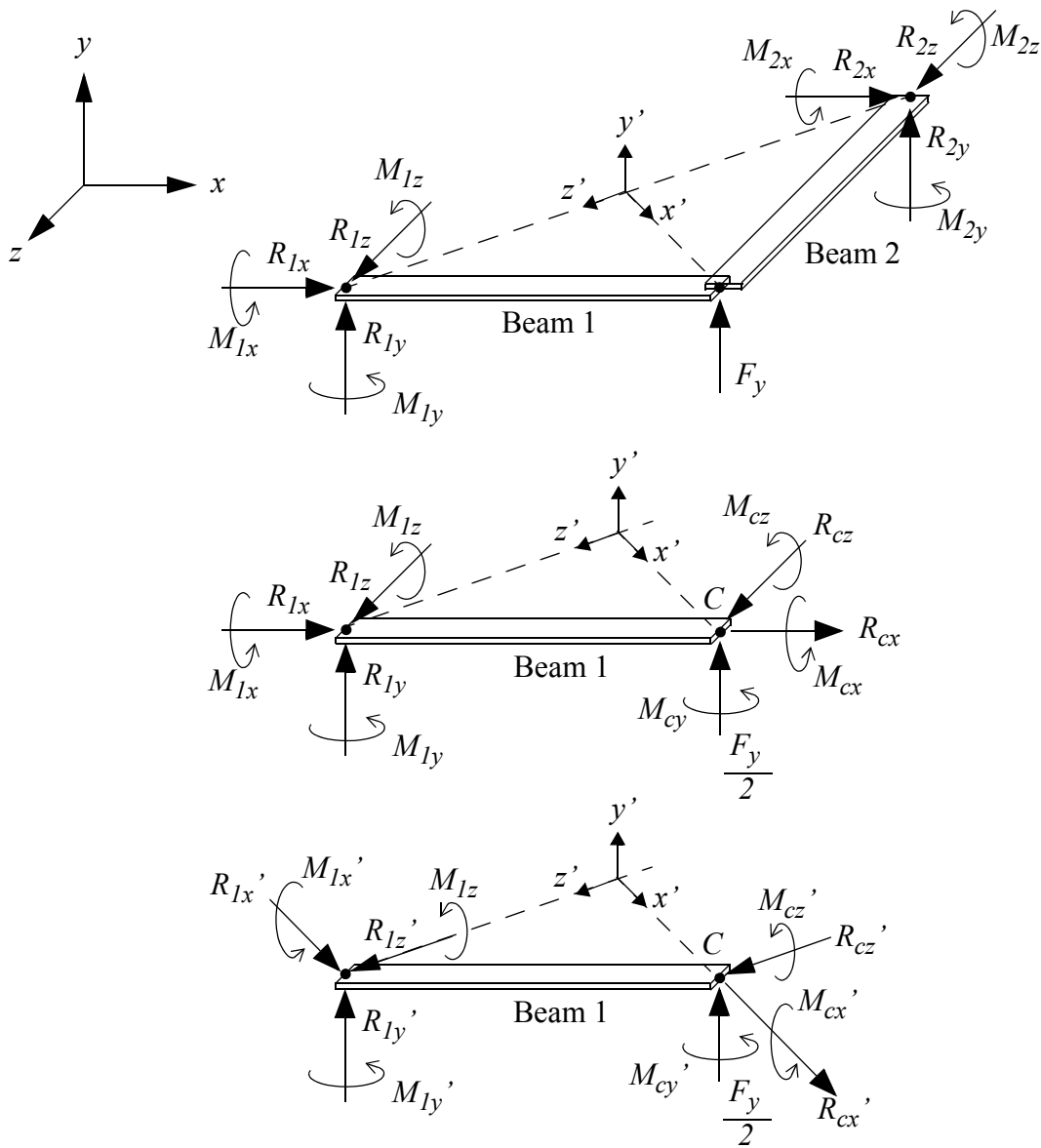


Figure A.2 Free-body diagram of compliant A-Arm mechanism

reaction forces and moments at the joint, C . A free-body diagram with reactions in the x' , y' , and z' axes is also shown for Beam 1.

Summing forces in x' direction yields

$$R_{1x'} + R_{cx'} = 0 \quad (\text{A.1})$$

Summing forces in y' direction yields

$$R_{1y'} = -\frac{1}{2}F_y \quad (\text{A.2})$$

Summing forces in z' direction yields

$$R_{1z'} + R_{cz'} = 0 \quad (\text{A.3})$$

Summing moments about the x' axis at ground for beam 1 yields

$$M_{1x'} + M_{cx'} + \frac{1}{2}F_y L \sin\left(\frac{\alpha}{2}\right) = 0 \quad (\text{A.4})$$

Summing moments about the y' axis at ground for beam 1 yields

$$M_{1y'} + M_{cy'} - R_{cx'} L \sin\left(\frac{\alpha}{2}\right) - R_{cz'} L \cos\left(\frac{\alpha}{2}\right) = 0 \quad (\text{A.5})$$

Summing moments about the z' axis at ground for beam 1 yields

$$M_{1z'} + M_{cz'} + \frac{1}{2}F_y L \cos\left(\frac{\alpha}{2}\right) = 0 \quad (\text{A.6})$$

A.1 Spherical Joint Approximation

Using a spherical joint approximation the following reactions become zero:

$$M_{cx}' = 0 \quad (\text{A.7})$$

$$M_{cy}' = 0 \quad (\text{A.8})$$

$$M_{cz}' = 0 \quad (\text{A.9})$$

Using linear approximations, the following reaction become zero:

$$R_{1x}' = R_{cx}' = 0 \quad (\text{A.10})$$

$$R_{1z}' = R_{cz}' = 0 \quad (\text{A.11})$$

Substituting Equations (A.8), (A.10), and Equation (A.11) into Equation (5) yields

$$M_{1y}' = 0 \quad (\text{A.12})$$

Substituting Equation (A.7) into Equation (A.4) yields

$$M_{1y}' = -\frac{1}{2}F_y L \sin\left(\frac{\alpha}{2}\right) \quad (\text{A.13})$$

Substituting Equation (A.9) into Equation (A.6) yields

$$M_{1z}' = -\frac{1}{2}F_y L \cos\left(\frac{\alpha}{2}\right) \quad (\text{A.14})$$

In terms of x - y - z coordinate axes, reactions at ground for Beam 1 become

$$M_{1x} = 0 \quad (\text{A.15})$$

$$M_{1z} = -\frac{1}{2}F_y L \quad (\text{A.16})$$

This is equivalent to a cantilever beam. Stiffness calculations will result in

$$\delta_y = \frac{\frac{1}{2}F_y L^3}{3EI} \quad (\text{A.17})$$

This is equivalent to two cantilever beams in parallel having equal dimensions of one of the A-Arm beams.

A.2 Fixed Joint Connection

Linear approximations still yield

$$R_{1x}' = R_{cx}' = 0 \quad (\text{A.18})$$

$$R_{1z}' = R_{cz}' = 0 \quad (\text{A.19})$$

$$M_{cy}' = 0 \quad (\text{A.20})$$

$$M_{cz}' = 0 \quad (\text{A.21})$$

Substituting Equations (A.18), (A.19), and (A.20) into Equation (A.5) yields

$$M_{1y}' = 0 \quad (\text{A.22})$$

From the original six static equations, only Equations (A.4) and (A.6) are left to solve for the three remaining unknowns. Substitute Equation (A.21) into Equation (A.6) yields

$$M_{1z}' = -\frac{1}{2}F_y L \cos\left(\frac{\alpha}{2}\right) \quad (\text{A.23})$$

and from Equation (A.4):

$$M_{1x}' + M_{cx}' = -\frac{1}{2}F_y L \sin\left(\frac{\alpha}{2}\right) \quad (\text{A.24})$$

In terms of the beam coordinate x-y-z axes there are two equations with four unknowns:

$$M_{1x} + M_{cx} = 0 \quad (\text{A.25})$$

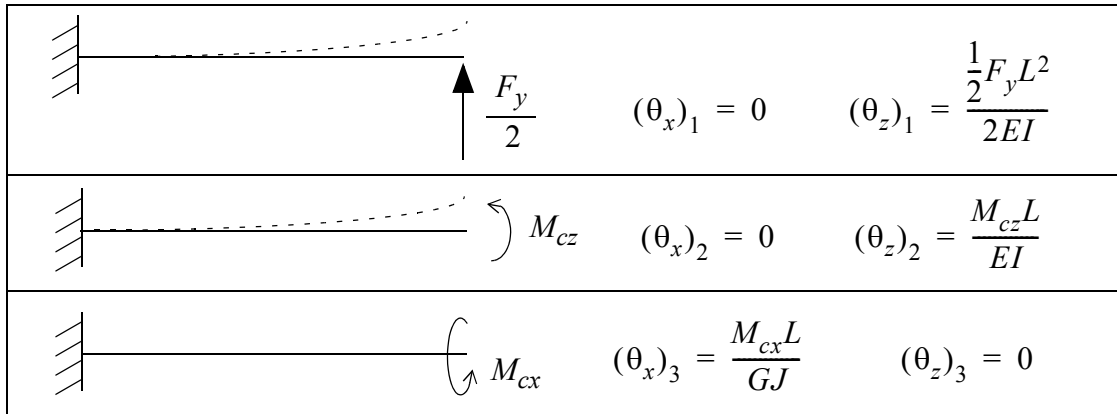
$$M_{1z} + M_{cz} = -\frac{1}{2}F_y L \quad (\text{A.26})$$

This structure is statically indeterminate to the second degree. The moments, M_{cx} and M_{cz} are chosen as the redundant reactions. By equating the rotations of the end point C of Beams 1 and 2 due to the applied force, $F_y/2$, and the redundant reactions, the redundant reactions may be solved. Each load is applied separately to each beam as shown in Figure A.3. Compatibility equations and the principle of superposition are used to yield:

$$(\theta_x)_1 + (\theta_x)_2 + (\theta_x)_3 = (\theta_x)_4 + (\theta_x)_5 + (\theta_x)_6 \quad (\text{A.27})$$

$$(\theta_z)_1 + (\theta_z)_2 + (\theta_z)_3 = (\theta_z)_4 + (\theta_z)_5 + (\theta_z)_6 \quad (\text{A.28})$$

Beam 1



Beam 2

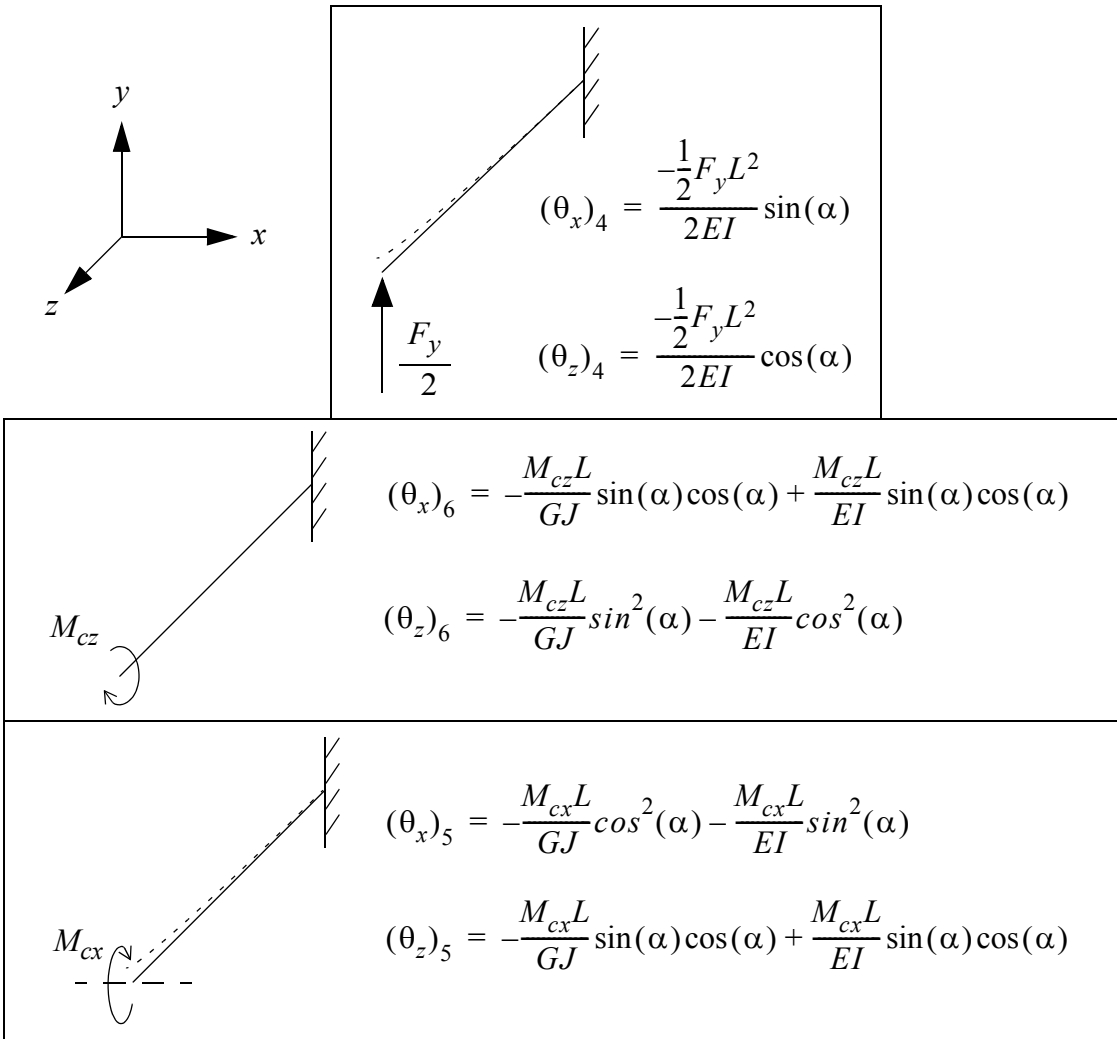


Figure A.3 Deflections due to applied loads and redundant loads

where θ_x and θ_z are rotations about the x and z axes respectively. In terms of the applied loads given in Figure A.3, these equations become:

$$\frac{M_{cx}L}{GJ} = \frac{-\frac{1}{2}F_yL^2}{2EI} \sin(\alpha) - M_{cx}L \left(\frac{\cos^2(\alpha)}{JG} + \frac{\sin^2(\alpha)}{EI} \right) - M_{cz}L \sin(\alpha) \cos(\alpha) \left(\frac{1}{JG} - \frac{1}{EI} \right) \quad (\text{A.29})$$

$$\frac{\frac{1}{2}F_yL^2}{2EI} + \frac{M_{cz}L}{EI} = \frac{-M_{cz}L}{GJ} \sin^2(\alpha) - \frac{M_{cz}L}{EI} \cos^2(\alpha) + \frac{\frac{1}{2}F_yL^2}{2EI} \cos(\alpha) + M_{cx}L \sin(\alpha) \cos(\alpha) \left(\frac{1}{EI} - \frac{1}{JG} \right) \quad (\text{A.30})$$

Solving these equations for M_{cx} and M_{cz} and simplifying yields

$$M_{cx} = \frac{\frac{1}{2}F_yL}{2EI} \left[\frac{(\cos(\alpha) - 1)AB + A^2 \sin(\alpha)}{A^2B - B^2C} - \frac{\sin(\alpha)}{B} \right] \quad (\text{A.31})$$

$$M_{cz} = \frac{-\frac{1}{2}F_yL}{2EI} \left[\frac{(\cos(\alpha) - 1)B + A \sin(\alpha)}{A^2 - BC} \right] \quad (\text{A.32})$$

where A , B , and C are

$$A = \sin(\alpha) \cos(\alpha) \left(\frac{1}{JG} - \frac{1}{EI} \right) \quad (\text{A.33})$$

$$B = \frac{1 + \cos^2(\alpha)}{JG} + \frac{\sin^2(\alpha)}{EI} \quad (\text{A.34})$$

$$C = \frac{1 + \cos^2(\alpha)}{EI} + \frac{\sin^2(\alpha)}{JG} \quad (\text{A.35})$$

Substituting Equations (A.31) and (A.32) into Equations (A.25) and (A.26) yield the reactions at ground:

$$M_{cx} = \frac{1}{2}F_y L \left[\frac{\sin(\alpha)}{B} - \frac{(\cos(\alpha) - 1)AB + A^2 \sin(\alpha)}{A^2 B - B^2 C} \right] \quad (\text{A.36})$$

$$M_{cz} = \frac{1}{2}F_y L \left\{ \frac{\frac{1}{2EI}[(\cos(\alpha) - 1)B + A \sin(\alpha)]}{A^2 - BC} - 1 \right\} \quad (\text{A.37})$$

Because torsion of the beams is also present, the cantilever beam linear stiffness relationship given in Equation (A.17) is not valid. Energy methods may be used to determine the stiffness of this structure. Energy storage, U , may be expressed as a function of the internal moment and torsion of Beam 1:

$$U = \frac{1}{2EI} \left[\int_0^L \left(M_{cz} + \frac{1}{2}F_y x \right)^2 dx \right] + \frac{1}{2GJ} \left[\int_0^L M_{cx}^2 dx \right] \quad (\text{A.38})$$

Applying Castigliano's theorem gives us the deflection in the direction of the force $F_y/2$ by taking the partial derivative of the energy function with respect to the force $F_y/2$:

$$u_y = \frac{1}{EI} \left[\int_0^L \left(M_{cz} + \frac{1}{2}F_y x \right) \left(\frac{\partial \left(M_{cz} + \frac{1}{2}F_y x \right)}{\partial \left(\frac{1}{2}F_y \right)} \right) dx \right] + \frac{1}{GJ} \left[\int_0^L M_{cx} \frac{\partial M_{cx}}{\partial \left(\frac{1}{2}F_y \right)} dx \right] \quad (\text{A.39})$$

Substituting Equations (A.36) and (A.37) into Equation (A.39) and solving yields:

$$u_y = \frac{1}{2}F_y L^3 \left(\frac{M}{EI} + \frac{N}{JG} \right) \quad (\text{A.40})$$

where:

$$M = \frac{1}{3} - \frac{1}{2EI} \left(\frac{(\cos(\alpha) - 1)B + A \sin(\alpha)}{A^2 - BC} \right) \left(1 - \frac{1}{2EI} \left(\frac{(\cos(\alpha) - 1)B + A \sin(\alpha)}{A^2 - BC} \right) \right) \quad (\text{A.41})$$

$$N = \left[\frac{1}{2EI} \left(\frac{(\cos(\alpha) - 1)AB + A^2 \sin(\alpha)}{A^2 B - B^2 C} - \frac{\sin(\alpha)}{B} \right) \right]^2 \quad (\text{A.42})$$

This relationship may be used for stiffness calculations at small deflections for all values of α between 0 and 90 degrees.